UNCLASSIFIED

ANL-5060(Del.)

UNITED STATES ATOMIC ENERGY COMMISSION

REACTOR ENGINEERING DIVISION QUARTERLY REPORT [FOR] MARCH 1, 1953 THROUGH MAY 31, 1953

June 15, 1953

Argonne National Lab
Lemont, Illinois

Technical Information Service Extension, Oak Ridge, Tenn.

Photostat Price $ 24.30
Microfilm Price $ 7.50

Available from the
Office of Technical Services
Department of Commerce
Washington 25, D. C.

UNCLASSIFIED

ANL-5060

ARGONNE NATIONAL LABORATORY
P. O. Box 299
Lemont, Illinois

REACTOR ENGINEERING DIVISION

QUARTERLY REPORT

March 1, 1953 through May 31, 1953

Compiled by

Members of the Reactor Engineering Division

June 15, 1953

Previous Reports:

ANL-5012	December 1, 1952 through February 28, 1953
ANL-4951	September 1, 1952 through November 30, 1952
ANL-4925	June 1, 1952 through August 31, 1952

Operated by The University of Chicago
under
Contract W-31-109-eng-38

5

TABLE OF CONTENTS

REACTOR DESIGN AND DEVELOPMENT

ARGONNE RESEARCH REACTOR (CP-5) - G. A. Anderson

Work on the Argonne Research Reactor is progressing according to schedule. The Reactor Shield is completed and the graphite work is approximately half finished. Piping has been completely fabricated, disassembled for cleaning, and is ready for reassembly and leak testing. All control room panels are installed and interconnecting wiring is progressing.

POWER BREEDER REACTOR (PBR)

A. Reactor Design and Evaluation - E. Hutter, L. J. Koch, M. J. Steckler (CR&D), J. E. Wellman (CR&D)

Conceptual design studies of reactor configurations are being made to identify the engineering problems, and to suggest solutions and available alternates. The most promising concept developed to date involves a contained primary coolant circuit, or package arrangement, in which the reactor proper and primary coolant circuit are contained in a single large vessel. This approach eliminates all exposed piping in the primary circuit, and results in a very compact primary unit with individual primary coolant circuits (probably four) surrounding the reactor. The design should result in the optimum utilization of shielding, since all components in the circuit requiring shielding are contained in a single shielded package. The "primary system package" approach requires that the intermediate heat exchangers, and primary coolant system pumps be submerged in the coolant (sodium). This appears to be a feasible application for d-c electromagnetic pumps.

Methods of fuel element unloading are being evaluated, assuming a box-type fuel element, which would be applicable to the various types of fuel elements being considered. Shutdown cooling of the fuel elements, and the activity of the fuel elements and adhering coolant complicate the procedure for removing these elements from the reactor. It has been assumed that subsequent processing of the fuel elements will require some cooling time following reactor shutdown. The most promising procedure developed thus far utilizes this cooling time by transferring the fuel elements from the reactor core to a storage facility within the reactor vessel. The fuel elements are kept submerged in sodium during transfer and in storage, and are not removed from the vessel until they have cooled sufficiently to meet the requirements of the succeeding operations.

Design studies have been made of fuel element configurations for the "particulated fuel element." The studies include facilities for the handling operations, provisions for coolant flow, and structural stability particularly in the core section. One design involves an element of hexagonal cross section containing triangular cross section tubes spaced on a triangular pitch. The tubes containing the "particulated fuel" have ribs at each corner which make contact with the flat side of each adjacent tube providing a stable structure and the necessary coolant flow passages. The hexagonal unit, approximately 3 in. across the flats, provides a reasonable size unit which permits handling of a relatively small number of "packages" in a reactor loading.

A preliminary analysis is being made of a heat removal system for a prototype or pilot plant reactor. The objective is to provide the steam generating equipment and turbo-generator unit to permit demonstrating the operating characteris :cs of the unit, and also permit the flexibility of operation required for an experimental unit. It is anticipated that the prototype reactor must be operable over a wide temperature and power range as well as the reference design conditions. Results thus far indicate that considerable operational flexibility can be achieved with only slight modifications in the plant arrangement.

B. Reactor Physics and Critical Assembly Work - R. Avery, D. Okrent

1. Two-Group Calculations

Further two-group diffusion theory calculations in spherical geometry have been made in order to obtain preliminary estimates relative to the PBR.

The fast group represents neutrons above the fission threshold of U^{238} ($\approx$1.6 mev) and the slow group neutrons below that energy. The following macroscopic cross sections (cm^{-1}) were used:

Fast Group

	U^{235}	U^{238}	Pu^{239}	Na	Fe	Pb	K
$\Sigma_{fission}$	0.0591	0.0297	0.0746	0	0	0	0
$\Sigma_{absorption}$	0.0698	0.0297	0.0836	0.0000044	0.002964	0.000528	0.000268
$\Sigma_{transport}$	0.203	0.180	0.173	0.066	0.296	0.165	0.0472
$\Sigma_{inelastic}$	0.0851	0.1135	0.0725	0.00088	0.0847	0.0396	0.000268

Slow Group

	U^{235}	U^{238}	Pu^{239}	Na	Fe	Pb	K
$\Sigma_{fission}$	0.0662	0	0.0705	0	0	0	0
$\Sigma_{absorption}$	0.0781	0.00237	0.0790	0.0000176	0.002964	0.000928	0.000268
$\Sigma_{transport}$	0.264	0.378	0.242	0.088	0.296	0.165	0.0268

$$\left.\begin{aligned} {}_1U^{235} &= {}_2U^{238} = 2.5 \\ {}_2Pu^{239} &= 2.9 \end{aligned}\right\} \text{ number of neutrons emitted per fission}$$

0.47 of the neutrons go into the fast group and 0.53 into the slow group.

Calculations were made on the following general systems:

I Converter

II Breeder

III Pilot Plant (Converter or Breeder)

Some of the results given below were reported previously.[1] They are included in order to facilitate comparison with the new results.

The core radius for the converter or breeder was, in all cases, 52.34 cm (volume equal to a cylinder with H = D = 36 in.). The pilot plant core radius was 24.3 cm (1/10 the volume of the full-size core). Unless otherwise stated, the reference core and standard blanket compositions were, by volume fraction,

Ref. 25	Ref. 49	Core	Standard Blanket Composition (SBC)
U^{235}	Pu^{239}	0.30	
U^{238}	U^{238}		
Na		0.55	0.20
Fe		0.15	0.10

[1] Reactor Engineering Division Quarterly Report, ANL-5012, March 15, 1953, p.6.

I. Converter

Core	Reflector Thick., in.	Reflector Composition	Blanket Thick.,* in.	Volume Fraction of U^{233} in Core	Atoms U^{233} / Atoms U^{233} in Core	Critical Mass U^{233}, kg
Ref. 25		None	12	0.05365	4.60	594
Ref. 25		None	25	0.05327	4.63	590
Ref. 25		None	24	0.05355	4.64	589
Ref. 25		None	∞	0.05321	4.64	589
Ref. 25		None	infinite	0.05321	4.64	589
Ref. 25	3	Na	12	0.05436	4.52	603
Ref. 25	6	Na	12	0.05478	4.48	607
Ref. 25	12	Na	12	0.05484	4.47	608
Ref. 25	∞	Na	infinite	0.05404	4.53	599
Ref. 25	3	Fe	12	0.05382	4.79	574
Ref. 25	6	Fe	12	0.05397	4.68	565
Ref. 25	12	Fe	12	0.05340	4.85	559
Ref. 25	6	Fe	infinite	0.05388	4.80	564
Ref. 25	3	Pb	12	0.05256	4.71	583
Ref. 25	6	Pb	12	0.05287	4.79	574
Ref. 25	12	Pb	12	0.05256	4.93	565
Ref. 25	12 (to volume)	Pb	infinite	0.05364	4.95	559
Ref. 25	3	(50 Na, 50 S.S.C.)	12	0.05369	4.59	591
Ref. 25	3	(50 Na, 50 Fe)	12	0.05290	4.67	586
Ref. 25	3	(50 Na, 50 Pb)	12	0.05343	4.61	582
Ref. 25	6	(50 Na, 50 S.S.C.)	12	0.05371	4.59	595
Ref. 25	6	(50 Na, 50 Fe)	12	0.05293	4.72	581
Ref. 25	6	(50 Na, 50 Pb)	12	0.05315	4.69	589
Ref. 25	6	(50 mod, 50 S.S.C.)	12	0.05576	4.38	616
Ref. 25	3	(S.S.C. with .0020 Pu^{239} replacing .0020 U^{238})	12	0.05306	4.66	587
Ref. 25, with Fe replaced by Na		None	12	0.04997	5.00	554
Ref. 25, with Fe replaced by U^{238}		None	12	0.05480	7.35	609

II. Breeder

Core	Reflector Thick., in.	Reflector Composition	Blanket Thick.,* in.	Volume Fraction of Pu^{239} in Core	Atoms U^{233} / Atoms Pu^{239} in Core	Critical Mass Pu^{239}, kg
Ref. 46		None	12	0.03813	8.36	362
Ref. 46	6	Na	12	0.03853	7.83	351
Ref. 46	6	Fe	12	0.03840	8.30	364

III. Pilot Plant (Converter or Breeder)

Core	Reflector Thick., in.	Reflector Composition	Blanket Thick.,* in.	Volume Fraction U^{233}	Volume Fraction Pu^{239}	Atom Ratio U^{233}/U^{235}	Atom Ratio U^{233}/Pu^{239}	Critical Mass, kg U^{233}	Critical Mass, kg Pu^{239}
Ref. 25		None	24	0.1322	---	1.27	---	248.6	---
Ref. ($\frac{\text{vol } U^{233}}{\text{vol } Pu^{239}}$ = 2)		None	24	0.0892	0.02973	2.63	7.55	98.9	39.5
Ref. ($\frac{\text{vol } U^{233}}{\text{vol } Pu^{239}}$ = 1)		None	24	0.0527	0.0527	3.70	4.30	98.4	52.8
Ref. 46		None	24	---	0.0936	---	2.67	---	95.7
Ref. 25	6	Na	24	0.1132	---	0.839	---	181.0	---
Ref. 25	6	Fe	24	0.1243	---	1.41	---	138.1	---
Ref. 46	6	Na	24	---	0.1136	---	1.98	---	111.7
Ref. 46	6	Fe	24	---	0.1065	---	2.90	---	98.6

*Standard Blanket Composition

2. One-Group Calculations

In addition to the two-group calculations, some one-group calculations were made to obtain rough estimates of various effects. In the following series of calculations, the one-group macroscopic cross sections were:

	U^{235}	U^{238}	Na	Fe	Pb
$\Sigma_{fission}$	0.0657	0.00218	0	0	0
$\Sigma_{absorption}$	0.0775	0.00918	0.0000166	0.002964	0.000528
$\Sigma_{transport}$	0.278	0.363	0.086	0.296	0.165

In the blanket the fission cross section of U^{238} was assumed to be zero. This assumption should not produce an appreciable error for the effects under investigation.

a. Comparison of Critical Mass for Pb-Bi vs Na Cooling

Calculations were made for a "Reference 25" core and an infinite S.B.C. blanket. With Na as the coolant, the critical volume fraction of U^{235} was .0531. With Pb-Bi as the coolant (in both core and blanket), the mixture was assumed to have cross sections equal to that of Pb of .90 density. The critical U^{235} volume fraction was .0528. Since the absorption cross section of Pb might be considerably lower than that assumed above, the calculation was repeated with this absorption cross section reduced by a factor of eight (the microscopic cross section was reduced from .016 to .002 barns). This changed the critical volume fraction of U^{235} to .0502.

b. Comparison of Critical Mass for UO_2 Core Alloy vs Uranium

The effect on critical mass of the replacement of all core uranium with UO_2 having a density 10 was investigated. Again the calculations were made on a "Reference 25" core with an infinite S.B.C. blanket. When the uranium was replaced by UO_2 the critical mass of U^{235} was reduced about 10%.

	Volume Fraction	
Core	U^{235}	U^{238}
Uranium	0.0531	0.2469
UO_2	0.0477	0.0937

It is estimated that the 28 fissions in the core per U^{235} fission would drop from .177 for the uranium fuel to .105 for the UO_2 fuel. This would have an adverse effect on the breeding ratio, producing a drop of 0.09 (i.e., if it were 1.20, it would become 1.11). Furthermore, there would be less internal breeding with a resultant increase in the problem of control.

c. *Effect of Blanket Thickness on Leakage Out of Blanket*

Calculations were made on a "Reference 25" core with S.B.C. blankets of thicknesses of 1 ft, 2 ft and 3 ft. The number of neutrons escaping the blanket per U^{235} fission in the core were for the three cases:

1 ft	2 ft	3 ft
0.251	0.044	0.007

3. Multi-Group Calculations

A multi-group diffusion theory set-up has been coded for solution by IBM. The method of solution and the programming are similar to that developed and used by KAPL.[2] It is anticipated that even with the large uncertainties in cross section, the multi-group calculations will afford more reliable estimates than heretofore possible to many of the problems involved in a detailed PBR design. The first of these calculations has been completed and the results are being analyzed.

C. Fuel Elements and Fuel Media

1. Corrosion - J. C. McGuire

Semi-static corrosion tests of materials in liquid sodium are being conducted. The main program at present is a cooperative effort with the Detroit Edison Company in testing proposed fuel alloys. Unless otherwise noted, the tests are made in AISI type 347 stainless steel capsules.

A uranium-iron eutectic alloy containing 40 atomic per cent iron, showed no deleterious effect after exposure in sodium at 550C (1022F) for periods of 1, 3, and 7 weeks.

A uranium-chromium alloy containing 20% chromium, showed no evidence of corrosion after 1, 3, and 9 weeks at 550C. Similar results were obtained on samples tested in Globe iron capsules.

Titanium, containing 6% aluminum, was unaffected after two weeks at 550C.

An effort was made to determine the temperature at which the natural surface film on Inconel X would be removed. Samples tested for 24 hr at 150, 250, and 300C (402, 482, 572F, respectively) showed little or no effect on the surface film.

---

[2] H. Hurwitz, R. Ehrlich, "Further Developments of Multi-Group Method for Intermediate Piles," KAPL-39, March 1, 1948.

2. Escape of Fission Products from Uranium - M. Sivetz

Because uranium or uranium alloy is to be used for reactor fuel at temperatures of 600C and higher, data on the amounts of fission products escaping by diffusion from the uranium metal into the sodium coolant at these temperatures are required to enable proper design of the fuel elements (or fuel cans). Since corrosion of uranium also would be expected to contribute fission products to the sodium, additional knowledge of the extent of corrosion is necessary. Consequently, a dynamic 30 gpm liquid sodium loop, of 20 gallons volume and 2-inch pipe size, is being constructed to study release of fission products and corrosion.

3. Manufacture of Ball-Type Fuel Elements - E. L. Currier

Tests have been made to determine operating characteristics of equipment for the manufacture of metal balls. The apparatus consists of a resistance-heated steel pot and a needle valve - nozzle arrangement in the bottom for generating molten metal drops which fall into a quenching medium placed directly beneath the pot. The controllable variables are: Molten metal temperature, nozzle diameter, rate of drop generation, dropping height (distance between tip of nozzle and surface of quenching medium), quenching medium, depth of quench, and temperature of quench. The product is classified according to screen size and packing fraction in 3/8 in. ID tubes.

Only lead drops have been made, with the following reference parameters arbitrarily selected for comparison of variables:

Temperature of lead, F	800
Nozzle diameter, in.	0.020
Drop rate, drops/sec	3
Drop rate, gm/hr	570
Dropping height, in.	1
Quench medium	HyVac Oil
Quench depth, in.	28
Quench temperature, F	90

The drops are usually oblate spheroids or tear drops with shrink hole surface defects. A high degree of size control has been obtained; for example, 11 random samples from one melt showed an average diameter of 0.105 in., with the smallest being 0.100 in., and the largest being 0.109 in.

The results of the packing tests of balls manufactured under these varying conditions allow the following observations:

(1) The packing fraction in the 3/8 in. tube is not increased by increased dropping height.

(2) The packing fraction may be increased by decreased drop rate.

(3) The packing fraction is increased with increased lead temperature.

(4) The packing fraction is increased with increased temperature of quench.

(5) The packing fraction is larger for the oblate spheroids than for the tear drops.

The highest packing fraction obtained was 58.7%, for rolling oblate spheroids of the following screen analysis:

- 8 + 10 mesh	413.6 gm
-10 + 12 mesh	1.6 gm

Rolling oblate spheroids are those which roll freely down an inclined glass surface. A typical low packing fraction for rolling oblate spheroids was 53.3%, obtained for balls which were screened as follows:

-7 + 8 mesh	308.7 gm
-8 + 10 mesh	14.3 gm

4. Ball-Type Fuel Element Packing Studies - W. A. Neisz

In order to determine how balls would pack in a tube under compressive loads, a series of compactions were made with lead shot of 0.095 in. diameter in a one-inch mold at pressures up to 12,000 psi. More flattening of the lead shot occurred at or near that surface of the compact which received the force. The compacts resulting from the pressing of lead shot at 4000 psi and 8000 psi (Figure 1), in Lucite tubing with a Lucite plunger, show this effect, especially at the higher pressure.

A maximum pressure of 1100 psi was required to remove the compacts from the molds. Usually when the applied pressure had exceeded 6000 psi, the upper portion of the compact cohered while the lower balls were free and able to fall out of the mold. An attempt to make a permanent compact was unsuccessful.

5. Gas Entrapment in NaK-Steel Ball Columns - W. K. Anderson, E. L. Currier, W. C. Dzombak, and J. W. Frank

Preliminary tests have been made to determine the extent of gas entrapment in liquid metal columns packed with steel balls. These tests are related to a projected fuel element composed of small spherical particles

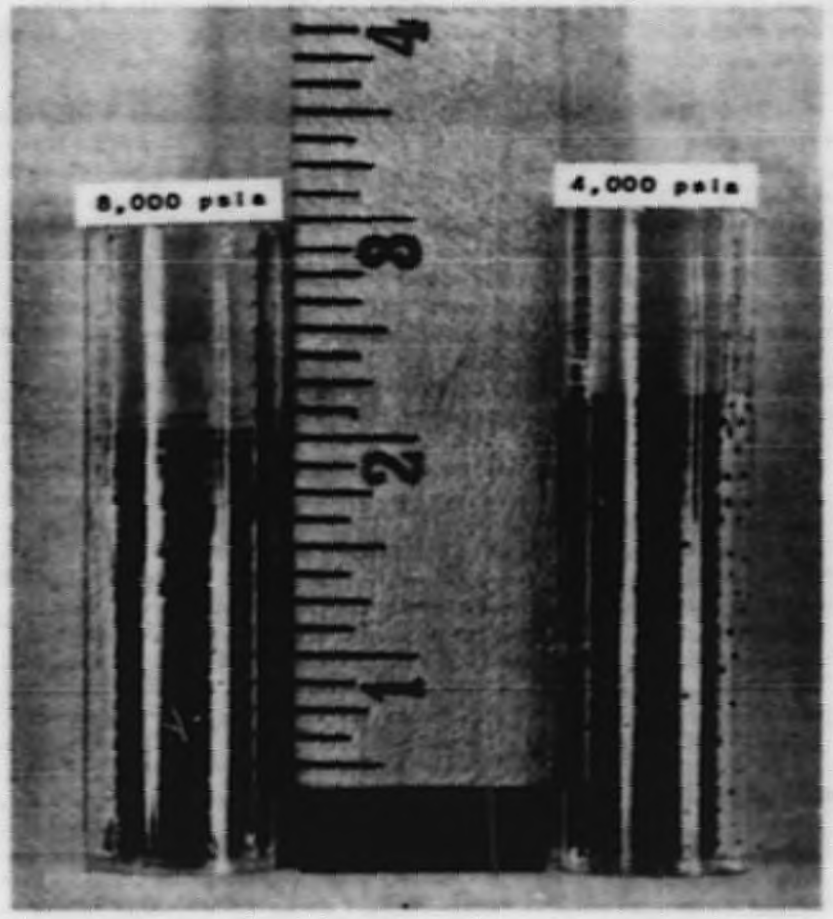

FIG. 1
LEAD SHOT COMPACTED AT 4,000 AND 8,000 psia

of fuel immersed in liquid sodium in a small diameter tube. It is desired to ascertain whether fission product gases, particularly xenon, will collect as bubbles acting as heat transfer barriers or whether the gases will pass up through the fuel bed into a collector above the element proper. The tests were made with NaK at room temperature and with sodium at 600C (1112F), in different equipment.

The apparatus for the first experiment with NaK consisted of a vertical glass tube closed by a rubber stopper through which a hypodermic needle could be inserted. The tube was about one-third filled with NaK and SAE 52100 steel balls were dropped into the NaK until the balls were visible at the top. More NaK was added to cover the balls, and a hydrocarbon fluid added to protect the meniscus. A cathetometer was focused on this meniscus to observe the liquid level. One cc of argon, introduced at the bottom of the tube with a hypodermic syringe, lodged within the space between the outermost balls and the walls of the tube. Second and third portions of argon (1 cc each) were added in the same way; the third cc passed through. It was noted on disassembly that the balls had not been wetted by the NaK and that large aggregates of Na_2O were present.

For the second experiment with NaK, equipment was completely redesigned and procedure replanned in order to eliminate the lack of wetting and the presence of Na_2O. The apparatus, shown in Figure 2 consists of a tube which is partially filled with degreased, pickled and dried SAE 52100 steel balls. At the bottom is attached another tube bearing a stopcock which terminates in a sintered glass filter, by means of which NaK is admitted. Also located at the bottom is a short length of small-bore rubber tubing closed at one end, through which the hypodermic needle is inserted. The top of the column is connected to an argon cylinder and a vacuum pump. For the test, the apparatus was evacuated, filled with argon and re-evacuated; this cycle was repeated twice. The ball column was heated with an open flame while under vacuum, argon was admitted, and the system re-evacuated in order to outgas the balls. The lower stopcock was then opened slowly in order to admit clean NaK. The column containing the NaK and balls was heated with a flame to insure wetting. This was verified by observation after pushing out the NaK with argon pressure. The NaK was replaced, the lower stopcock closed, and argon admitted at a pressure of one atmosphere. The level of the NaK was read on the cathetometer scale, the hypodermic syringe was inserted into the rubber tube, and argon was admitted in 1-cc portions. The gas remained lodged among the balls until the third cc was added. This was shown by a rise in the liquid level, as well as by the absence of any bubbles rising to the top surface. On disassembly the balls were found to be completely wet by the NaK, except for three or four in the top center of the column.

For the tests with sodium at 600C (1112F), a small amount of argon gas is released at the bottom of a resistance-heated 3/8 in. ID stainless steel tube 10 in. high filled with 1/16 in. diameter stainless steel

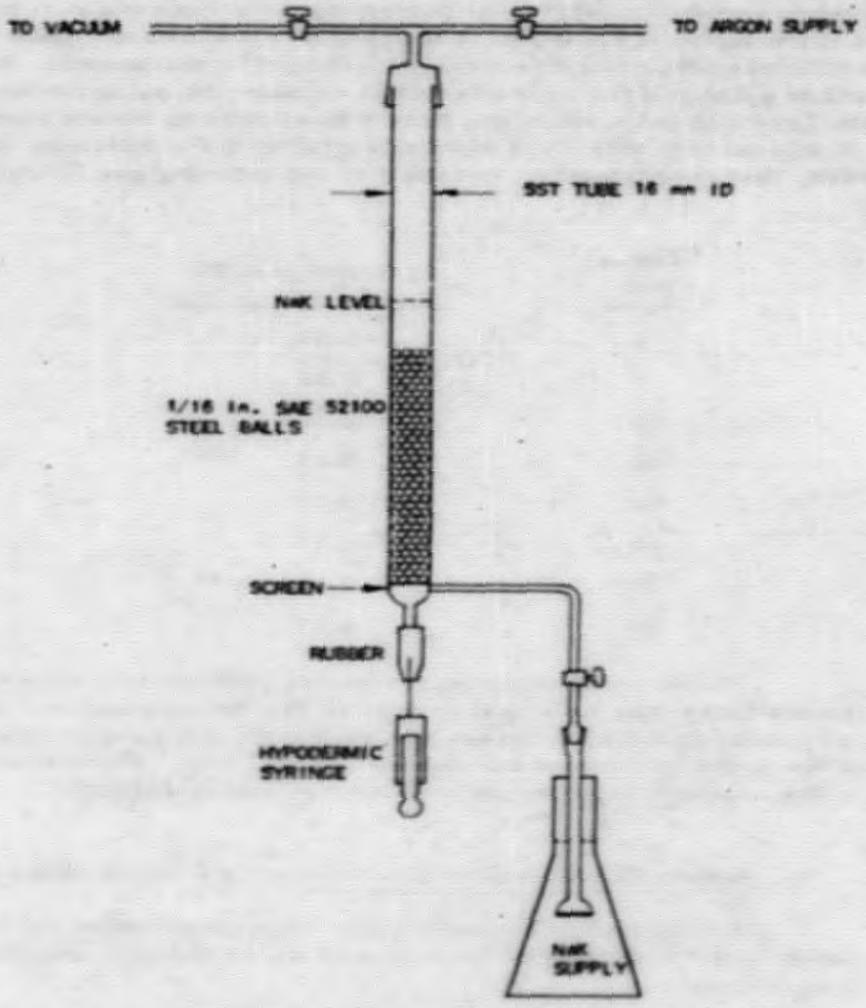

RE-7-11451-A

FIG. 2
APPARATUS FOR DETERMINING GAS ENTRAPMENT IN NaK-STEEL BALL COLUMNS

J. R. FRANKLIN, 7-13-53

balls submerged in liquid sodium. Volumetric measurements with an electric probe are made at regular intervals to determine the volume of gas remaining in the tube at atmospheric pressure. The apparatus is shown in Figure 3. Early tests with AISI type 440C stainless steel balls showed no entrapment. It is not known whether wetting of the balls affects gas entrapment, but in the later experiments with Type 304 balls sufficient time was allowed to insure complete wetting. A typical test with Type 304 balls produced the following averaged data, showing that approximately one-half of the entering gas is trapped in the balls:

Time, min.	cc argon at 600C
0	0.33
5	0.33
20	0.30
40	0.23
50	0.17
60	0.17
70	0.17
80	0.17

These preliminary experiments indicate that with this type of fuel element there may be a real danger of gas entrapment inside the fuel element, assuming that fission gases are generated and escape through the surface of the uranium balls at a sufficiently rapid rate. Future tests will be made using uranium balls in convection-circulating sodium.

6. Xenon Diffusion Through Uranium - J. C. McGuire

Experimental equipment has been constructed and is now in operation to determine the diffusion rate of xenon through uranium at various temperatures.

The test apparatus consists of a uranium membrane, .020 in. thick and 11 sq in. in area, exposed to xenon at atmospheric pressure on one side and to vacuum on the other side at any desired temperature. In test, the exhaust is cut off and the pressure increase caused by diffusion of xenon through the membrane is indicated by a calibrated Pirani gage. The diffusion rate can be calculated from the rate of pressure rise and the volume of the evacuated system.

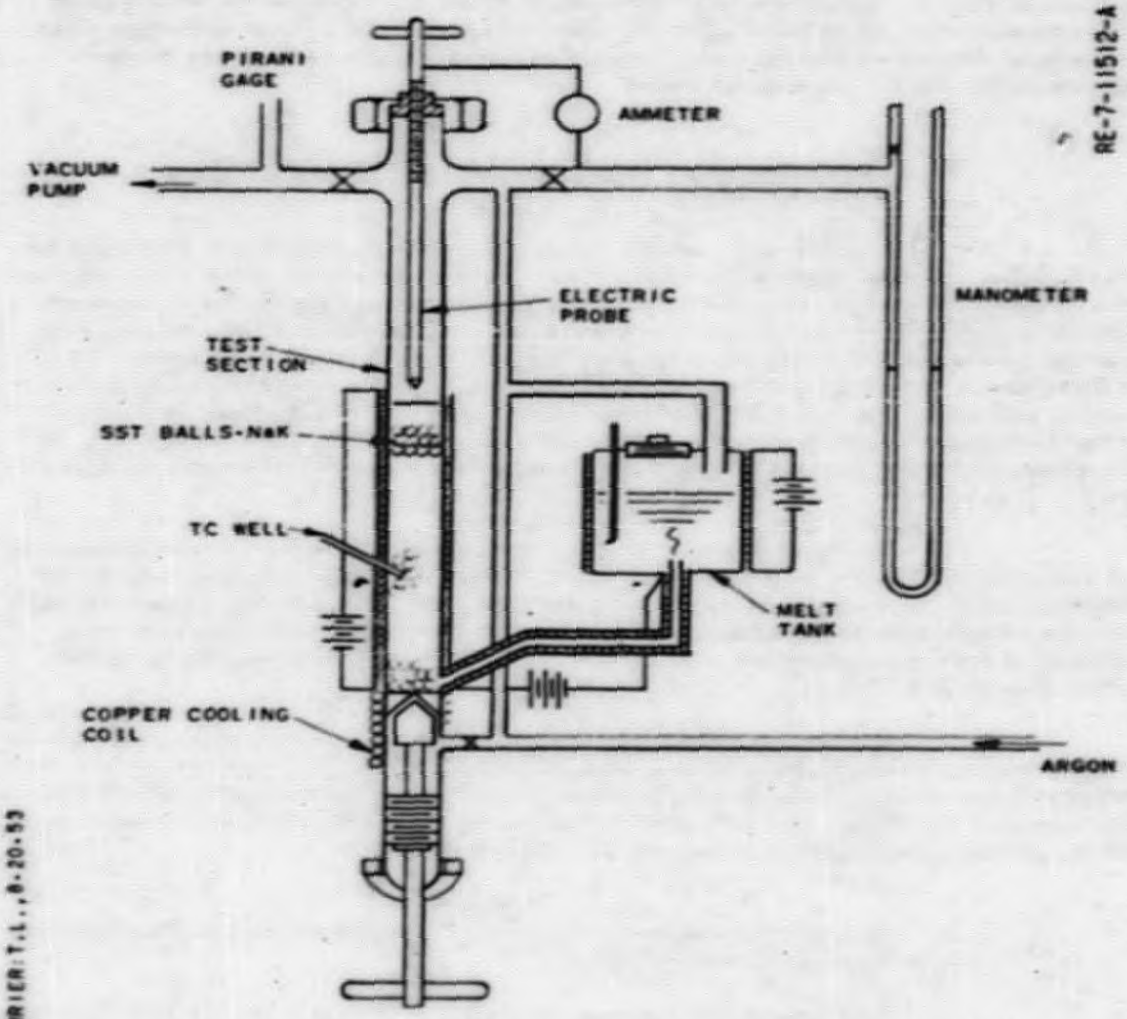

FIG. 3
APPARATUS FOR GAS ENTRAPMENT STUDIES

Preliminary tests with argon showed a significant rise in diffusion rate at temperatures above 450C (842F). Initial tests with xenon at temperatures up to 625C (1157F) showed an extremely low diffusion rate barely in excess of background. Tests in the uranium beta phase range above 660C (1220F) are to be made.

7. Impregnation of UO_2 with NaK by Vacuum Technique
W. A. Neisz

A putty-type of fuel such as a UO_2-NaK mixture that may be extruded or pushed through a reactor has advantages over solid fuel rods in that growth distortion may be overcome and reprocessing of the component materials may be simplified. Consideration of various methods of impregnating powdered UO_2 with NaK led to the choice of vacuum technique. To determine whether UO_2 is wet by NaK, the mixing was performed under an argon blanket. This was done by outgassing the UO_2 and NaK in individual containers in a glass vacuum system and then adding the NaK to the UO_2 by inverting the NaK container. All the experiments were performed in a dry box.

The compounds in their individual containers were outgassed at room temperature to a pressure of 10^{-5} mm Hg. The UO_2 was heated to 300C (572F) and outgassed again to a pressure of 10^{-5} mm Hg. The UO_2 was allowed to cool to room temperature under vacuum and then the NaK was added. Argon was admitted and the UO_2-NaK mixture was heated to about 150C (about 302F).

The mirror-like appearance of the inside of the heated glass container indicated wetting of the container and of the UO_2 powder by the NaK. Microscopic examination under oil also showed that the particles of UO_2 were surrounded by NaK. The UO_2-NaK mixture was successfully extruded from a 30 cc syringe through the enlarged (3/8 in.) exit hole.

8. Sodium Filling and Cleaning of Fast Exponential Experiment Fuel Cans - M. Sivetz

Equipment has been prepared for filling 3 in. by 3 in. by 24 in. fast exponential experiment fuel cans with sodium by drawing up molten sodium into the evacuated cans. For this purpose, a 1/4-inch pipe thread is to be provided in the brazed top cover and in the bottom of the can. The sodium will be removed by reverse-flow, followed by an ethanol rinse at 30C (86F) to remove residual Na and Na_2O. It is planned to use this procedure on 64 fuel cans per month throughout the course of the experiment.

9. Physical and Mechanical Properties - A. E. Dwight

The thermal conductivity of a uranium-15% plutonium alloy after 2-1/2 weight per cent of the plutonium has been burned up has been calculated to vary between 0.04 cal/(cm)(sec)(C) at 100C to 0.06 cal/(cm)(sec)(C) at 600C.

Measurements have been made of the thermal conductivity of Type 440C stainless steel balls in liquid sodium. The experimentally determined conductivities vary up to 20% higher than those calculated from Tareevs' equation. The latter equation, in the form applicable to spheres in a homogeneous medium is

$$k_{avg} = \frac{2+n+2e(n-1)}{2+n-e(n-1)}$$

where e is the volume concentration of sphere material and n is its thermal conductivity relative to that of the medium.

10. Thermal Stability Tests - W. S. Fagan

An apparatus for high temperature thermal cycling (Figure 4) has been built to study the behavior of fuel element materials under temperature changes. The temperature cycling is accomplished by moving the sample from a region containing hot eutectic lead-bismuth alloy to a region containing colder alloy, while controlling the holding time in each environment and the transit time between environments.

The sample, welded into a NaK-filled cold-rolled carbon steel capsule attached to a Type 347 stainless steel rod, is moved up and down in a vertical pipe filled with molten lead-bismuth alloy. Large diameter sections at the top and bottom ends of the pipe provide the necessary heat capacity. A helium blanket prevents oxide formation at the gas-liquid interface.

The samples are uranium cylinders prepared by a powder metallurgy technique with resultant random orientation. One sample, cycled 400 times from 200C (392F) to 600C (1112F), showed no change in visual appearance and small dimensional change. Another sample cycled 400 times from 200C (392F) to 725C (1337F) showed considerable growth, distortion, and deterioration. A sample cycled from 200 C (392F) to 825C (1517F) has not been inspected.

Build-up of alloy on the rod as it leaves the liquid and enters the gas results in a very great increase in the diameter of the rod and a reduction of the liquid level. A redesigned apparatus is being built to overcome this difficulty and to allow 24-hour unattended operation.

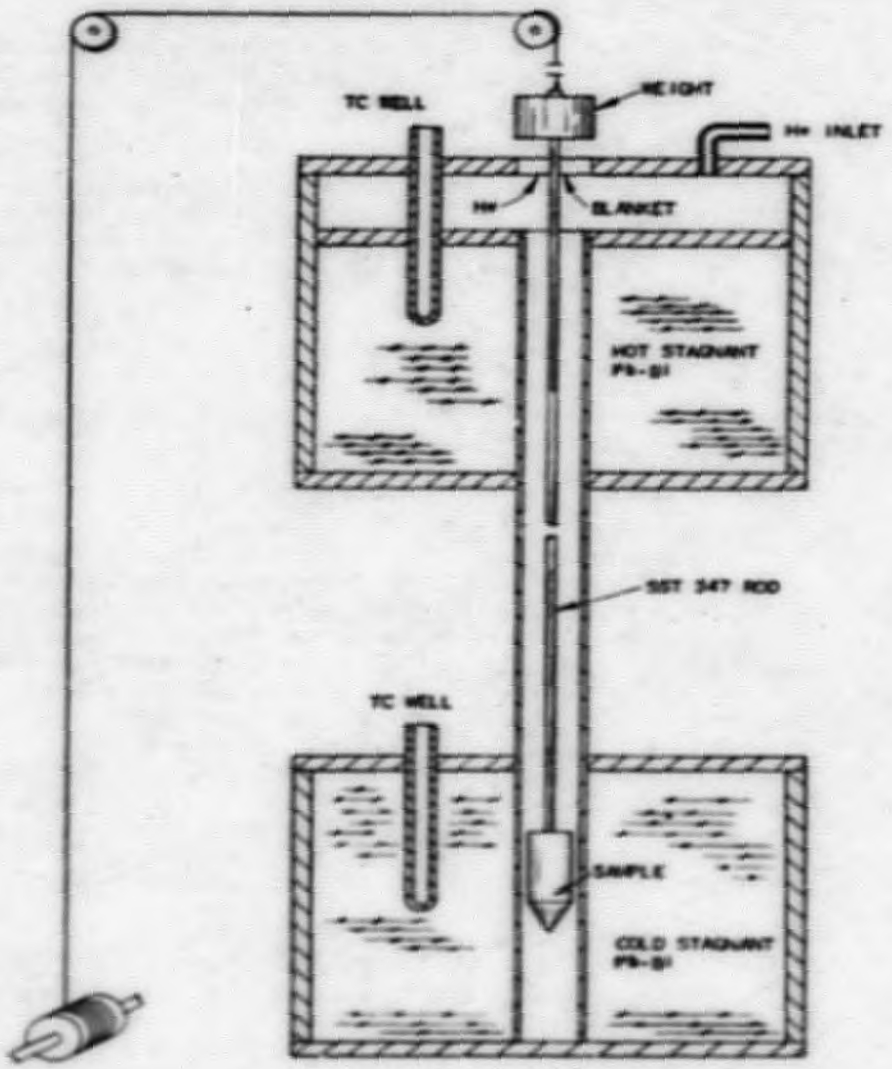

RE-7-11450-A

FIG. 4
SCHEMATIC OF LEAD-BISMUTH
THERMAL CYCLING APPARATUS

D. Reflector and Structural Materials

Mass Transport - C. H. Scheibelhut

Much additional information is required on the causes and extent of mass transport and redeposition of containing materials and their corrosion products in liquid metal systems at high temperature. It is intended initially to investigate the behavior of liquid sodium systems, both dynamic and static, employing containing material of stainless steel and maximum temperatures of 400 to 800C (752 to 1472F).

A dynamic system (loop) of Type 347 stainless steel has been designed and is under construction. A schematic drawing of this loop is shown in Figure 5. The main components are a high temperature (heat input) section, a low temperature (heat removal) section, a surge tank, an electromagnetic pump, a flow rate control valve, and an electromagnetic flowmeter, through which the circulating sodium flows in the order named. Auxiliaries include a secondary liquid metal-to-air heat exchanger system for dissipating the heat extracted from the low-temperature section, and a bypass filtering system for removing sodium oxide from the circulating sodium when operating at 100 to 110C (212 to 230F).

The high temperature section consists of a three-foot length of 0.25 in. OD, 16 gage (0.065 in. wall thickness) stainless steel tubing through which electric current is passed longitudinally to effect the desired heat input. The design heat input is zero to 12 kw, sufficient to provide a maximum sodium temperature rise from inlet to outlet of about 200C (392F) at a sodium velocity of 25 fps. The low-temperature section consists of a removable five-foot length of 0.50 in. OD, 16 gauge tubing positioned concentrically inside a two-inch pipe. Sodium-potassium alloy flowing through the annulus and through a fintube heat exchanger in the secondary system dissipates the heat to air. At present, all the loop components are available and welding has been completed on some parts, such as the surge tank, the adapter elbows, and the heat exchanger tee ends.

Apparatus for study of the transport of radioactivity from stainless steel under static conditions in liquid sodium with various impurities and temperatures is also being built. The test sample (2-in. length of irradiated 1/8 in. OD stainless steel tubing and a similar unirradiated piece) are placed in a 7-in. long, 1 in. OD, 16 gage stainless steel tube c' sed at one end and connected to a 3/8 in. OD copper tube at the other e .or evacuating and filling. A schematic of the apparatus is shown in Figure 6. Sodium is distilled into the tube under vacuum and the tube is sealed and placed in a pyrometer-controlled furnace. The transport of activity is to be determined by radiochemical methods.

C.H.SCHEIBELHUT:E.K.,7-13-53

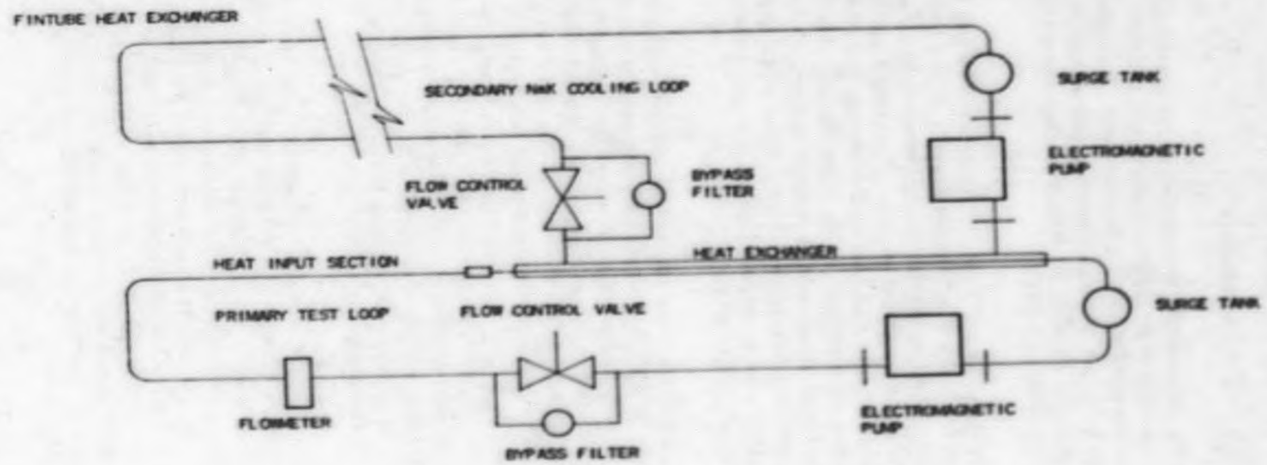

FIG. 5
SCHEMATIC OF DYNAMIC LOOP
FOR MASS TRANSPORT STUDIES

RE-7-11453-A

C.H.SCHEIBELHUT:E.K.,7-13-53

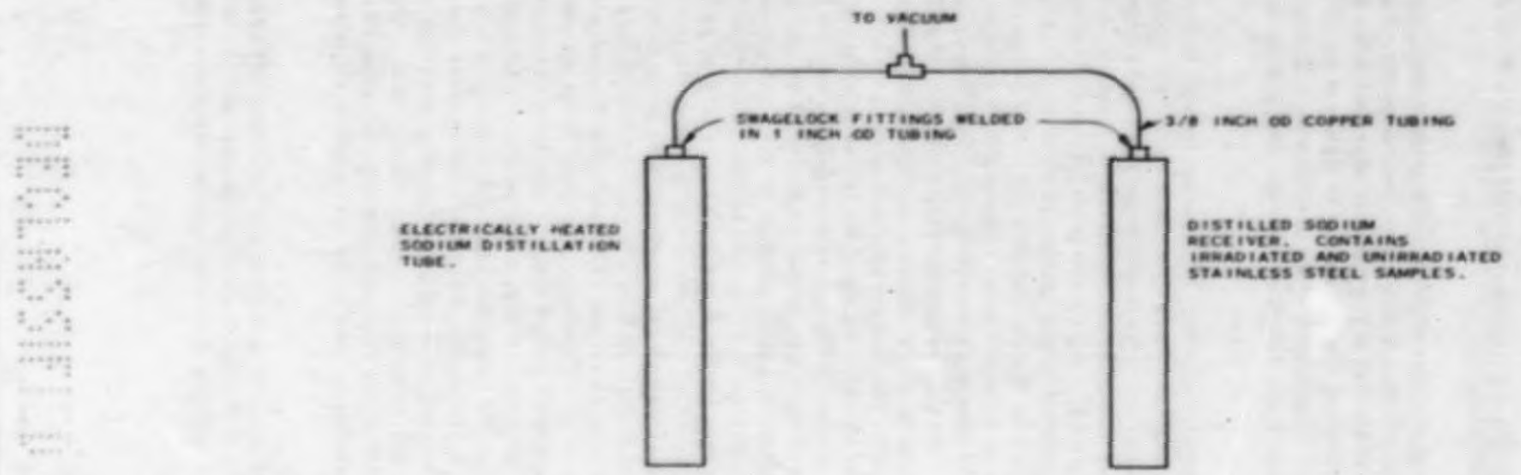

FIG. 6
SCHEMATIC OF APPARATUS FOR STUDY OF TRANSPORT OF RADIOACTIVITY UNDER STATIC CONDITIONS

RE-7-11452-A

E. Reactor Coolant, Heat Transfer and Power Generation

1. Sampling and Analysis of Liquid Metals - W. C. Dzombak, J. R. Humphreys

The occurrence of corrosion in a liquid metal coolant system is dependent upon the presence of impurities, such as oxides, in the coolant. Knowledge of the concentration of impurities is important in the operation of any liquid metal system and is also required in studies of the purification of alkali metal coolants. The purpose of the present work is to provide adequate methods and facilities for the sampling, analysis, and purification of liquid metal coolants.

A portable apparatus has been constructed to facilitate the removal of samples of alkali metals from static or dynamic experimental systems. The sample is delivered at the temperature of the liquid metal system into evacuated metal or glass receivers. A schematic of the apparatus is shown in Figure 7. Liquid metal is forced into the evacuated sampling apparatus by the pressure existing in the liquid metal system. The sample flows from the system through a 1/8 in. OD stainless steel capillary delivery tube, through a bellows-sealed needle valve, and through an additional length of steel capillary tubing which terminates inside an evacuated chamber. The bellows-sealed needle valve and the entire sample delivery line are heated to a temperature equal to or greater than that of the liquid metal system. The delivery tube is located on the axis of a flexible metal bellows welded to the top of the vacuum chamber of the sampling apparatus. Evacuation of the apparatus causes the bellows to collapse and the delivery tube to move 3 in. toward the bottom of the vacuum chamber. As the bellows collapses, it is tilted manually to direct the delivery tube into one of the sample receivers. The collapsed bellows comes to rest on a metal collar holding the bellows and the delivery tube in an inclined position aligned with a sample receiver. As the bellows is displaced vertically, the end of the delivery tube passes through one of several holes in the bottom of the vacuum chamber, and through the bore of a stopcock connecting a glass or metal sample receiver to the vacuum chamber. After discharge of some liquid metal into the receiver, inert gas is admitted to the apparatus to permit the bellows to expand and the sample delivery tube to be withdrawn from the stopcock bore. The stopcock is closed either before or after subsequent evacuation of the apparatus so that the liquid metal specimen is sealed in an inert atmosphere or under vacuum. Since four receivers are connected to the bottom of the vacuum chamber, the delivery line may be flushed and three samples obtained without allowing air to enter the apparatus. Vacuum leaks have been eliminated from the all-metal assembly; the apparatus will be subjected to sampling tests as soon as the vacuum pump and accessories have been mounted.

Since it would be desirable to have sampling equipment permanently connected to each liquid metal experimental facility, an inexpensive and easily duplicated sampling apparatus has been designed which, it is hoped,

RE-6-11120-1

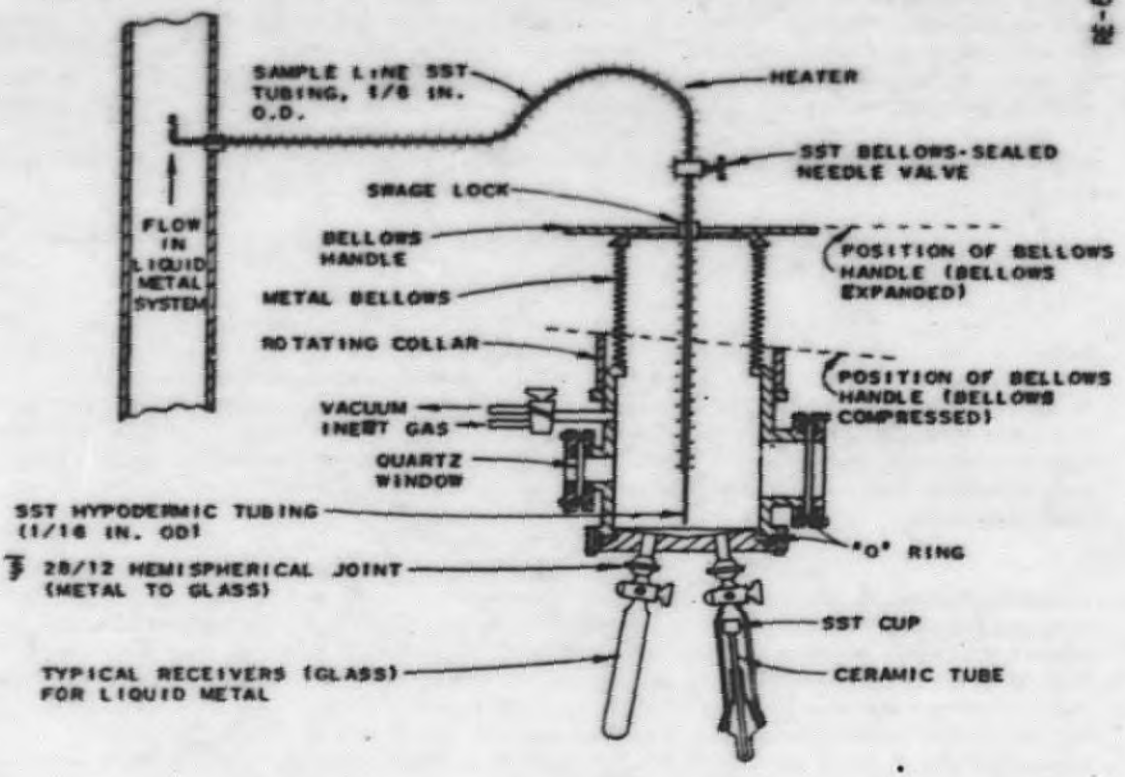

FIG. 7
PORTABLE LIQUID METAL SAMPLING APPARATUS

R.C.DZOMBAK:H.C.:6-10-53

may be used to replace the portable unit. In the alternate design, now under construction, the costly bellows is replaced by a piston moving in two "O" rings which permit vertical displacement and rotation of the piston and sample delivery tube.

The accepted procedures for the chemical analysis of alkali metals have been reviewed and steps taken to procure the apparatus and chemicals needed. For the determination of the oxygen content of alkali metal samples, two methods of analysis will be available: the amalgamation method, in which mercury separates liquid metals from the oxides; and the Wurtz method, in which liquid metal, but not the oxide, reacts with an organic halide. In addition, an attempt will be made to employ vacuum distillation with induction heating to effect a quantitative separation of liquid metal from the oxide.

2. Heat Transfer Analysis - L. L. Kintner, J. B. Reynolds, W. R. Simmons

Three types of fuel elements for the reference design reactor were analyzed to establish the highest permissible coolant temperatures attainable with each type for an assumed maximum fuel element temperature limitation. The effect of velocities and geometry different from the reference design was determined for the flat plate-type. The other two types analyzed were tubes containing (1) a mixture of fuel alloy particles and sodium, and (2) seven fuel alloy pins with voids between the pins filled with sodium.

The reference reactor design[3] was used as a base for comparison of these fuel elements. Where the core geometry was changed, the core power (500 mw) and the core volume (600 liters), and hence the power density, were maintained constant. The maximum to average heat flux was assumed to be 1.45 in all cases, and constant coolant temperature rise through all sections of the reactor was assumed. The physical properties of the sodium coolant were assumed constant at 760F (thermal conductivity = 41.2 Btu/(hr)(ft)(F); specific heat = 0.305 Btu/(lb)(F); density = 53.2 lb/cu ft). The film coefficient was assumed to be one-half of the value computed from Martinelli's theoretically predicted value for flat plates.[4] For the flat plate-type element the transformation temperature of the fuel alloy (1202F) was assumed to be limiting, while for the other two types the boiling point of the stagnant sodium bond at atmospheric pressure (1612F) was assumed to be limiting. A sketch of the three types of fuel elements is shown in Figure 8.

---

[3]Reactor Engineering Division Quarterly Report, ANL-5012, March 15, 1953.

[4]Liquid Metals Handbook, NAVEXOS - P-733 (Rev.), June, 1952, p. 207.

L.L.KINTNER: J.B.REYNOLDS. T.L.7-13-53

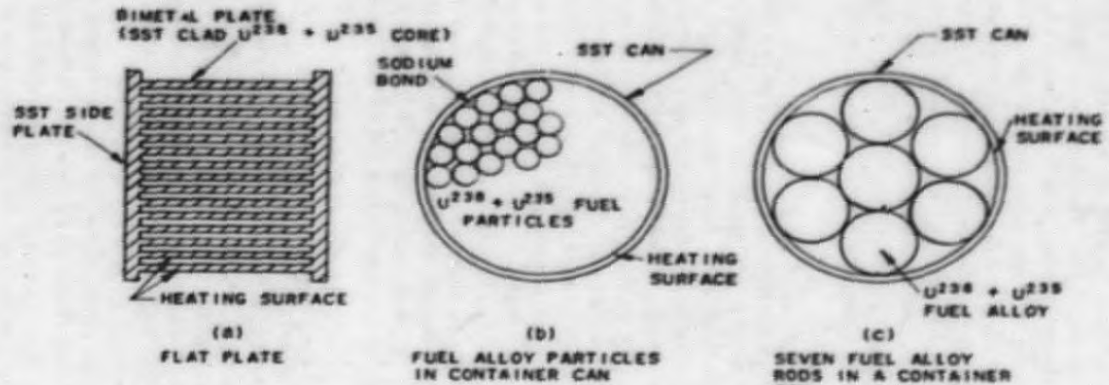

(a) FLAT PLATE

(b) FUEL ALLOY PARTICLES IN CONTAINER CAN

(c) SEVEN FUEL ALLOY RODS IN A CONTAINER CAN

FIG. 8
SCHEMATIC OF FUEL ELEMENTS USED FOR HEAT TRANSFER STUDIES

RE-7-11449-A
ANL-ASJ-11449

a. Flat Plate-Type Fuel Element

The highest coolant temperatures permissible with the flat plate-type element were calculated for a range of velocities from 20 to 40 fps, fuel plate thicknesses from 0.075 in. to 0.105 in. and length to diameter ratios of the active core from 0.7 to 1.0. The core composition was held constant at the reference design composition of 55% coolant, 15% stainless steel structural material, and 30% fuel alloy (volume per cent). The thermal conductivity of stainless steel and fuel alloy were assumed to be 16 and 16.5 Btu/(hr)(ft)(F), respectively. Hot spot factors to allow for deviations in subassembly dimensions, heat flux distribution, and flow distribution, were included in the calculation of maximum core alloy temperatures. The total factor on the over-all temperature difference from the maximum uranium temperature to the inlet coolant temperature was 1.34.

The results of the analysis are given in Figures 9 to 14. Figures 9 to 11 inclusive, show the effect of the variables on the inlet coolant temperature for a core power output of 500 mw. Reference conditions indicated in the figures refer to the preliminary reference design plate thickness of 0.075 in., maximum coolant velocity of 25 fps, and length to diameter ratio of the active core of 1.0. Since an increase in coolant temperature results in higher permissible steam pressures and superheat, and therefore higher thermal efficiency, it is desirable to have coolant temperatures as high as possible. From Figures 9 to 11, it is seen that increasing the coolant velocities has the greatest effect on increasing coolant temperatures for the range of variables considered. Increasing the plate thickness while holding core volume and composition constant decreases the inlet temperature and is therefore not desirable. Decreasing the plate thickness for constant core volume and composition below 0.075 in. would result in clad thicknesses less than 0.007 in. and may increase problems of fabrication and decrease the rigidity of the fuel plate.

The effect of increasing velocity on pressure drop through the reactor core is shown in Figure 12. The preliminary reference velocity of 25 fps was selected because of insufficient data on corrosion at higher velocities. However, if corrosion is not appreciable at higher velocities, it is possible that coolant velocities greater than 25 fps could be used, since even at 40 fps the pressure drop is not untenable (Figure 12).

Increased velocity at constant core coolant volume results in greater total weight rate of flow (Figure 13). At reference conditions four external circuits, consisting of 12 in. (nominal) pipe will handle the total flow of 15,400,000 lb/hr with an estimated total circuit pressure drop of 70 psi. Increasing the velocity to 35 fps at an L/D of 1.0 increases the total flow rate to 21 500,000 lb/hr. However, by increasing the external pipe circuits to 16 in. nominal size, the estimated circuit pressure drop is 76 psi. Thus the increased flow rate may be partially compensated for by increasing the external circuit pipe diameter.

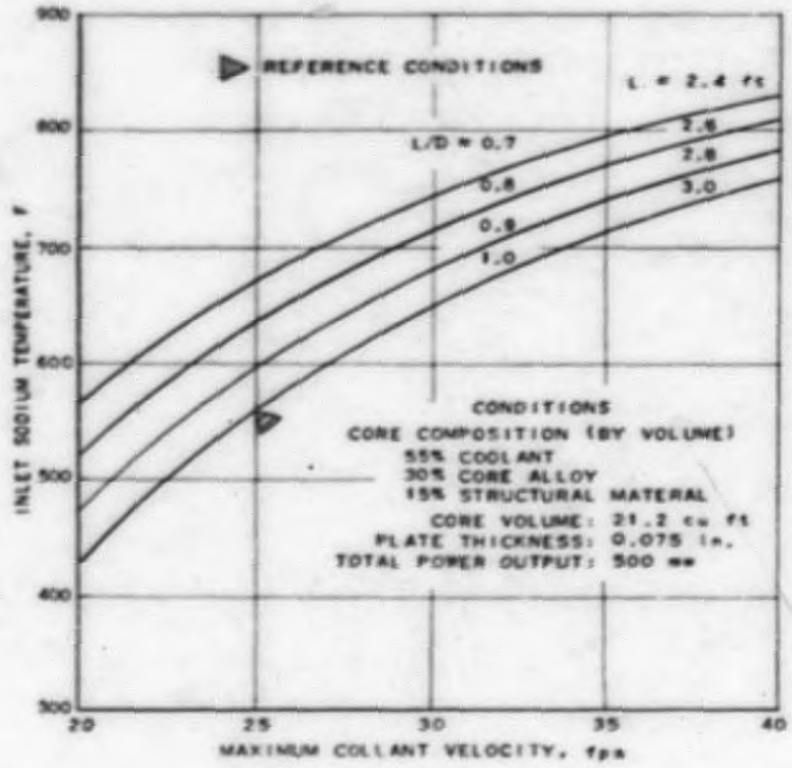

FIG. 9
EFFECT OF COOLANT VELOCITY AND REACTOR CORE L/D ON INLET SODIUM TEMPERATURE

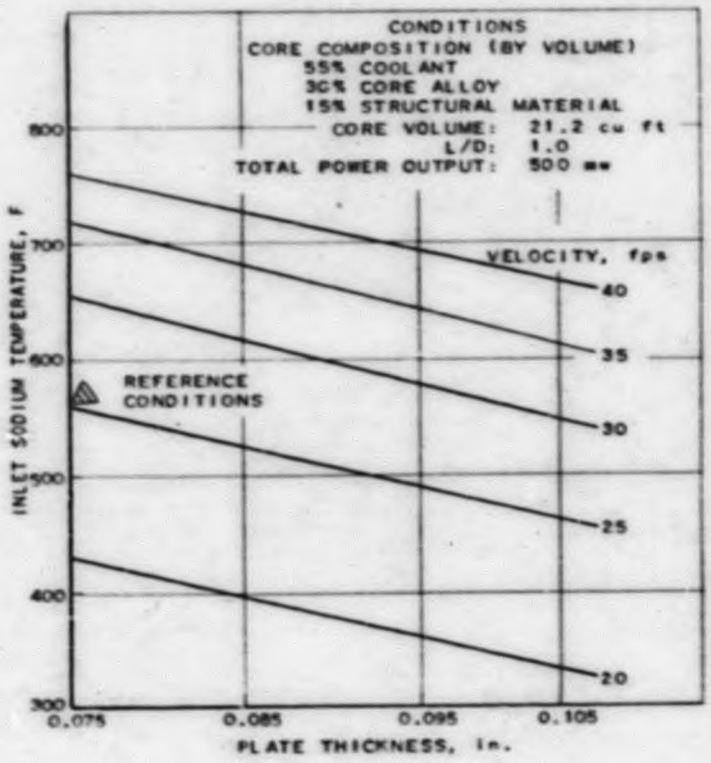

FIG. 10
EFFECT OF PLATE THICKNESS AND COOLANT VELOCITY ON INLET SODIUM TEMPERATURE

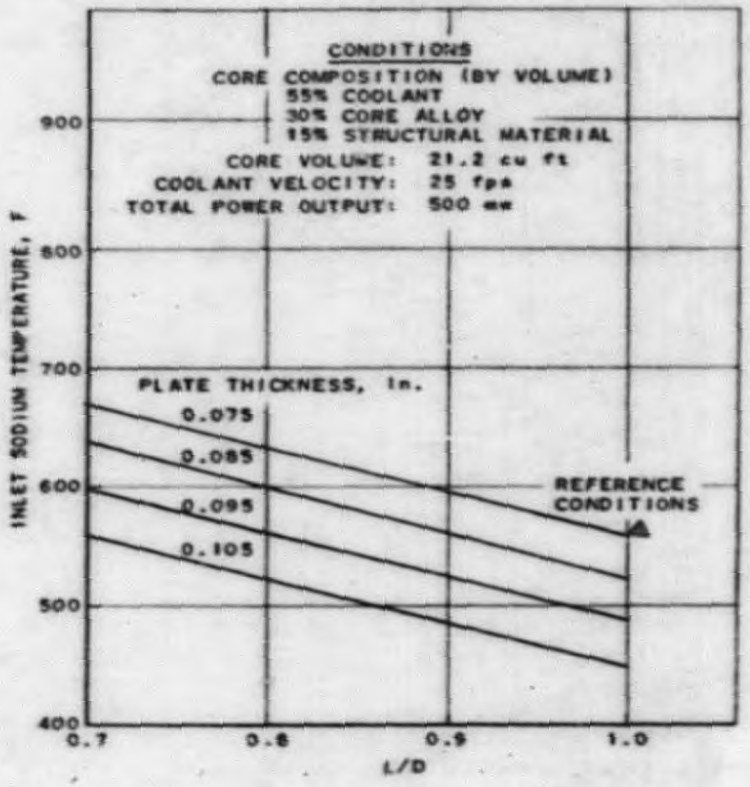

FIG. 11
EFFECT OF REACTOR CORE L/D AND PLATE THICKNESS ON INLET SODIUM TEMPERATURE

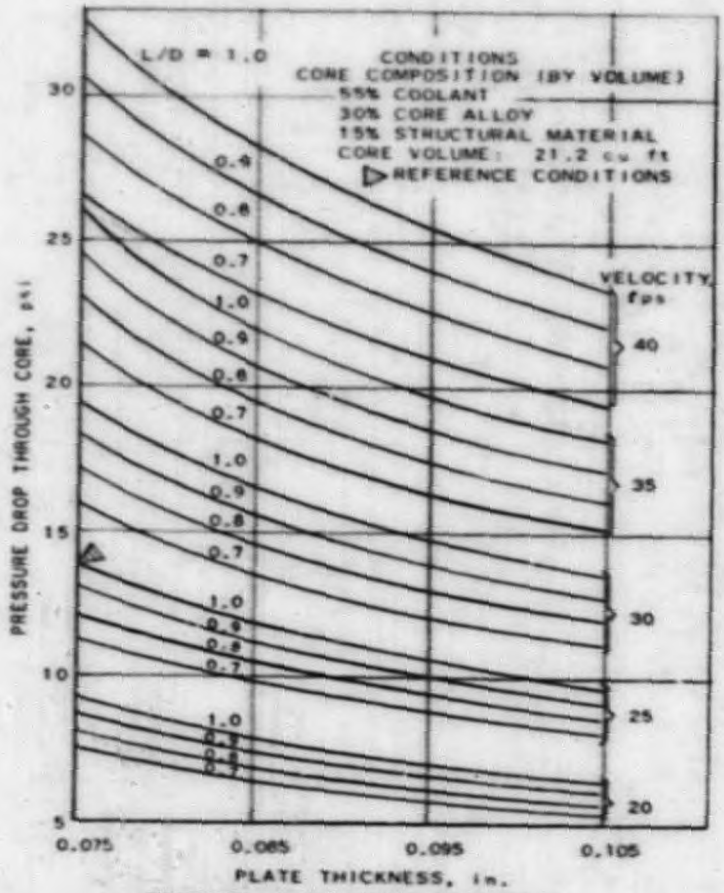

FIG. 12
EFFECT OF COOLANT VELOCITY, PLATE THICKNESS, AND L/D ON PRESSURE DROP THROUGH CORE

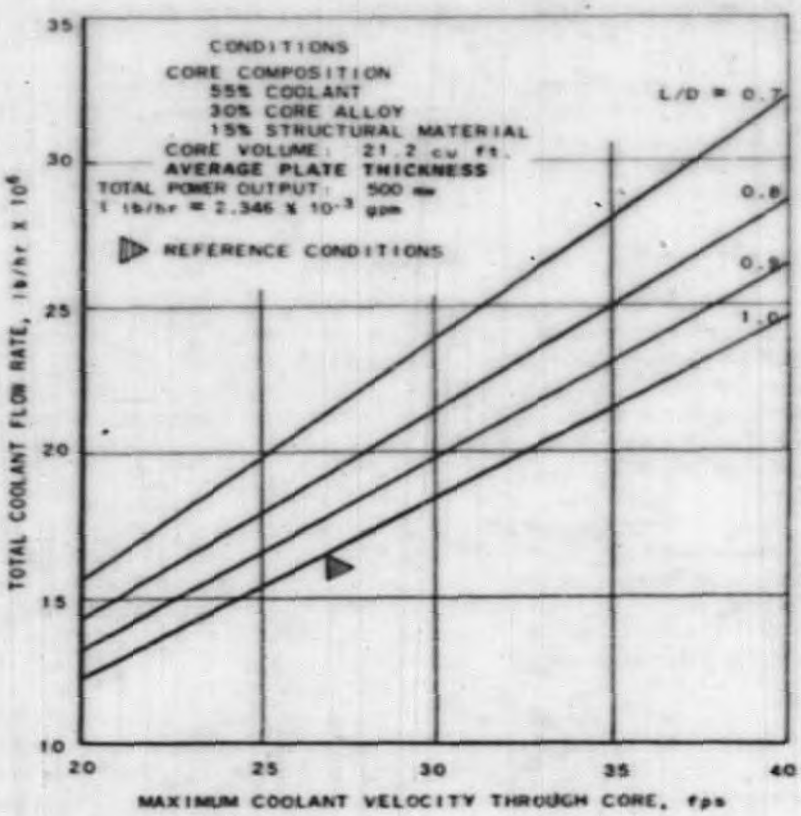

FIG. 13
EFFECT OF COOLANT VELOCITY AND REACTOR CORE L/D ON TOTAL COOLANT FLOW RATE

Increasing the velocity at constant core composition and volume may be accomplished without increasing the critical mass requirements. However, decreasing the L/D ratio would increase the critical mass. Therefore the gain in efficiency of the steam cycle is offset somewhat by the decrease in specific power and the advantages obtained by reduction of L/D will not be as large as the thermal analysis indicates when the fuel requirements are considered.

The temperature rise of the coolant for various flow rates is given in Figure 14. As the coolant temperature rise increases, the problems in designing the system to avoid thermal shock accompanying a sudden power cutoff become greater. For the present, temperature rises up to 400F have been considered feasible.

b. Ball-Type Fuel Element

The ball-type fuel element, as shown in Figure 8 (b), consists of fuel alloy particles, 1/16 in. diameter or less, packed in a stainless steel tube. The interstices are filled with sodium which serves as a heat transfer medium. The assembly is cooled by sodium flowing on the outside of the container tube. The assemblies are arranged in the core on an equilateral triangular pitch to give the desired coolant volume in the active core (3 ft diameter by 3 ft high).

The variables in this analysis were the size of the container tube (1/4 in. to 3/8 in. inside diameter), the per cent of core volume allotted to sodium coolant (35 to 55 per cent), the per cent of the container tube volume allotted to fuel alloy (60 to 80 per cent), thermal conductivity of the fuel alloy (10 to 23.2 Btu/(hr)(ft)(F)), and the heat transfer medium used inside the container tube (Na or NaK).

The stainless steel tube wall was assumed to be 0.020 in. thick in all cases. The coolant velocity was maintained constant at 25 fps and the inlet coolant temperature was assumed to be 560F. Uniform heat generation in the mixture of fuel and sodium in the container tube was assumed.

The results of the analysis are given in Figures 15 to 19. Figure 15 shows the apparent thermal conductivity of the mixture of fuel alloy particles and liquid sodium inside the tube, assuming the heat transferred by convection of the liquid metal is negligible. Figure 16 shows the temperature drop through the fuel alloy - liquid metal mixture for the range of variable covered. Since this temperature drop is large, the effect of thermal conductivity of the fuel alloy and the method of computing apparent conductivity has an appreciable effect on the reactor performance. The method used was the one described by Jakob[5] which gives values that lie in between the upper limit obtained by assuming the resistances of liquid metal and fuel alloy are in layers parallel to the heat flow and the lower limit obtained by assuming that these layers are perpendicular to the heat flow.

[5] M. Jakob, "Heat Transfer," Vol. I, p. 85.

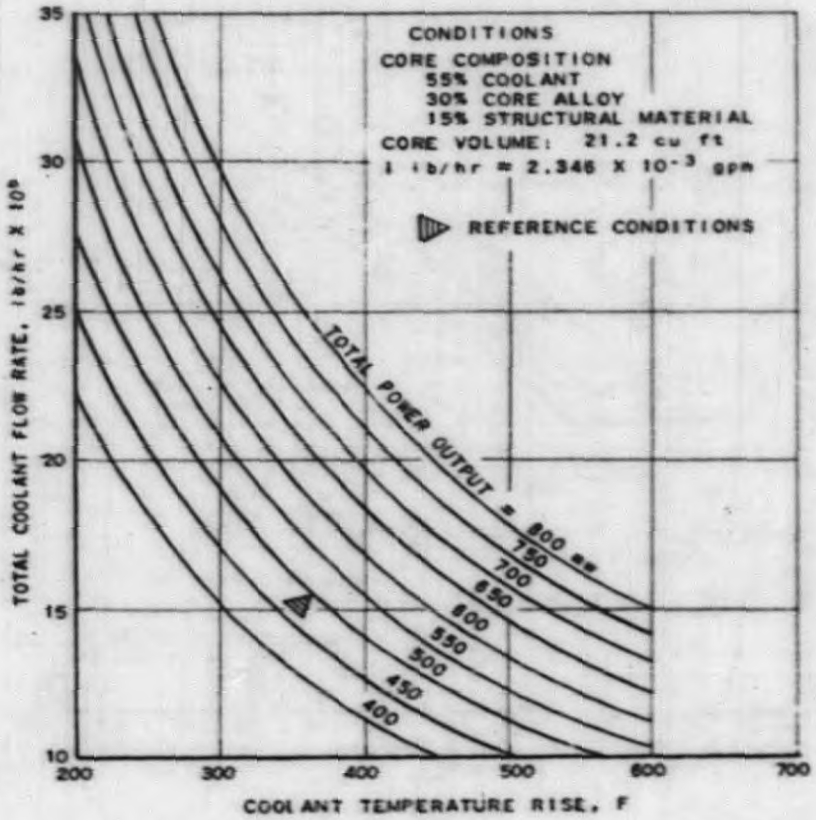

RE-7-11454-A

FIG. 14
COOLANT TEMPERATURE RISE AS A FUNCTION OF TOTAL FLOW RATE AND TOTAL POWER OUTPUT

J.B.REYNOLDS & L.L.KINTNER:T.W.L.,7-13-63

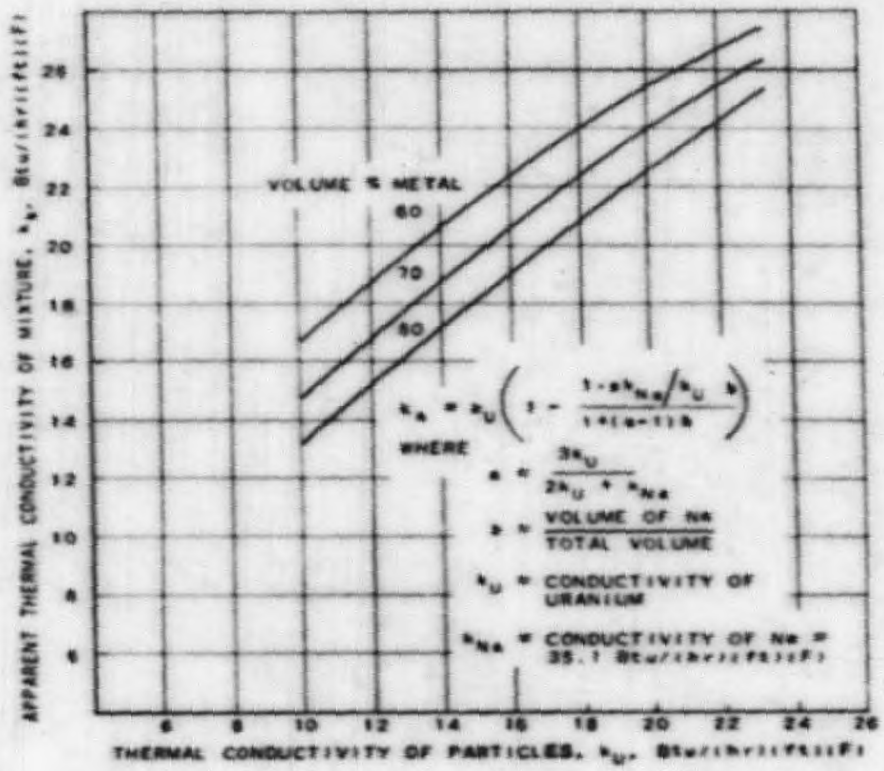

FIG. 15
APPARENT THERMAL CONDUCTIVITY OF A MIXTURE OF URANIUM PARTICLES IN SODIUM

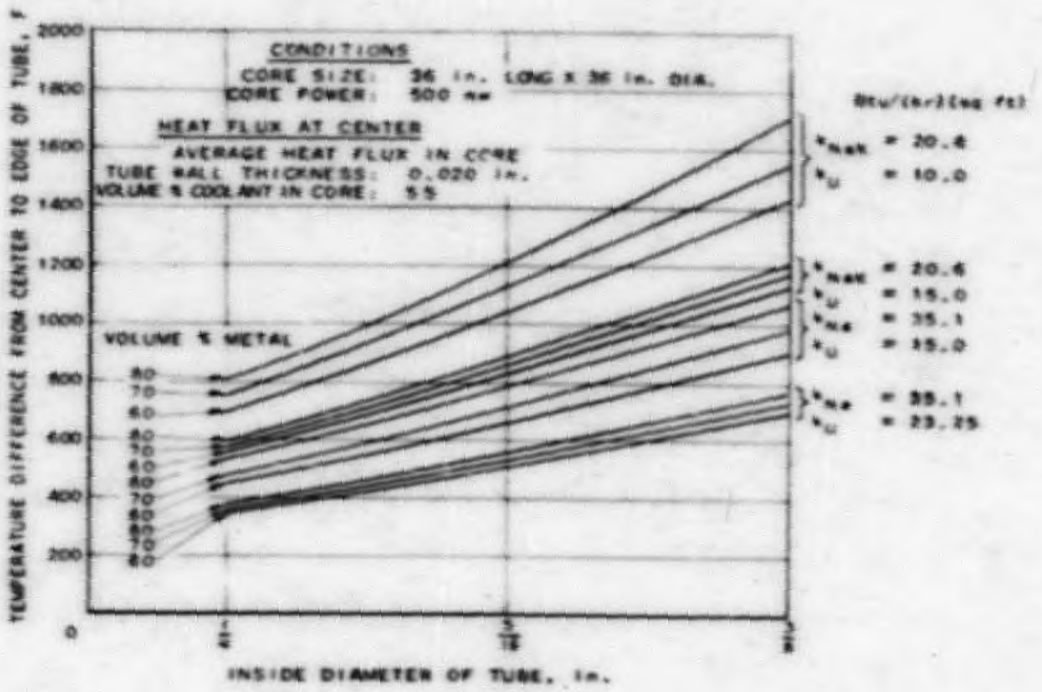

FIG. 16
TEMPERATURE DROP THROUGH FUEL TUBE
(BASED ON APPARENT THERMAL CONDUCTIVITY)

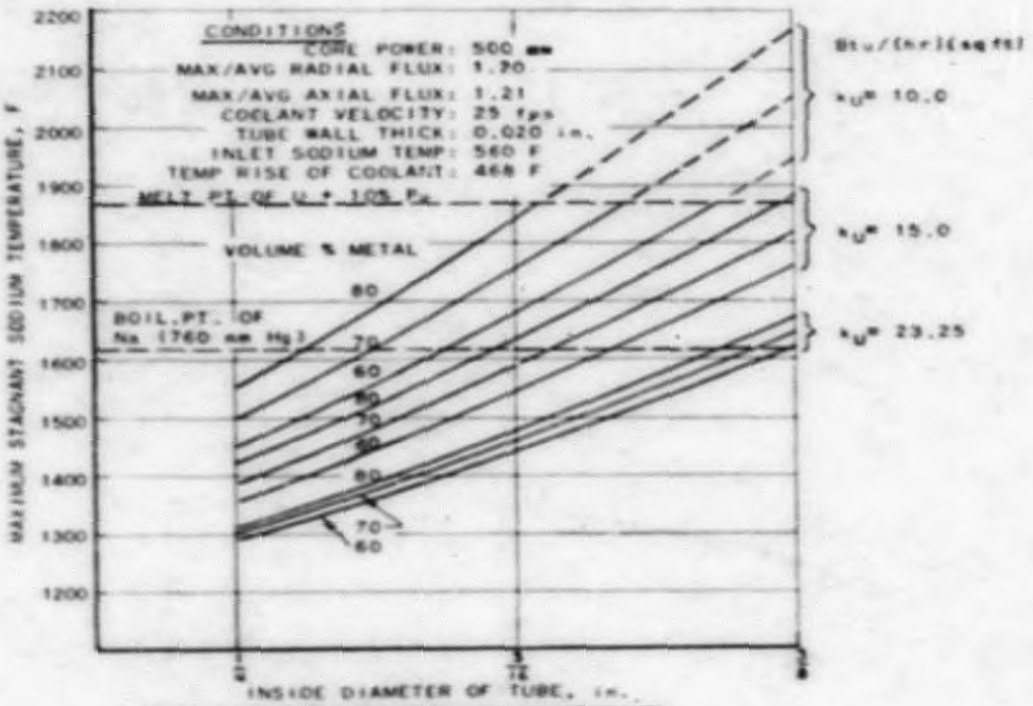

FIG. 17
MAXIMUM SODIUM TEMPERATURE
INSIDE OF FUEL ELEMENT FOR
35 VOLUME PER CENT COOLANT SODIUM

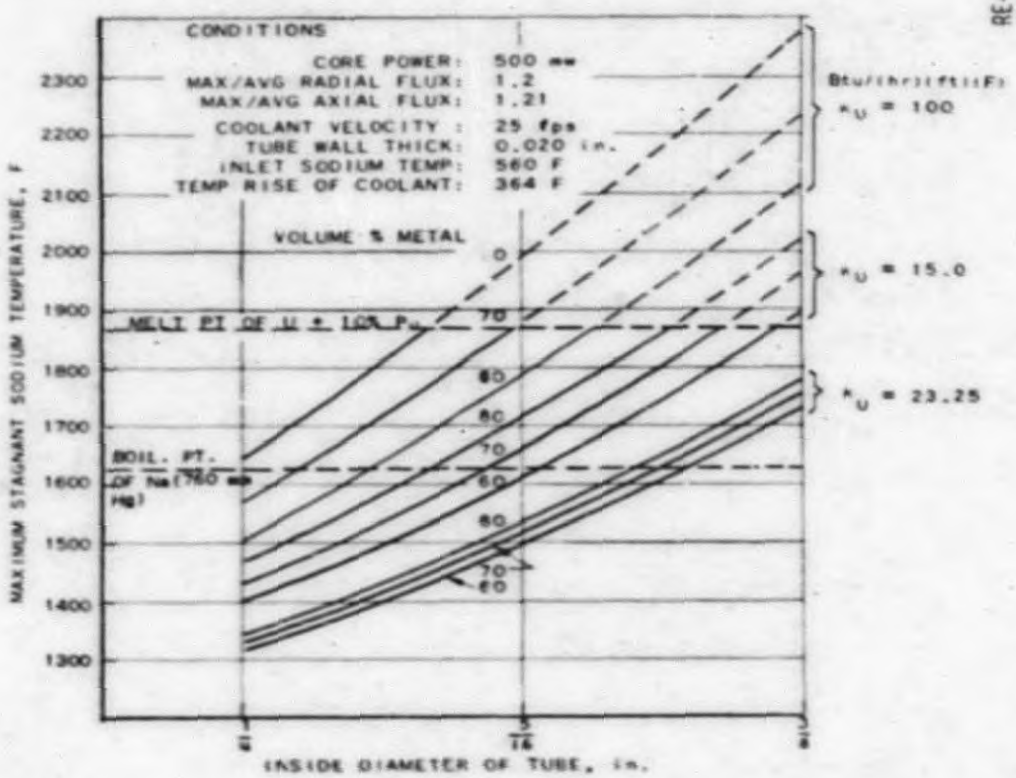

RE-7-11498-A

L.L.KINTNER:T.W.L.,8.18.53

FIG. 18
MAXIMUM SODIUM TEMPERATURE INSIDE OF FUEL ELEMENT FOR 45 VOLUME PER CENT COOLANT SODIUM

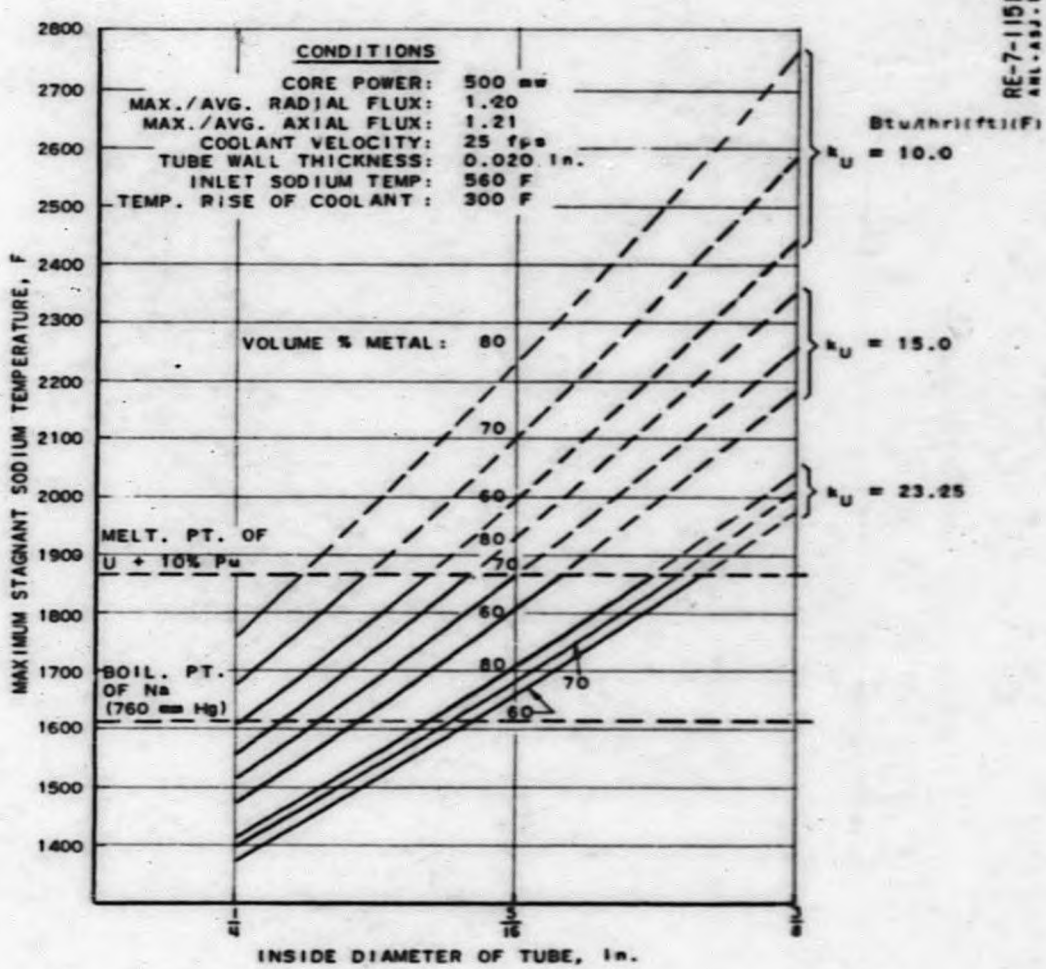

L L.KINTNER:T.L.,8-21-53

FIG. 19
MAXIMUM SODIUM TEMPERATURE INSIDE OF FUEL ELEMENT FOR 55 VOLUME PER CENT COOLANT SODIUM

Figures 17, 18, and 19 show the maximum calculated sodium temperature inside of the fuel element for coolant volume of 35, 45, and 55%, respectively. The boiling point of sodium at 760 mm Hg abs. pressure (1621F) is indicated as a possible limit for the maximum stagnant sodium temperature, since boiling of the sodium would generate vapor bubbles thus decreasing the apparent conductivity of the mixture and increasing the temperatures. Another possible limit would be the melting point of the fuel alloy (estimated at 1870F), assuming that the tube could be pressurized to a few atmospheres to prevent sodium boiling.

The packing of the fuel alloy in the container tubes is approximately 60% if the particles are not plastically deformed under pressure. The thermal conductivity of the fuel alloy, especially after it has been in the pile for some time and contains fission products, is not known. The thermal conductivity of 85% U^{238} - 15% Pu has been estimated as 14 Btu/(hr)(ft)(F) at 1500F. Assuming that the boiling point of sodium at atmospheric pressure is the limiting temperature in the fuel element, Figure 18 shows that a container tube 5/16 in. ID with an inlet temperature of 560F, satisfies this condition. The temperature rise of the coolant is 364F with 45% of the core volume allotted to coolant. Thus, the ball-type fuel element with a limiting temperature of 1621F gives reactor performance comparable to the reference plate-type fuel element with a limiting temperature of 1202F. The reason for this is the thicker fuel element in the tubular element with a longer heat flow path and correspondingly higher temperature difference through the element.

The volume per cent stainless steel in the reactor for the 5/16-inch container tube and 45% coolant volume mentioned above is 11.6%. This leaves 26% of the core volume for fuel alloy and 17.4% of the core volume for stagnant sodium inside the container tubes.

c. Pin-Type Fuel Element

The pin- or wire-type fuel element is similar to the ball-type element except the fuel alloy is in the form of seven pins in the container tube. Theoretically, this arrangement provides 77.8% of the tube volume in fuel alloy. Therefore, the temperatures in this type of fuel element are comparable to the 80% packing of the ball-type fuel element.

The assumptions for the analysis of this element are essentially the same as for the ball-type element. The fuel element temperatures were obtained from a Teledeltos electrical analog, which was designed by members of the Heat Engineering Section of the Reactor Engineering Division. The analogue model was made for a 3/8 in. ID tube of 0.020 in. wall thickness containing seven 1/8 in. diameter fuel alloy pins. The void space between the pins was assumed to be filled with sodium.

The temperatures obtained from the analog are subject to the following conditions and assumptions:

(1) Two dimensional heat flow (no flow axially along the fuel element).

(2) Constant thermal conductivity of the materials in the fuel element as given below:

	Btu/(hr)(ft)(F)
Sodium	35.2
Fuel Alloy	11.7
Stainless steel	11.7

(3) No convection occurs in the sodium.

(4) No contact resistance between any mediums.

(5) Uniform heat generation over the cross section of the uranium fuel pins.

(6) A uniform heat transfer coefficient around the surface of the tube of 15,000 Btu/(hr)(sq ft)(F).

A plot of the isothermal pattern in the 3/8 in. ID fuel element is given in Figure 20 for 35% coolant volume. The temperatures indicated are the temperatures in excess of the coolant temperature at the center of the reactor. The heat liberation in the fuel element at the center of the reactor is 169,000 Btu/(hr)(ft of length). From Figure 20, the maximum stagnant sodium temperature is 1240F above the coolant temperature and the maximum fuel alloy temperature is 1380F above the coolant temperature. This plot shows that the heat from the center fuel pin tends to go between the outer fuel pins at their points of contact. However, once beyond this heat barrier, the heat flow spreads out through the sodium. This is assisted by the stainless steel tube wall. Since the thermal conductivity of the tube wall is lower than the sodium, the tube wall serves as a heat barrier and the heat flows preferentially through the sodium. This reduces the heat flux variation along the surface of the tube. The greatest surface heat flux and correspondingly the maximum film temperature difference occurs on a line with the center of the tube and the point of contact between two outer fuel pins.

Since the temperature pattern in the fuel element is a function of geometry only, provided the thermal conductivity of the materials remains the same, the pattern in other sizes of fuel elements is the same as long as the relative dimensions are constant. The temperature level is directly proportional to the total heat per unit length generated in the fuel element. Thus the temperatures in fuel element sizes from 1/4 in. to 3/8 in. were computed from the analog for coolant volumes in the reactor of 35% to 55%. The maximum sodium temperatures and maximum fuel alloy temperatures are plotted in Figures 21 and 22, respectively. In these figures, the film heat transfer coefficient, the clad thickness, and the thermal conductivity of stainless steel were made the same as in the ball-type element so that the results may be compared with that element.

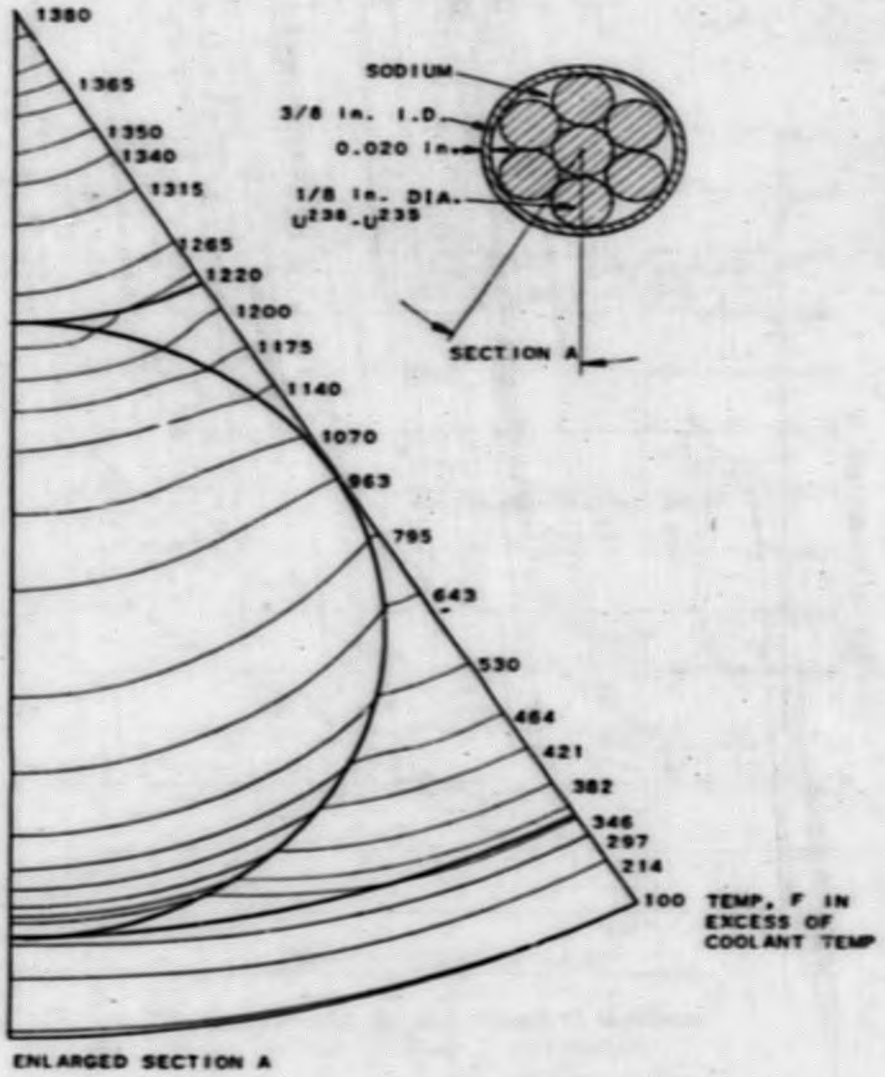

RE-7-11517-A

W.R. SIMMONS: E.A.K., 8-21-53

FIG. 20
ISOTHERMAL PATTERN IN A LUMPED DISTRIBUTED HEAT SOURCE

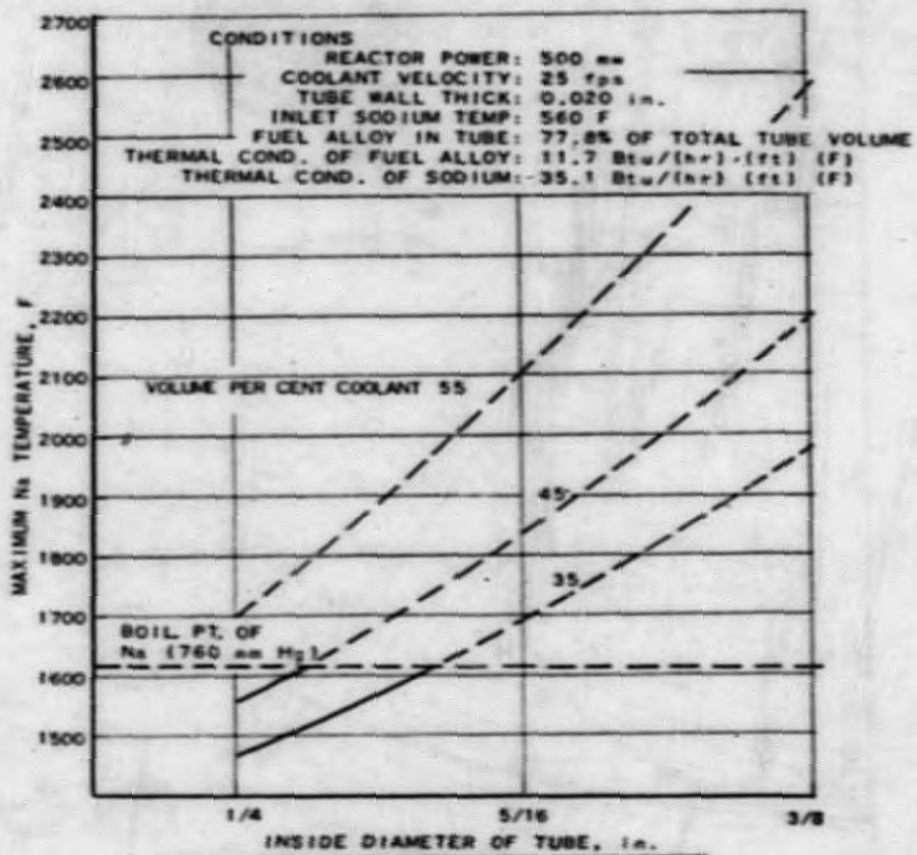

FIG. 21
MAXIMUM STAGNANT SODIUM TEMPERATURE.
PARAMETER - COOLANT VOLUME

L.L.KINTNER:T.M.L.,7.17.53

RE-7-11493-A
ANL-4812-11493

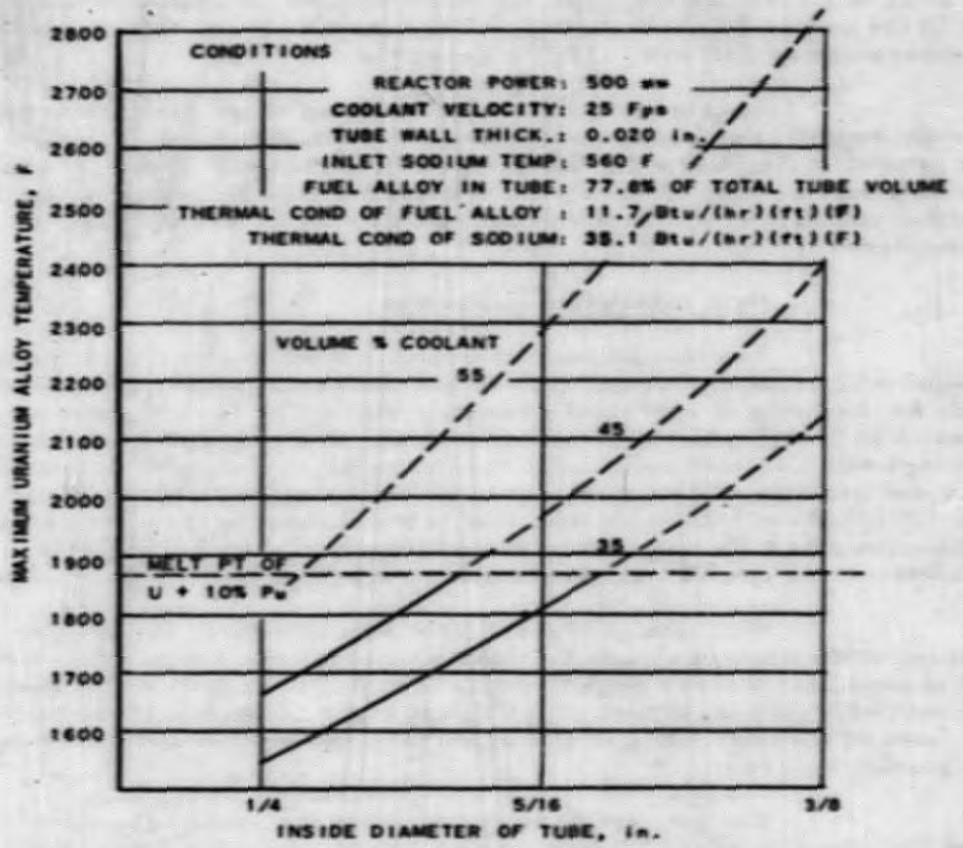

RE-7-11497-A

L.L.KINTNER:T.W.L.,8-18-53

FIG. 22
MAXIMUM URANIUM TEMPERATURE.
PARAMETER - COOLANT VOLUME

Other types of fuel elements are being considered. One variation of the pin type discussed above is to make the central pin of the 7-rod group of U^{238}. This results in most of the heat being generated near the outside tube surface and lowers the maximum sodium and fuel alloy temperature by about 90F and 160F, respectively. Another variation, putting the fuel alloy in a circular ring with a sodium annulus on each side and a U^{238} rod in the center (70 % fuel alloy), lowers the maximum sodium and fuel alloy temperature by 40F and 110F, respectively.

Another fuel rod type is a group of six fuel alloy rods bonded with sodium in an equilateral triangular container tube. This fuel element geometry simplifies the spacing problem since the corner of one triangle may serve as the contact point against the side of another triangle. The thermal analysis of a core composed of this type of fuel element is being undertaken.

d. Heat Liberation in Blanket

The fission heat liberated in the blanket after 100 days of operation was estimated to be 7.7 % of the total core power. The estimate was made on the basis of spherical geometry with a 2 ft thick blanket section composed of 80 % U^{238} and 20 % sodium coolant. The heat flux distribution thus obtained was assumed to be valid for the radial direction in cylindrical geometry and a cosine distribution was used for the axial direction of the cylinder. The ratio of maximum heat flux in the blanket to the average heat flux in the core was 0.05, and beyond the mid-point of the blanket in the radial direction, the fission heat production dropped off to negligible amounts.

With this heat production, and assuming the limiting temperature in the blanket was 1202F (same as in the plate type core) the analysis showed that nuclear requirements of high U^{238} density in the blanket could be met with stainless steel clad U^{238} rods in a hexagonal subassembly 2.562 in. across the flats. The total number of subassemblies required for the side blanket was 260.

The subassemblies adjacent to the side of the core contained 19 rods of 0.99 in. OD (including 0.005 in. stainless steel clad) which gives a composition of 14 % coolant, 82 % U^{238}, and 4 % stainless steel. The remaining subassemblies contained 9 rods of 1.62 in. OD giving a blanket composition of 15 % coolant, 81 % U^{238} and 4 % stainless steel. The reason for the smaller diameter rods in the assemblies adjacent to the core is that the heat generation is higher there.

Results of the analysis showed that a blanket of the above configuration could be maintained at temperatures below 1200F with proper orificing of the flow. The coolant stream for the side blanket is assumed to be in parallel with the core coolant stream while the upper and lower blanket coolant stream is assumed to be in series with the core coolant

stream. The total coolant flow rate required for the side blanket is about 7.5% of the core coolant flow which results in approximately the same outlet temperature for core and blanket coolant streams. The friction pressure drop in the blanket is about 8 psi.

e. Preliminary Sizing of Heat Exchangers - L. L. Kintner, J. B. Reynolds, R. R. Rounsley

(1) Intermediate Heat Exchanger

The size of a shell and tube, counterflow, heat exchanger for transfer of 500 mw of heat from sodium to NaK has been calculated. The size is based on the following conditions for the NaK and Na:

	Na	NaK
Flow rate, lb/hr	15,400,000	21,800,000
Average velocity, fps	10	10
Inlet temperature, F	930	529
Outlet temperature, F	560	899

The NaK was assumed to be inside the tubes. The tubes were made of 1/2 in. OD, 23 BWG (0.025 in.), stainless steel. The effect of tube diameter on the size of the heat exchanger was found to be small in the range of tube diameters from 1/4 in. to 1/2 in. However, about five times as many 1/4-inch tubes were required. The heat exchanger size given below is based on 1/2 in. OD tubes.

Log mean temperature difference, F	31
Over-all heat transfer coefficient, Btu/(hr)(sq ft)(F)	2,180
Number of tubes required	7,100
Heating surface, sq ft	25,000
Tube length, ft	27
Approximate ID of shell, ft	5.3

Other types of heat exchangers are being considered for heat transfer between liquid metals which will take advantage of the relatively low pressure required and the exceptionally good heat transfer coefficients. Plate-type exchangers are being considered which have a minimum amount of metal per unit volume for the heat to be transferred through.

(2) NaK to Water and Steam Heat Exchangers (Steam Generator)

Preliminary sizing of steam generator components must be accompanied by an appropriate steam cycle. Steam cycles

are being studied to determine the effects of reheating, regeneration, split NaK flow, etc., for the NaK temperatures available. Appropriate sizes for these components may then be calculated.

Prelimary estimates of a steam cycle assuming the NaK flows in series through a superheater, boiler, and preheater, indicate that a cycle operating at 1000 psia boiler pressure is feasible with the present reference reactor coolant temperatures. The over-all plant efficiency for such a cycle is about 28%, assuming 80% turbine efficiency, 760F superheat temperature, 2 in. Hg abs. condenser back pressure, and 10% of the electrical output for auxiliary plant equipment. Work is continuing on this phase to determine more efficient cycles.

Rough estimates of the component sizes for the above steam conditions have been made. The estimates include provisions for preventing the direct mixing of NaK and water. The reaction between Na or NaK and dry steam has been found to be considerably lower than with water.[6] Therefore, in the superheater, single wall tubes were used. Since the reaction of NaK in water is more violent, double wall tubes were used in the boiler and preheater, with a detecting fluid (helium) between the tubes. Experimental values of the over-all coefficient for such a double-walled tube when generating steam with hot NaK was found to be approximately 500 Btu/(hr)(sq ft)(F) by King and Tidball.[7] The approximate heating surface areas required for the superheater, boiler, and preheater were estimated to be 3000, 12,500 and 11,000 sq ft, respectively.

f. Thermal Stress Analysis of Clad Plate-Type Fuel Elements - W. S. Flinn

Calculations were made of the thermal stresses in a proposed stainless steel clad, uranium core fuel plate, .061 in. thick with a cladding thickness of .007 in. (Figure 23). No particular bond between the clad and core was considered but it was assumed that there was no thermal resistance or lack of strength at this bond.

The thermal stresses in an unrestrained bimetallic fuel plate can be subdivided into two general categories.

(1) Thermal stresses due to temperature distribution through the fuel plate (σ_T).

(2) Thermal stresses due to the relative expansions of the clad and core caused by the various temperature levels (σ_M)

---

[6] Liquid Metals Handbook, NAVEXOS, P-733 (Rev.), June, 1952.

[7] E. C. King, and R. A. Tidball, "Heat Fluxes from Liquid Metal to Boiling Water," NP-4047, August 8, 1952.

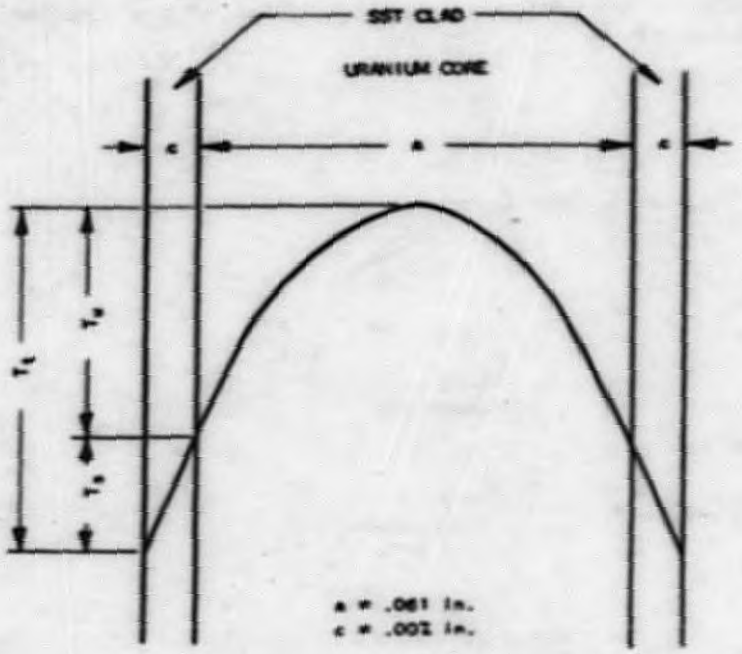

FIG. 23
TEMPERATURE DISTRIBUTION
IN PROPOSED BIMETALLIC
FUEL PLATE

RE-7-11440-A

R.S.FLINN:E.C.F.,8/13/53

to which the plate is subjected, i.e., rolling temperature*, room temperature, and operating temperature. Therefore from the equation:

$$\text{Total stress} = \sigma_o = \sigma_T + \sigma_M$$

the total stresses in the stainless clad (σ_{s-o}) and in the uranium core (σ_{u-o}) may be expressed as:

$$\sigma_{s-o} = \sigma_{s-T} + \sigma_{s-M}$$
$$\sigma_{u-o} = \sigma_{u-T} + \sigma_{u-M}$$

The stresses σ_T and σ_M are further broken down as follows:

$$\underline{\sigma_T}$$

Uranium core

Center

$$\sigma_{u-T\ (\text{center})} = \sigma_{u\ (\text{center})} + \sigma_{u-s}$$

Outside surface

$$\sigma_{u-T\ (\text{outside})} = \sigma_{u\ (\text{outside})} + \sigma_{u-s}$$

where:

$\sigma_{u\ (\text{center})}$ = thermal stress in the center of the uranium core due to the temperature distribution within the uranium.

$\sigma_{u\ (\text{outside})}$ = thermal stress at the outside surfaces of the uranium core due to the temperature distribution within the uranium.

σ_{u-s} = uniform thermal stress in the uranium caused by the relative expansions of the core and clad due to the temperature distribution in the total thickness of the fuel plate.

---

*It will be assumed that this temperature is the one of original zero stress level of the bimetallic fuel plate. Possible subsequent Beta stress reliefs may change this. Since the exact manufacturing process is not known, a rolling temperature of 1340F was considered to be the zero stress reference temperature.

Stainless clad

Inside surface

$$\sigma_{s\text{-}T\ (inside)} = \sigma_{s\ (inside)} + \sigma_{s\text{-}u}$$

Outside surface

$$\sigma_{s\text{-}T\ (outside)} = \sigma_{s\ (outside)} + \sigma_{s\text{-}u}$$

where:

$\sigma_{s\ (inside)}$ = thermal stress at the inside surface of the stainless clad due to the temperature distribution within the clad.

$\sigma_{s(outside)}$ = thermal stress at the outside surface of the stainless clad due to the temperature distribution within the clad.

$\sigma_{s\text{-}u}$ = uniform thermal stress in the stainless caused by the relative expansions of the core and clad due to the temperature distribution in the total thickness of the fuel plate.

σ_M

Uranium core

$$\sigma_{u\text{-}M} = \sigma_{u\text{-}M_1} + \sigma_{u\text{-}M_2}$$

Stainless clad

$$\sigma_{s\text{-}M} = \sigma_{s\text{-}M_1} + \sigma_{s\text{-}M_2}$$

where:

$\sigma_{u\text{-}M_1}$ and $\sigma_{u\text{-}M_2}$ = respective uniform thermal stresses in the uranium caused by the relative expansion of the core and clad due to the fuel plate temperature changing from:

(1) rolling temperature to room temperature, and

(2) room temperature to fuel plate surface operating temperature.

$\sigma_{s\text{-}M_1}$ $\sigma_{s\text{-}M_2}$ = respective uniform thermal stresses in the clad caused by the relative expansion of the core and the clad due to the fuel plate temperature changing from: (1) rolling temperature to room temperature and (2) room temperature to fuel plate surface operating temperature.

From the above definitions it can be seen that σ_M is dependent upon rolling or manufacturing temperatures and operating temperature levels rather than upon heat flux. The stress σ_T, however, is proportional to heat flux and is not dependent upon these temperature level changes other than to the extent that some of the significant physical properties of uranium and stainless are affected by temperature. This means that, even with a uniform heat flux along the length of the core, there would be a changing total thermal stress value at any corresponding location in the fuel plate thickness as the location along the core length is varied. This change is due to the difference in temperature of the coolant. The actual total thermal stress values, of course, also vary because there is a flux variation along the length of the core.

The following equations were developed to express the thermal stresses at various locations in the fuel plate.

Uranium

$$\sigma_{u\text{-}T\ (\text{center})} = -\left[\frac{1}{3}\frac{E_u\ \alpha_u\ \Delta T_u}{(1-\mu_u)} + \frac{\alpha_u\ \theta_u - \alpha_s\ \theta_s}{\frac{a}{2cE_s} + \frac{1}{E_u}}\right]$$

$$\sigma_{u\text{-}T\ (\text{outside})} = \left[\frac{2}{3}\frac{E_u\ \alpha_u\ \Delta T_u}{(1-\mu)} - \frac{\alpha_u\ \theta_u - \alpha_s\ \theta_s}{\frac{a}{2cE_s} + \frac{1}{E_u}}\right]$$

$$\sigma_{u\text{-}M\ (\text{outside})} = -\left[\frac{T'(\alpha_s-\alpha_u)}{\frac{a}{2cE_s'} + \frac{1}{E_u'}} + \frac{T''(\alpha_s-\alpha_u)}{\frac{a}{2cE_s''} + \frac{1}{E_u''}}\right]$$

Stainless

$$\sigma_{s\text{-}T\ (\text{inside})} = \left[\frac{\alpha_u\ \theta_u - \alpha_s\ \theta_s}{\frac{1}{E_s} + \frac{2c}{aE_u}} - \frac{1}{2}\frac{E_s\ \alpha_s\ \Delta T_s}{(1-\mu_s)}\right]$$

$$\sigma_{s\text{-}T\ (\text{outside})} = \left[\frac{\alpha_u\ \theta_u - \alpha_s\ \theta_s}{\frac{1}{E_s}\ \frac{2c}{aE_u}} + \frac{1}{2}\frac{E_s\ \alpha_s\ \Delta T_s}{(1-\mu_s)}\right]$$

$$\sigma_{s\text{-}M} = \left[\frac{T'(\alpha_s-\alpha_u)}{\frac{1}{E_s'} + \frac{2c}{aE_u'}} - \frac{T''(\alpha_s-\alpha_u)}{\frac{1}{E_s''} + \frac{2c}{aE_u''}}\right]$$

where:

ΔT_u = temperature drop in the uranium = $\left(\frac{a}{a + 4c}\right) \Delta T_{Total}$ °F

ΔT_s = temperature drop in the clad = $\left(\frac{c}{\frac{a}{4} + c}\right) \Delta T_{Total}$ °F

$\theta_u = \Delta T_s + \frac{2}{3} \Delta T_u$

$\theta_s = \frac{\Delta T_s}{2}$

$T_T = \frac{\frac{Q}{A}}{12k}\left(\frac{a}{4} + c\right)$

$\frac{Q}{A}$ = heat flux, Btu/(hr)(sq ft)

k = thermal conductivity of stainless steel and uranium = 16 Btu/(hr)(ft)(F)

a = uranium core thickness = 0.061 in.

c = stainless clad thickness = 0.007 in.

T' = $T_o - 75$

T'' = $T_p - 75$

T_o = rolling temperature, F

T_p = operating surface temperature of fuel plate, F

The material property values used were:

E_u	= approximate effective moduli of	13×10^4
E'_u	= elasticity of uranium for the	10×10^4
E''_u	= various associated stresses and temperatures, psi.	20×10^4
E_S	= approximate effective moduli of	27×10^4
E'_s	= elasticity of Type 347 stainless	10×10^4

E_s''	=	steel for the various stresses and temperatures, psi.	22×10^6
α_u	=	approximate average coefficient of expansion for natural uranium	$7 \times 10^{-6}/F$
α_s	=	average coefficient of thermal expansion for Type 347	$11 \times 10^{-6}/F$
μ_u μ_s	=	Poisson's ratio for uranium and stainless steel, respectively	0.3

The uranium and stainless steel thermal stresses shown in Table I were calculated in an attempt to determine the approximate order of magnitude of thermal stresses that might exist in this type of fuel plate. This is particularly true of that portion of the stresses that are caused by manufacturing or heat-treating processes. The following assumptions were made:

(1) The heat flux at the middle of the fuel plate length is 990,000 Btu/(hr) (sq ft).

(2) The heat flux at the inlet and discharge end of a fuel plate in a core is 495,000 Btu/(hr) (sq ft).

(3) The fuel plate surface temperatures at the inlet, middle, and discharge position of the fuel plate are 600, 800, and 960F, respectively.

Table I

APPROXIMATE THERMAL STRESSES IN STAINLESS STEEL CLAD, URANIUM CORE FUEL PLATE

		Thermal Stress, psi			
		Uranium		Stainless Steel	
		Center	Outside	Inside	Outside
σ_T	Inlet	-2600	2540	30	7700
	Middle	-1200	5070	60	15,400
	Discharge	-2600	2540	30	7700
σ_M	Inlet	-1000		6460	
	Middle	2210		-9440	
	Discharge	4790		-20,800	
σ_R	Inlet	-3600	1540	4490	12,160
	Middle	-2990	7280	-9380	5960
	Discharge	2190	7330	-26,770	13,100

3. Heat Transfer Experiments - K. D. Kuczen

a. Heat Transfer Test Facilities

The first test loop to be built will be used primarily for basic heat transfer data in a round tube, rectangular channel, and an annulus. The test sections will be heated electrically with direct current. The coolant will be sodium and/or sodium-potassium alloy.

The tubular test section has been designed. It consists of a copper tube 3 ft long, 0.55 in. OD and a 0.25 in. ID with electrical terminals on each end. With these dimensions, 5% of the heat generated in the copper tube will be generated in the coolant.

To reduce the short-circuiting effect the loop will cause across the test sections, the loop will be built of sufficient length of 3/4 in. stainless steel piping to keep the heat generation in the loop to within 5% of that in the test section.

An electromagnetic pump will be used to pump the coolant through the loop. The required capacity of the pump is approximately 20 gpm against a head of 60 psi.

The heat generated in the test sections will be released to the atmosphere in a sodium-to-air cooler of approximately 380 kw capacity. A blower will be used to supply cooling air.

A contract has been placed to provide a rectifier a source of direct-current power. The capacity of the rectifier will be from 2 to 15 v at 30,000 amp.

The basic data obtained from the above mentioned tests will be used to design a liquid metal heat exchanger, the model of which will be tested in a second liquid metal test loop.

The second loop will consist of 2 in. stainless steel piping. The sodium or sodium-potassium alloy will be heated by passing direct current through the fluid. Direct current will flow into the center of a 1-1/2 in. stainless steel pipe and flow out at each end so that both ends of the heater section are at the same potential. This will prevent current flow through the loop external to the heater section.

The electromagnetic pump will have a capacity of 100 gpm at 50-60 psi of head.

Both the rectifier and sodium-to-air cooler will be common to both loops.

Piping and fittings for both loops have been ordered. Standard stainless steel valves are in the shop being redesigned with sealing bellows to prevent leakage. Drawings of the sodium-to-air cooler design are being prepared. Most of the component parts of the cooler are now on hand. The electromagnetic pumps are being made available.

b. Pressure Drop in Corrugated Plate Assemblies - R. J. Weatherhead

A series of isothermal pressure drop tests have been conducted on four corrugated plate assemblies having corrugation pitch angles of 0, 10, 30, and 45 deg, respectively.

All assemblies were alike except for the angle of corrugation, the angle between the incident flow direction and the corrugation axis. Each assembly consisted of fifteen 2S aluminum, 14 gage (.064 in.) plates stacked such that adjacent plates had the diagonal corrugations at alternate angles.

The tests were conducted in the Small Scale Heat Throughput Loop at a uniform pressure of 1000 psi and at water temperatures of 100, 200, 300, and 400F for each assembly. For all the water temperatures the flow was increased from minimum to maximum and then decreased to the minimum. Approximately 75 friction points were determined for each assembly.

The test data was correlated to the standard friction factor - Reynolds Number presentation by using the Gunter and Shaw[8] volumetric equivalent diameter

$$Dv = \frac{4 \times \text{net free volume}}{\text{friction surface}}$$

where the net free volume is considered to be the total space in the test section occupied by the flowing fluid. An average flow area of the test section, calculated by dividing the net free volume by the test section length, was used to calculate the average test section velocity of the fluid.

---

[8] A. Y. Gunter and W. A. Shaw, "A General Correlation of Friction Factors for Various Types of Surfaces in Crossflow," Trans. ASME 67, (1945), pp. 643-660.

The test results are given in Figure 24. The data for both the zero-degree and 45-degree plate assemblies showed little scatter and were used to determine the test curves for the 10-degree and 30-degree plate assemblies which showed an abnormal scattering. It was observed that the plates of both the 10-degree and the 30-degree assemblies had loosened in the holder during testing, the reduction in total plate thickness being from 1/32 to 1/16 in. This loosening of the plates in the holder is believed to be the cause of the excessive scatter in the 10-degree and 30-degree plate data. In evaluating the test points for curve plotting, it was assumed that the increase in pressure drop with the increase in angle of corrugation was directly proportional to the change in angle of corrugation since the angular change of direction of the fluid was directly proportional to the angle of corrugation. Using the curves for the zero-degree and 45-degree plate assemblies as the reference, the curves for the 10-degree and 30-degree plate assemblies were interpolated both as to slope and intercept and appear to fit the bulk of the data reasonably well.

BOILING REACTOR HEAT TRANSFER EXPERIMENTS

A. Boiling Density Tests - A. S. Jameson, E. A. Wimunc

The natural circulation boiling density tests, originally reported in ANL-4921[9] have been continued and extended to cover a range of variables. The results obtained from these tests are shown graphically in Figures 25 to 31 inclusive. The following tabulation lists the pertinent information regarding the test sections for which density data have been obtained.

Fig. 32 Ref.	Channel Geometry: Opening, in.	Width, in.	Height, in.	No. of Flow Channels	Material	Heat Transfer Area, sq ft.	Heat Water Volume, liters
(a)	1/8	5	24	20	"A" Nickel	32	4.87
(b)	1/4	5	24	18	"A" Nickel	31.6	8.68
(c)	1/4	5	9	18	"A" Nickel	11.9	3.25
(d)	1/4	5	24	4	Type 304	5.3	1.97
(e)	1/2	5	24	10	"A" Nickel	16.1	9.68
				5 - 3/4			
	3/4 x 1/4	5	24	4 - 1/4	"A" Nickel	14.2	9.27

[9] J. R. Dietrich, D. C. Layman, O. A. Schulze, "The Proposed Boiling Reactor Experiment," November 12, 1952.

R.J.WEATHERHEAD;E.A.K.,8-21-53

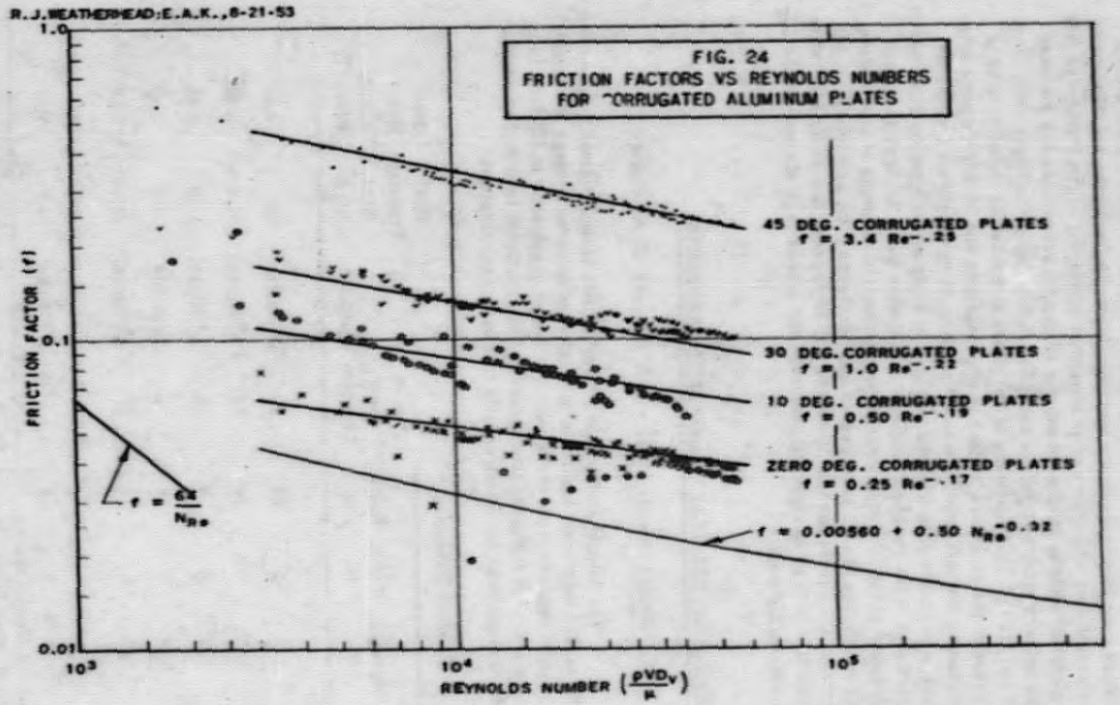

FIG. 24
FRICTION FACTORS VS REYNOLDS NUMBERS
FOR CORRUGATED ALUMINUM PLATES

RE-7-11527-A

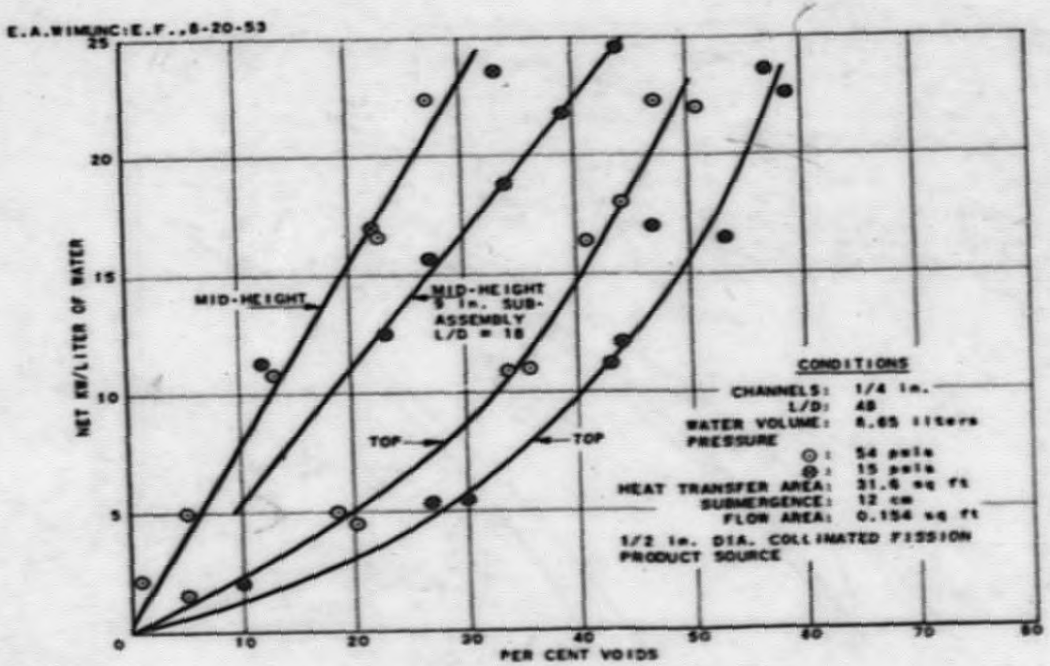

FIG. 25
POWER INPUT PER UNIT VOLUME
VS PER CENT VOIDS

RE-7-11514-A

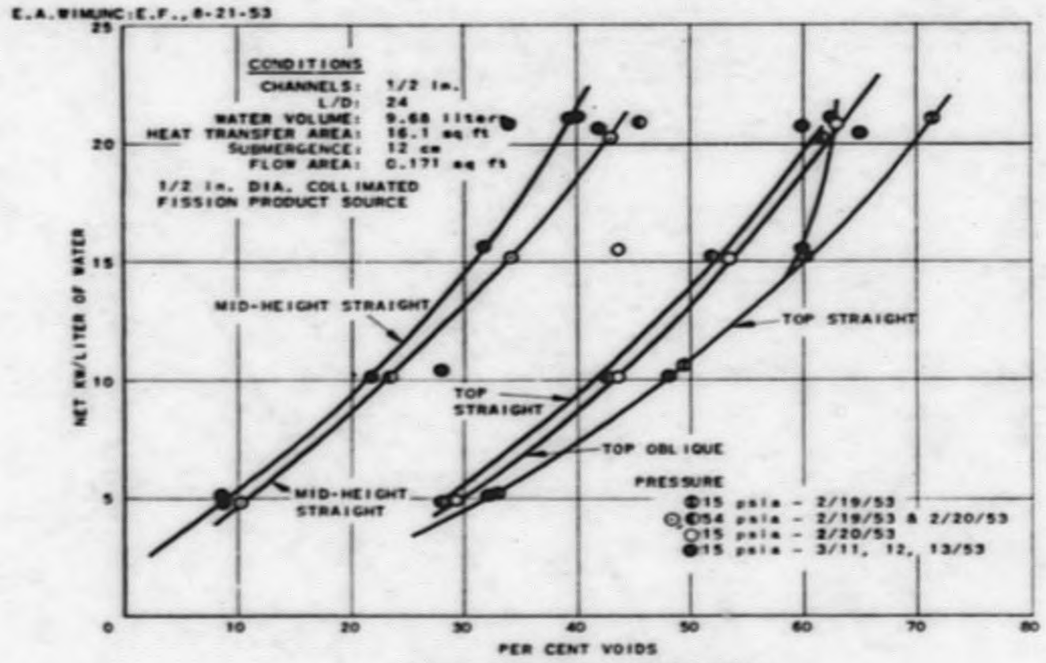

FIG. 26
POWER INPUT PER UNIT VOLUME
VS PER CENT VOIDS

RE-7-11518-A

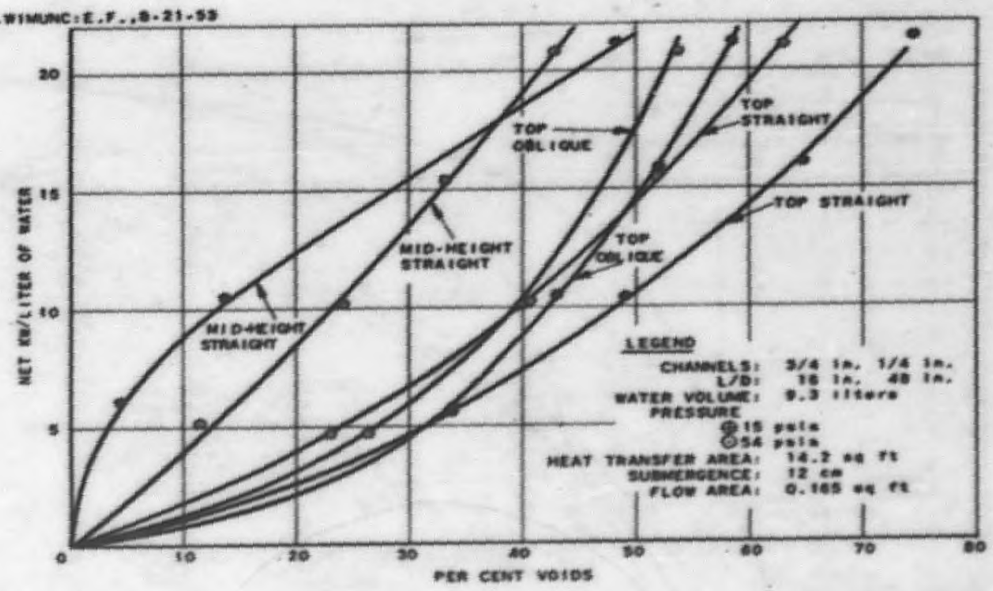

FIG. 27
POWER INPUT PER UNIT VOLUME
VS PER CENT VOIDS

RE-7-11529-A

E.A.WIMUNC:E.F.,7-12-53

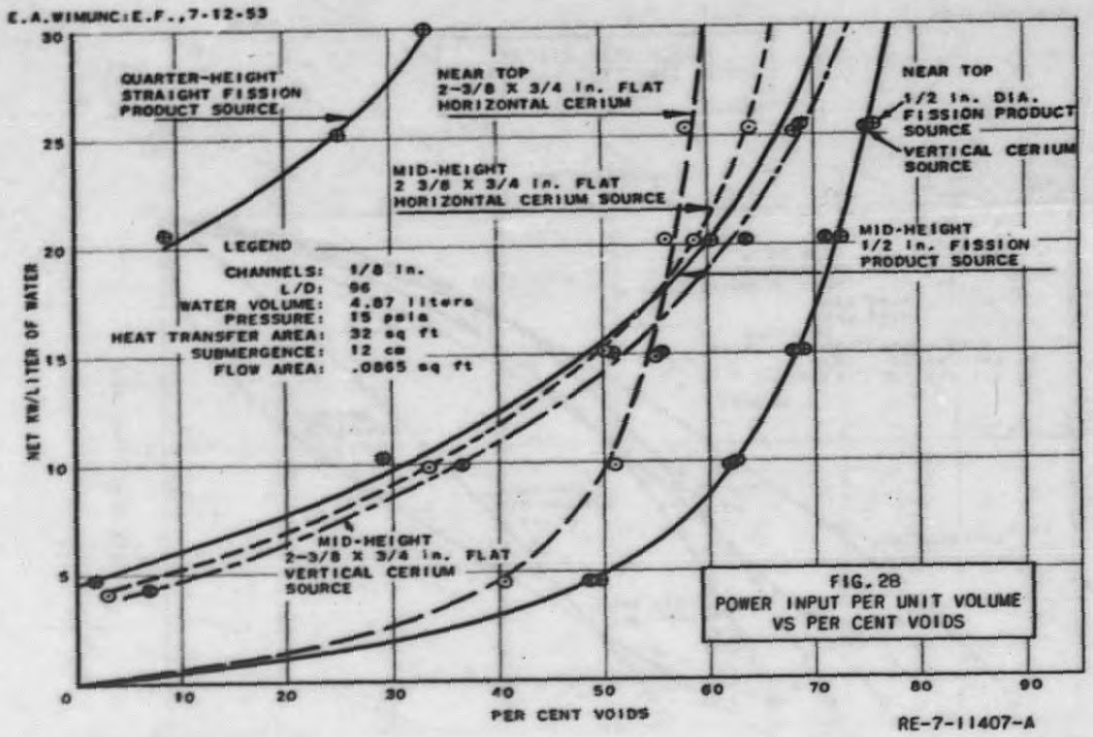

FIG. 28
POWER INPUT PER UNIT VOLUME VS PER CENT VOIDS

RE-7-11407-A

E.A.WIMUNC:E.F.,7-12-53

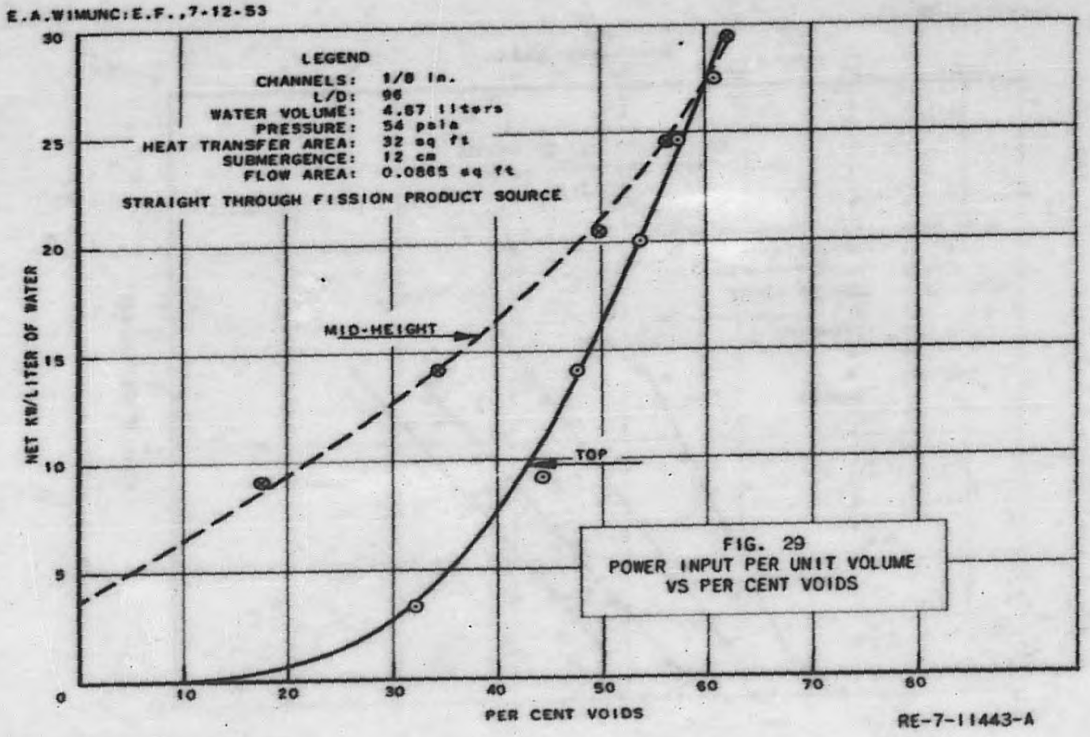

FIG. 29
POWER INPUT PER UNIT VOLUME
VS PER CENT VOIDS

RE-7-11443-A

E.A.WIMUNC:E.F.,7-11-53

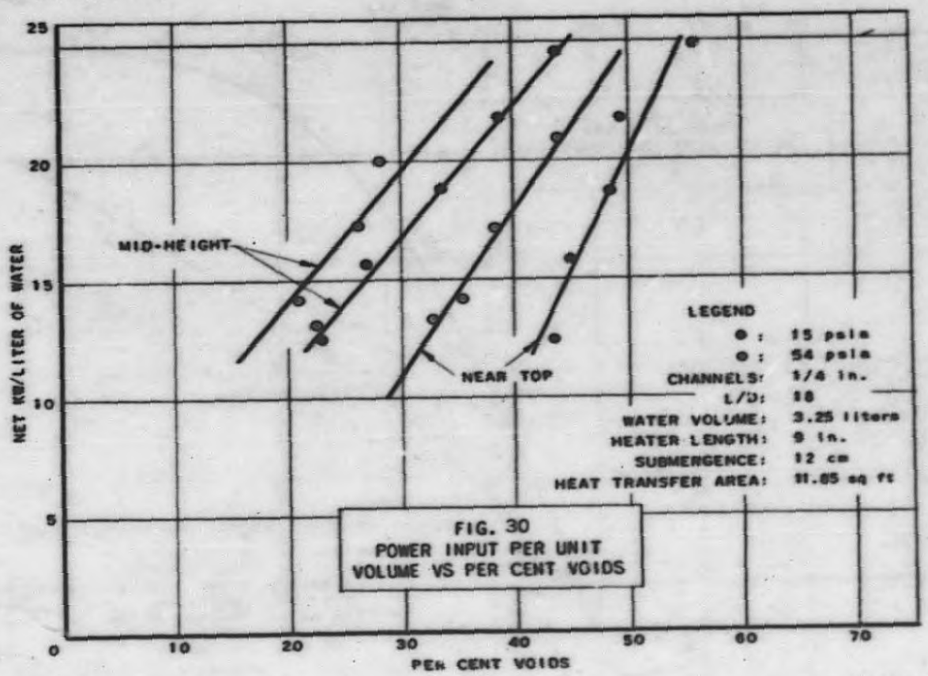

FIG. 30
POWER INPUT PER UNIT
VOLUME VS PER CENT VOIDS

RE-7-11444-A

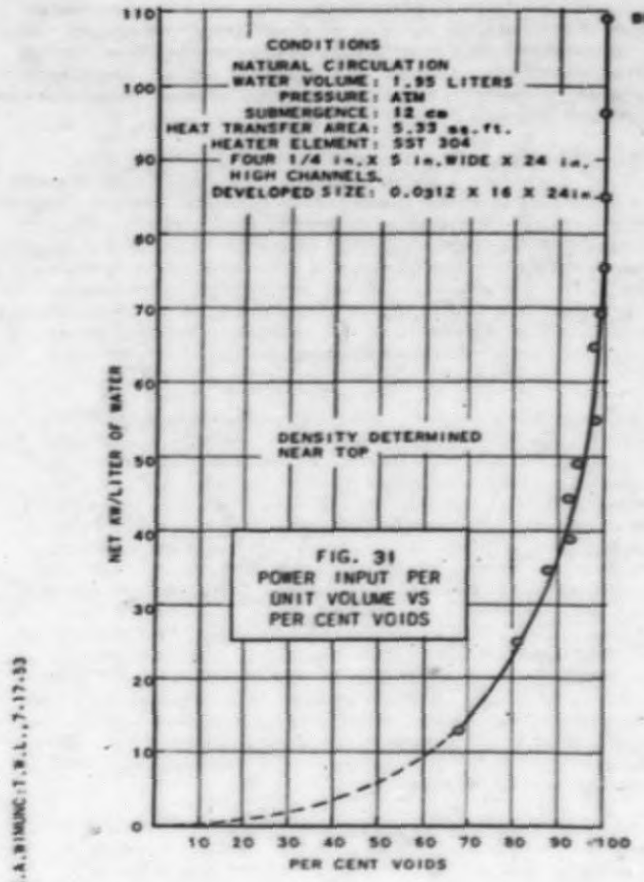

FIG. 31
POWER INPUT PER UNIT VOLUME VS PER CENT VOIDS

E.A. HIMMING: T.W.L., 7-17-53

RE-7-11402-A

The test sections (Figure 32) which were essentially resistance heaters, were all fabricated the same way, from 1/32 in. sheet folded in successive 5 in. widths, with the coolant channel formed between the folds. At the ends of the corrugated section, 1/4 in. thick, 5 in. wide copper plates were brazed to uniformly distribute the heating current along the height. The channel openings were maintained with two Teflon spacer combs inserted at both top and bottom of the assembly adjacent to the heater folds. Rigidity of the unit was accomplished with two electrically insulated spacer rods between the copper terminal plates at top and bottom.

Power to the submerged resistance heater (Figure 33), was conducted through 1-1/2 in. diameter copper electrodes screwed into threaded bosses brazed at the mid-height of the test section terminal plates. The copper electrodes were electrically insulated from the tank walls by Micarta adapters and water leakage was prevented by "O" rings mounted in the adapter. The bus bar connections between the 30,000-amp, 13-volt rectifier terminals and the test section electrodes were water-cooled to prevent overheating. Water cooling of the electrode terminals, in the vicinity of the bus bar connector, was also necessary. The heat rejection to the electrode cooling water, in addition to the heat losses to the surroundings were accounted for by conducting heat loss tests.

The measurement of the steam voids formed during the boiling process was by attenuation of gamma rays directed through the tank. Two sources were used during these tests. The first source tried was a 1/2 in. diameter collimated, natural uranium shielded fission product source. In use, the source was located against one side of the tank such that the beam was parallel to the flow channels. The Geiger-Mueller counter tube was also correspondingly positioned with its axis parallel to the channel walls and such that maximum sensitivity was obtained. With the 1/2 in. diameter beam, the number of channels surveyed was a function of the channel width. To check the steam void results, over a greater number of channels with the fission product source, the latter was mounted at an angle of 30 degrees with the channel axis. The indicated voids with the oblique source setting were lower at the same power density as shown in Figures 26 and 27, than that obtained with the source directed straight through and parallel with the channel walls. The reduction in indicated steam volume fraction can be attributed to the relatively dead boiling zone in the channel adjacent to the low heat flux copper terminal plate, which was partially scanned with the oblique setting of the source and G-M tube.

A further check to determine representative steam voids over a greater number of channels was made by using a flat cerium source, with exposure face dimensions 3/4 in. by 2-3/8 in. In use, the cerium source was positioned on the tank wall such that the flat exposure face was normal to the channel axis. This source was utilized during the atmospheric pressure tests of the 1/8 in. channel subassembly, the results of which are

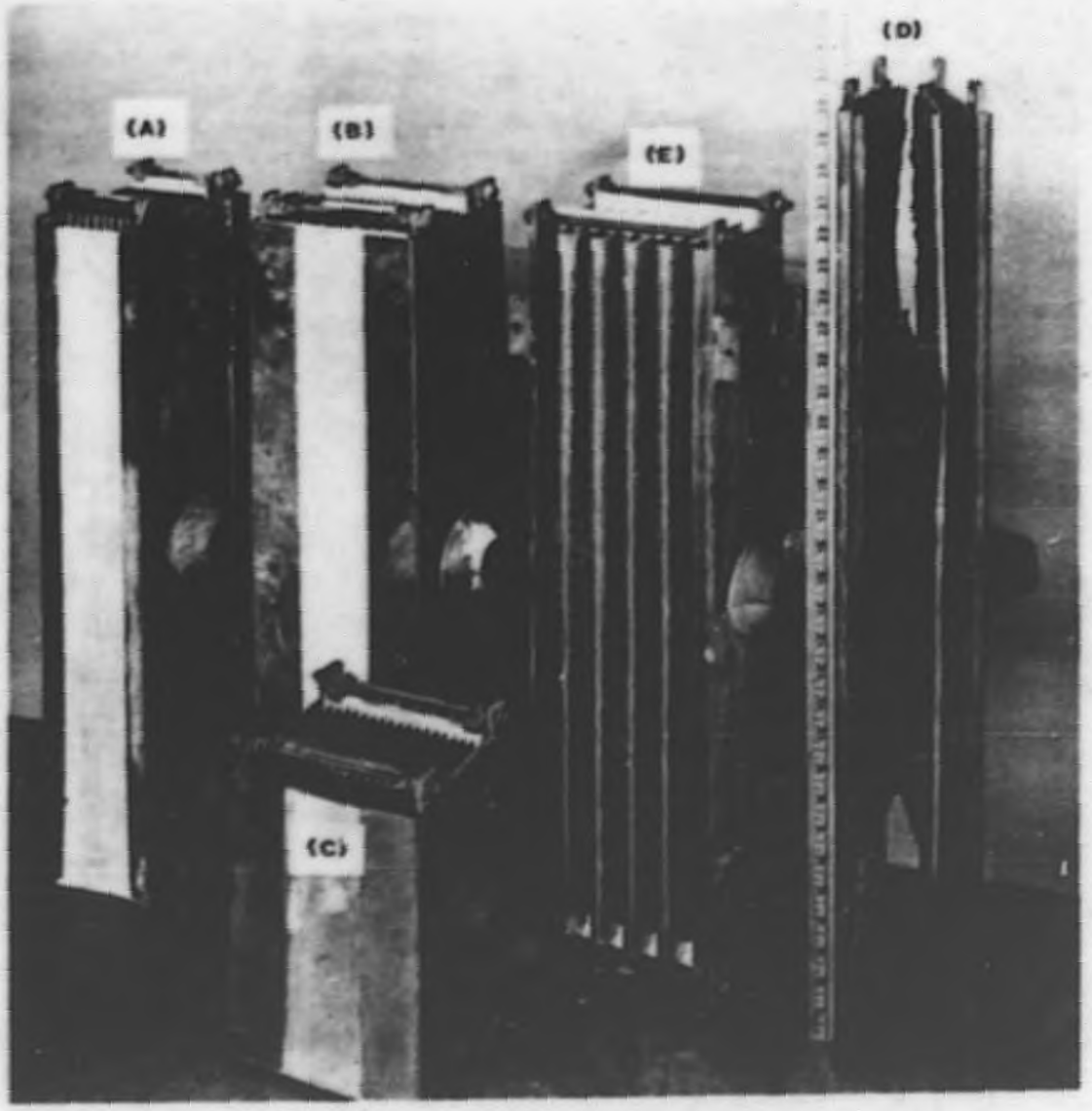

FIG. 32
TEST SECTIONS (RESISTANCE HEATERS)
USED IN BOILING DENSITY TESTS

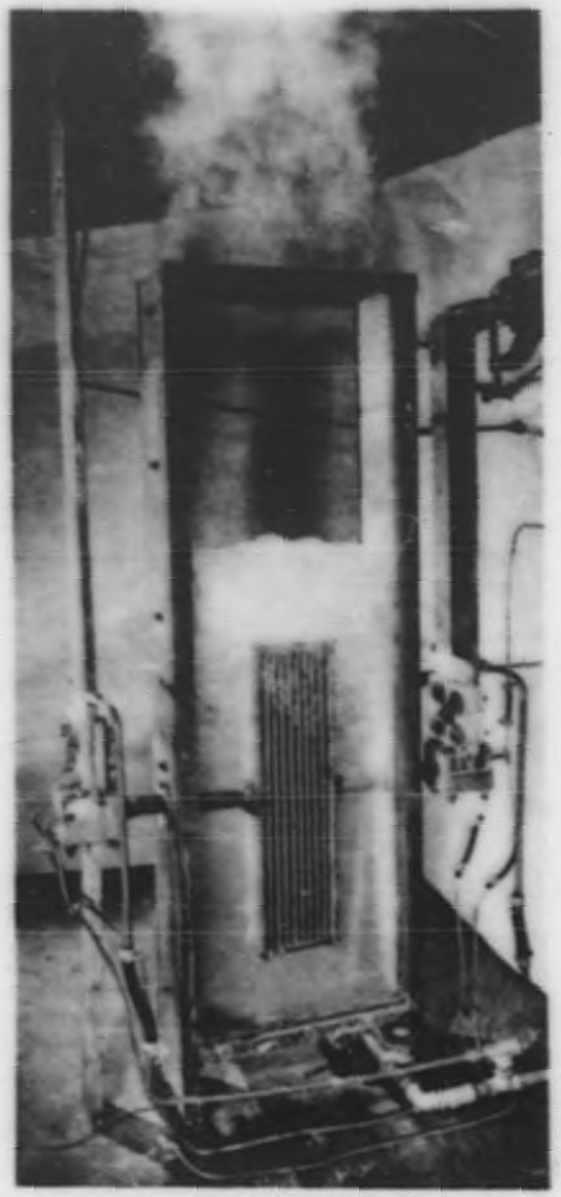

FIG. 33
BOILING AT 5 KW/LITER

shown in Figure 28. Relatively good agreement between results with the flat cerium source and the straight-through directed fission product source can be noted with the exception of the discrepancy in the results with the sources located at the "near top" position of the heater. An accounting of this discrepancy has not been completely resolved.

Both sources were calibrated to yield conversion of counting rates to void fractions. In the calibration setup the actual test section or a dummy section, was placed in an open tank in a horizontal position with the channel walls vertical. The corresponding total thickness of steel of the tank walls, Teflon of the side shrouds, and side water annulus, were reproduced in the calibration setup. The source was mounted with its axis vertical and underneath and in contact with the calibration tank. The G-M counter tube was mounted above the test section, at a height corresponding to the distance between the test section tank walls, and in line with the source axis. Successive increments of cold water to the tank between the bottom and top levels of the test heater, with the corresponding counter readings for each water level constituted the calibration. The results of the calibration are shown in Figure 34. With the fission product source and the G-M tube, the calibration curve was taken the same for all test sections since the calibration test points for the individual subassemblies agreed well within the accuracy of the measurements.

The normal operating procedure during any power run was to fix the desired power level, and operating pressure (when above atmospheric), and adjust the make-up feed flow rate until the pressure, metered feed rate and submergence (the water level above the test section top), were all constant. Not until these conditions were stable were the counter readings observed. During such a test run, stability was further indicated by the agreement between successive counter readings.

For all tests reported, the test section was completely shrouded, so that the steam bubbles could not leave the flow channel and enter the downcomer. Teflon sheets in contact with the folds of the test section, constituted the shroud. During these tests the ratio of the downcomer flow cross-sectional area to the riser flow area was varied from 2:1 to 4:1. Changes in the steam voids due to these variations were not detected.

Further tests to determine the effect of downcomer area size to riser flow area were carried out with dampers installed in the downcomer sections. The variation in the steam voids with the dampers wide open and full closed was negligible. Full blocking of the downcomers was not completely possible due to clearance between damper and tank walls. The opposite effect was observed when damper restrictions were installed above the heater top. Large increases in the steam void fraction were observed.

Tests to determine the effect of water level above the heated channel top were carried out and the results of this investigation are shown in Figure 35.

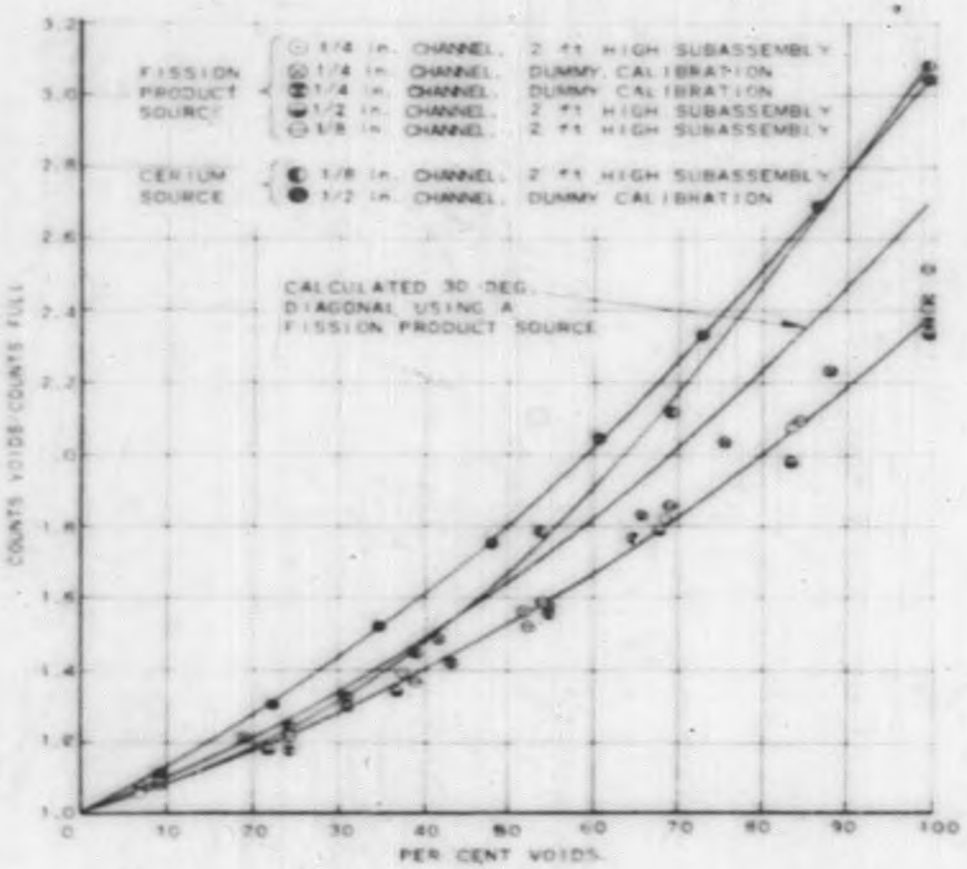

RE-7-11508-A

E.A. WUNC 7-1-, 8-21-53

FIG. 34
PER CENT VOIDS VS COUNT RATE RATIO

E.A.WIMUNC E.A.K.,M-21-53

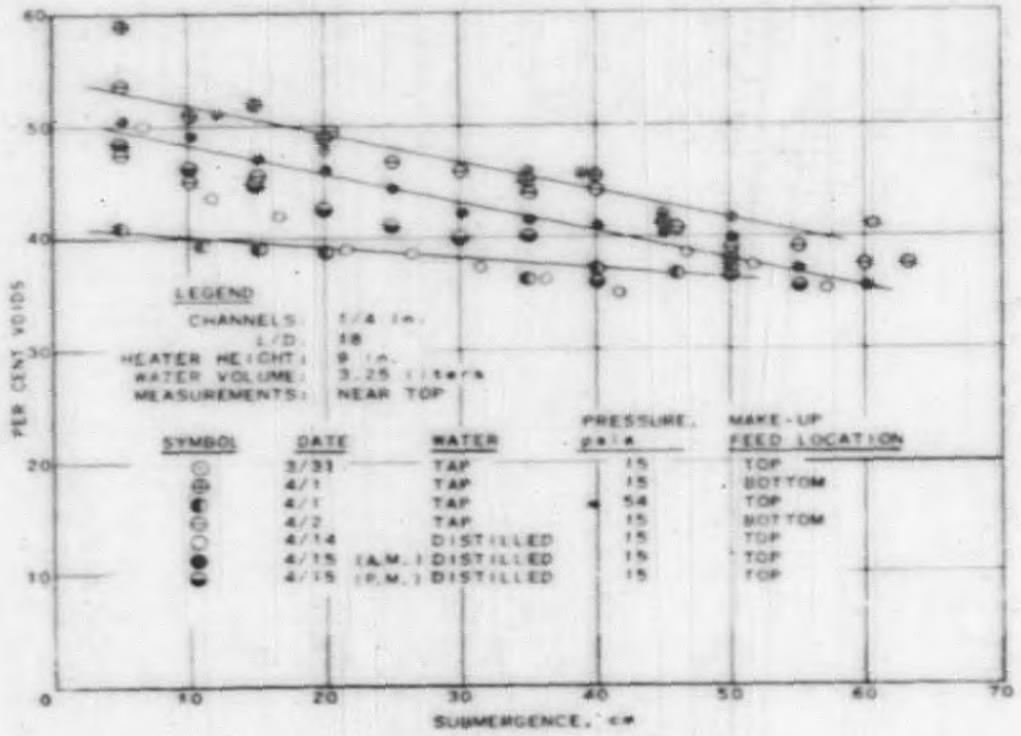

FIG. 35
EFFECT OF SUBMERGENCE VS PER CENT VOIDS AT 20 KW/LITER

RE-7-11526-A

Attempts to meter the water circulating rate were not too successful. Various pitot tube units were installed at the bottom of the heater but fouling of the static holes made them unreliable.

A source of major uncertainty in the test results can be attributed to the purity of the water used during tests. All tests except those for the 1/4 in. channel, 9 in. long subassembly and the 1/2 in. - 24 in. long stainless steel unit were conducted using laboratory "tap" water which had a total hardness of 60 ppm calcium and magnesium. The subassemblies after test had definitely been scaled and the flow resistance effected. Scaling was heavier on the side of each plate in the direction of the negative terminal and increased progressively in magnitude on the plates closer towards the positive terminal. Portions of channels of the 1/8 in. subassembly were partially blocked with scale.

It was observed that the use of distilled make-up water did not completely eliminate the scaling, but did reduce it in comparison to that resulting with "tap" water make-up feed. This was due to the steel tank and the corresponding accumulation of deposits during the sustained evaporation periods.

During the tests of the short, 9 in. length, 1/4 in. channel subassembly it was observed that the water surface oscillated about 1 cycle per sec. This see-saw, swashing action was also observed during the burnout tests of the long (24 in.), 1/4 in. channel stainless assembly. This cyclic motion most likely occurred with the other units tested but was not noticed at the time because the tank top, for the pressure runs, was installed.

The stainless steel test section was designed primarily for burnout determination. The results are shown graphically in Figure 31. During these tests it was necessary to add additional height to the tank to reduce splash-over. This was not completely eliminated even though the chimney added was 5-1/2 ft over the heater top. The burnout point, indicated by fluctuating voltage and ejection of molten metal from the tank top, was reached at a power density of 109 kw per liter, which corresponded to a thermal heat flux of 140,000 Btu/(hr)(sq ft). Figure 36 shows the test section appearance after burnout.

B. Boiling Experiments to Determine Natural Circulation Flow Rates - A. S. Jameson, D. H. Weiss

In order to check the results of the water-steam density experiments with the folded multi-channel heaters described on page 59, a much smaller and simpler apparatus, made primarily of glass in order to permit visual observation, was manufactured. The apparatus consisted of a 0.496 in. OD by 31 in. active length, 220-volt, 2500-watt copper calrod unit mounted in a 36 in. long Pyrex tube of such size as to provide annuli ranging from

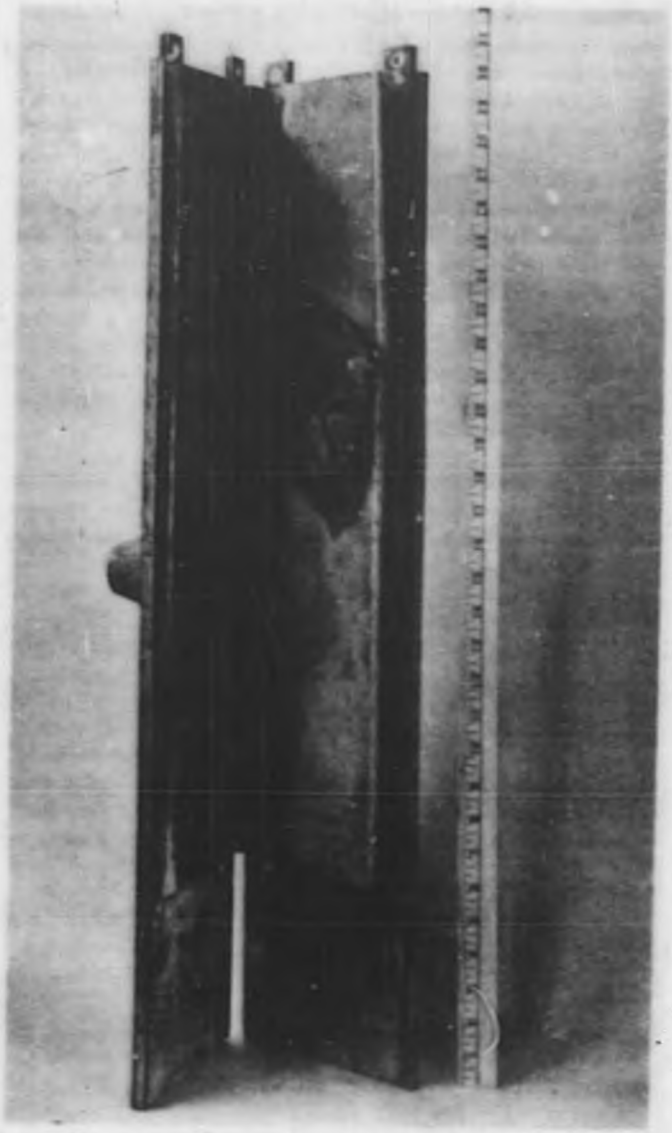

FIG. 36
APPEARANCE OF DISASSEMBLED STAINLESS STEEL HEATER FOLLOWING BURNOUT AT 109 KW/LITER

1/16 to 1/4 in. as was desired. At each end of the 16-inch length was attached a 6 in. deep by 6 in. diameter brass plenum chamber containing pressure taps, thermocouple thimbles and bleed valves. In addition, the lower plenums each contained a small copper calrod heater for heating the water up to saturation temperature. In order to make a complete natural circulation circuit, a 1-inch Schedule-40 pipe was connected in parallel with the plenum chamber - Pyrex tube - plenum chamber assembly to act as a downcomer. At the exit end of each downcomer was placed a bank of two rotameters in parallel to divide up and measure the flow rate. In addition, a bypass line was provided so that the rotameters might be bypassed when desired. All piping was covered (except on the 36 in. Pyrex lengths) with insulation to minimize heat loss.

With the testing of 1/16 and 1/8 in. annuli to 38 kw/liter (based on Pyrex tube water volume) at approximately atmospheric pressure and saturated inlet water, it was found that

(1) If the inlet temperature was allowed to go more than approximately 20F below saturation temperature, the flow became unstable as indicated by sharp changes in the rotor location in rotameter tube.

(2) With an increase in kw/liter beyond a certain value, the flow becomes unstable.

(3) Beyond $2\frac{1}{2}$ kw/liter, the larger annulus gives the larger flow, the maximum values occurring at approximately 16 kw/liter. At this power the 1/16 in. annulus passed 160 pph (1.0 fps) and the 1/8 in. annulus passed 400 pph (1.1 fps). Both units appeared to indicate a leveling off of flow at 16 kw/liter. The 1/16 in. unit indicated a slight decrease in flow from 16 to 38 kw/liter. With the modification of the present power supply, it is hoped to be able to raise the 1/8 in. unit power input from 16 kw/liter to 38 kw/liter.

An attempt will be made to eliminate the rotameters (which cause an excessive pressure drop in the circuit) by use of various electromagnetic flowmeters. The maximum heat flux reached in these tests was 27,000 Btu/(hr)(sq ft).

C. Instrumentation - A. S. Jameson

A density tube (Figure 37) was designed, built and tested and found to give reasonably good agreement with the density as measured with the fission product source. During the tests it was necessary to water cool the static pressure lines to eliminate steam formation. This feature was incorporated in the tubes to be used during the BORAX Experiment.

A.S. JAMESON T.L., 7-12-53

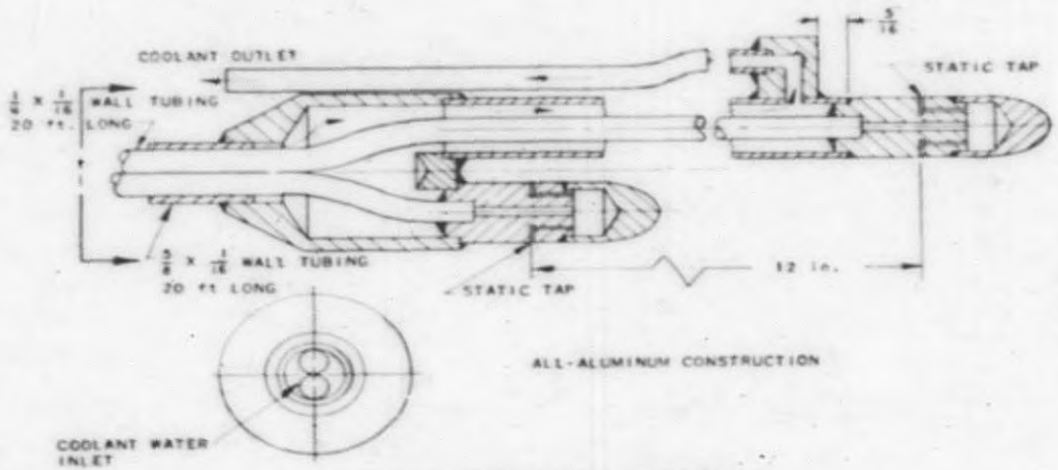

FIG. 37
WATER-COOLED DENSITY TUBES

RE-7-11408-A

Transient Tests - R. Schiltz

The requirement of a rapid response thermocouple, for observing fast fuel plate temperature changes, during the proposed power excursion BORAX tests resulted in the design of a thermocouple which is capable of measuring temperature transients of better than 25C/ms.

Transient tests of the thermocouple, in which each wire is individually percussion welded to the heat-emitting metal surface, were conducted by pulse resistance heating of the metal.

The apparatus, shown schematically in Figure 38, consisted of an 0.25 in. OD by 0.035 in. wall nickel tube 4 in. long at the center of which was welded a 22 gage (0.025 in. diameter) chromel-alumel thermocouple. Heating of the tube was provided by a low voltage transformer which was controlled by a timer and magnetic contactor in the primary circuit. An attempt to weld the two thermocouple wires in an equipotential plane to eliminate IR pickup due to the heating current was unsuccessful. Therefore the IR pickup was balanced by means of a potential obtained from a resistance circuit which in effect shifted the a-c potential of one lead to that of the other. The resistance of this balancing circuit was kept high (approximately 1000 ohms) to minimize the effect of a third thermocouple junction formed by it. The power measurements were made for the central 1 in. section of the heated element since it was felt that a temperature gradient existed from the center to each end. It was assumed that the temperature and heat flux were uniform in this section the mass of which was 3.65 gm.

The results of four tests are shown in Figures 39 and 40. The average rate of change of temperature varied from 25C/ms to 30C/ms. It will be noted that at power cut-off the temperature trace has reached at least 90% of its final value. This error is probably due to the thermocouple wires acting as heat sinks. The points of inflection in the temperature trace are what can be expected from a sinusoidal type heating.

The thermocouples which will be attached to the surface and core alloy of the fuel plates will be of 40-gage wire and thus should increase the response rate above that experimentally determined with the 22-gage couple wires. Figure 41 shows the details of the thermocouple mounting on the BORAX fuel plates.

HEAVY WATER BOILING REACTORS - FEASIBILITY STUDIES - M. Treshow

The reactor designs discussed below were developed as reference drawings for studies of atomic power plant economics. While it is recognized that a great deal of development work must be carried out both in the field of power plant engineering and reactor engineering, the designs are believed to limit the elements of uncertainty to a minimum.

R.J.SCHILTZ:W.I.K.,9-29-53

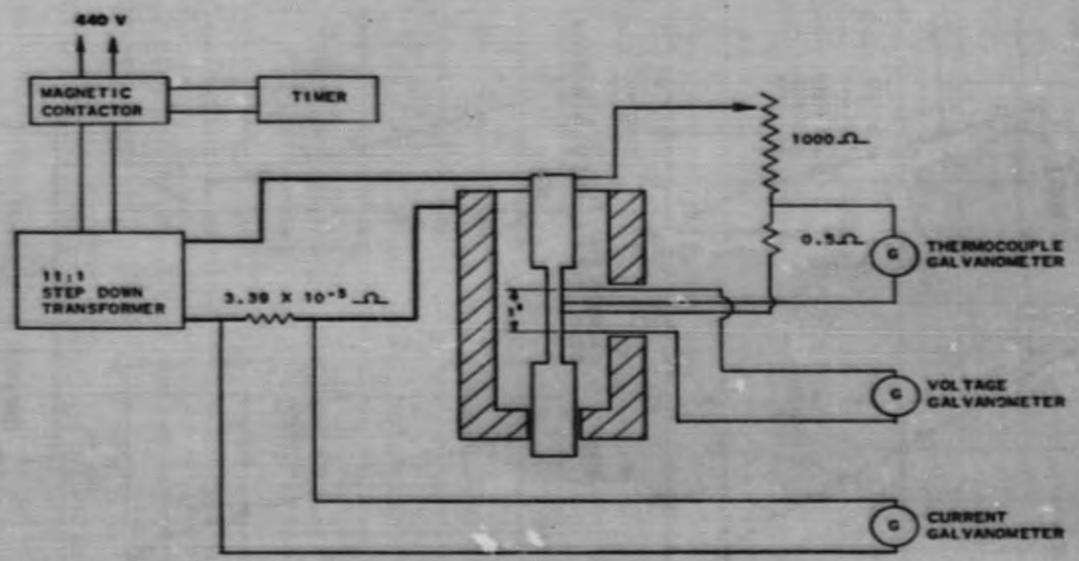

FIG. 38
THERMOCOUPLE RESPONSE APPARATUS

RE-7-11085-A

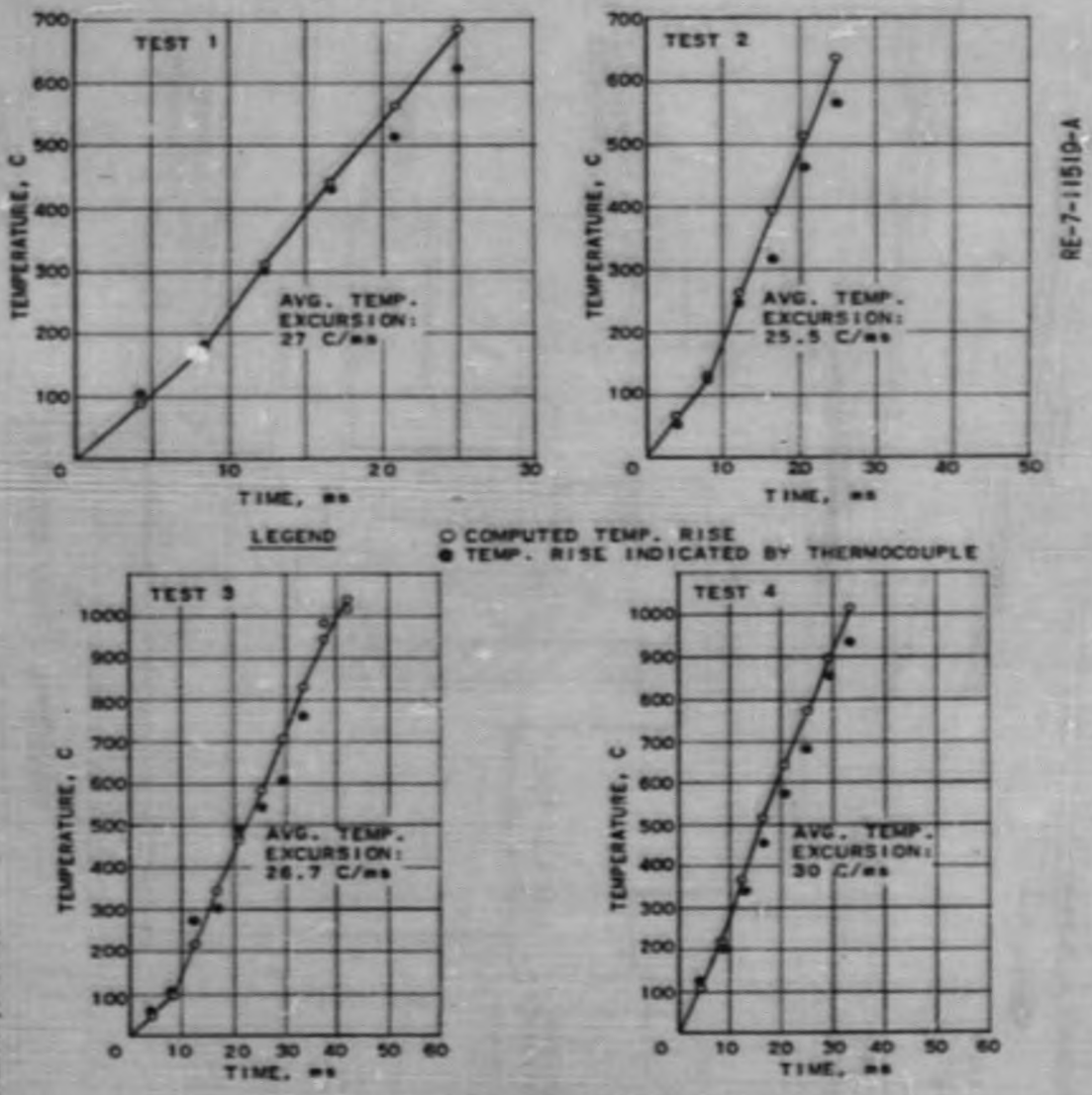

RE-7-11510-A

R. SCHILTZ: (A.E.C., 8-21-53)

FIG. 39
COMPARISON OF TEMPERATURE RISE OBSERVED AT INTERVAL OF 1/4 CYCLE WITH COMPUTED TEMPERATURE RISE

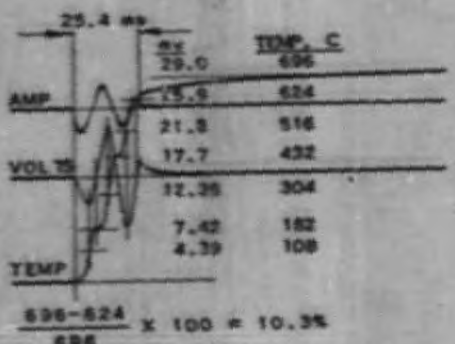

$\frac{696-624}{696}$ X 100 = 10.3%

AVG. TEMP. EXCURSION: 27 C/ms
TEST 1

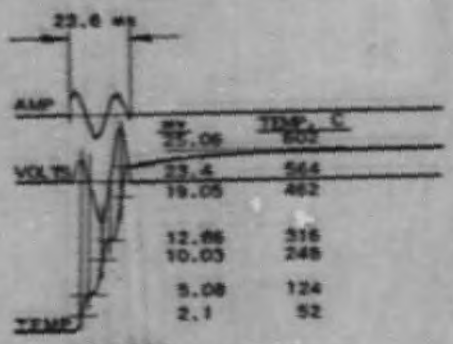

$\frac{602-564}{602}$ X 100 = 6.3%

AVG. TEMP. EXCURSION: 25.5 C/ms
TEST 2

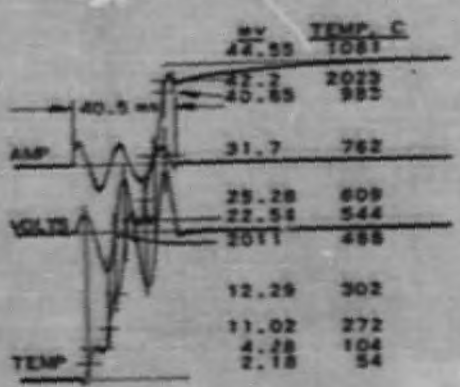

$\frac{1081-1023}{1081}$ X 100 = 5.4%

AVG. TEMP. EXCURSION: 26.7 C/ms
TEST 3

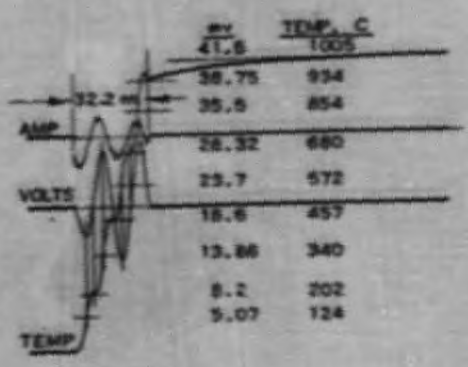

$\frac{1005-934}{1005}$ X 100 = 7.1%

AVG. TEMP. EXCURSION: 30 C/ms
TEST 4

FIG. 40
OSCILLOGRAPH TRACES OF
TEMPERATURE EXCURSIONS

RE-7-11513-A

R.J.SCHILTZ:E.A.K.,6-21-53

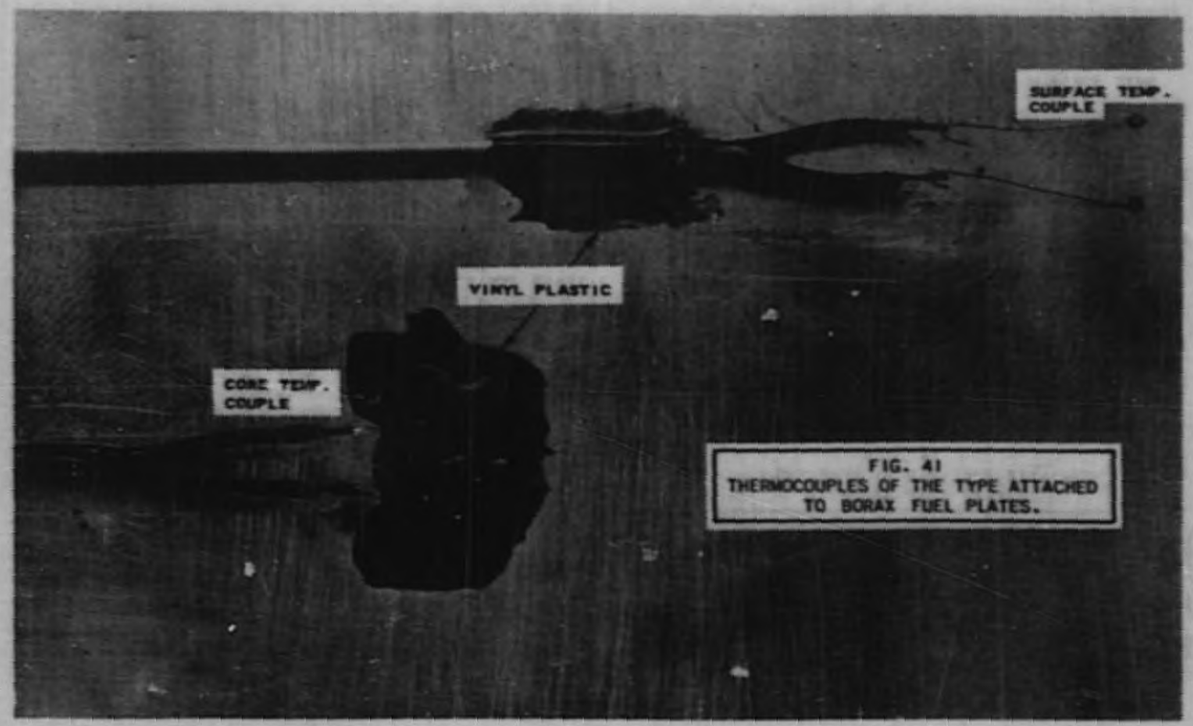

FIG. 41
THERMOCOUPLES OF THE TYPE ATTACHED TO BORAX FUEL PLATES.

A. General

1. Boiler Pressure

The obvious advantage in connection with Boiling Reactors or "Atomic Boilers" is that the steam is delivered to the power plant at "full value" at the same temperature and pressure which can be tolerated in the reactor. The steam cycle efficiency, therefore, can be higher than would be possible if secondary heat exchangers were employed.

The power which can be extracted from the channels in a boiling reactor depends largely on the mass flow of steam, and thereby on its density and pressure. This condition obviously encourages operating with high steam pressure. The reactor designs studied are considered for steam pressures of 500 to 700 psia. Superheating of this steam in a secondary reactor is visualized as a possible future step in the power plant development.

2. Temperature Coefficient

In case of heavy water boiling reactors the temperature and density characteristics are similar to those of pressurized reactors of the CP-7 type. This is self-evident up to the point where the boiling temperature is reached. The increased temperature will cause a gradual decrease in "k"; as boiling develops this will cause a further decrease.

It is essential that the change in reactivity is negative for any increase in bubble formation; this condition is easy to establish in case of D_2O-moderated reactors. The situation is more complicated for light water.

It is likewise important to avoid any too great variation in "k" related to small variations in the boiling. This might lead to very unstable conditions which could make control of the system problematic. It would also mean that the reactivity at the upper end of the reactor would be much smaller than at the lower end where the bubble formation has not yet started.

For this reason, it is an important advantage in case of D_2O boilers that the boiling can be confined to a relatively small area of each "cell." The water boils only inside the fuel tubes while most of the moderator area is unaffected. Therefore, the behavior of such boilers can be predicted reasonably well. Light-water boiling has much more influence on reactivity of a pile and conditions would be less predictable without experiments as a background.

The changes in reactivity associated with the rise in temperature and bubble formation are listed on page 89.

3. Fuel Elements.

Any water-cooled power reactor, boiling or not, depends on fuel plates and cladding having sufficient mechanical and chemical stability to withstand high temperature water and radiation for extended periods.

(1) The cladding and its welding must be completely tight and corrosion resistant.

(2) Radiation damage must not change the dimensions and cause the fuel to rupture the jacket.

(3) As far as possible, a metallurgical bond shall exist between fuel and cladding.

(4) Should a rupture or a "pin hole" occur, the subsequent rate of corrosion of the fuel alloy must be non-catastrophical, thus allowing time to exchange the damaged fuel assembly. The reactor designs provide for the use of unloading devices to permit exchange of fuel assemblies while the boiler is operating. In case the monitoring system should report a damaged fuel strip, it is hoped that the assembly can be exchanged before the damage has spread.

B. Boiling Reactor Type 1 - Spherical Boiler

1. Reactor Design

The preliminary design of a large-scale spherical boiling reactor was previously described in ANL-4843.[10]

The subsequent design shown in Figures 42 and 43 was based on the following specifications and assumptions:

(1) The heat transfer from fuel plates to coolant is accomplished by natural convection maintained by means of the lower density of boiling water in the tubes. Preliminary estimates indicated that this could be done at a satisfactory rate. Experiments are being conducted on a smaller scale with electrically heated plates, initial results are reported on page 59.

(2) A maximum heat flux of 300,000 Btu/(hr)(sq ft) was assumed. This value was derived from different sources and is believed to include a reasonable safety margin. No experiments "to full scale" have been attempted to conclusively determine the factor of safety.

[10] Reactor Engineering Division Semiannual Report, June 15, 1953.

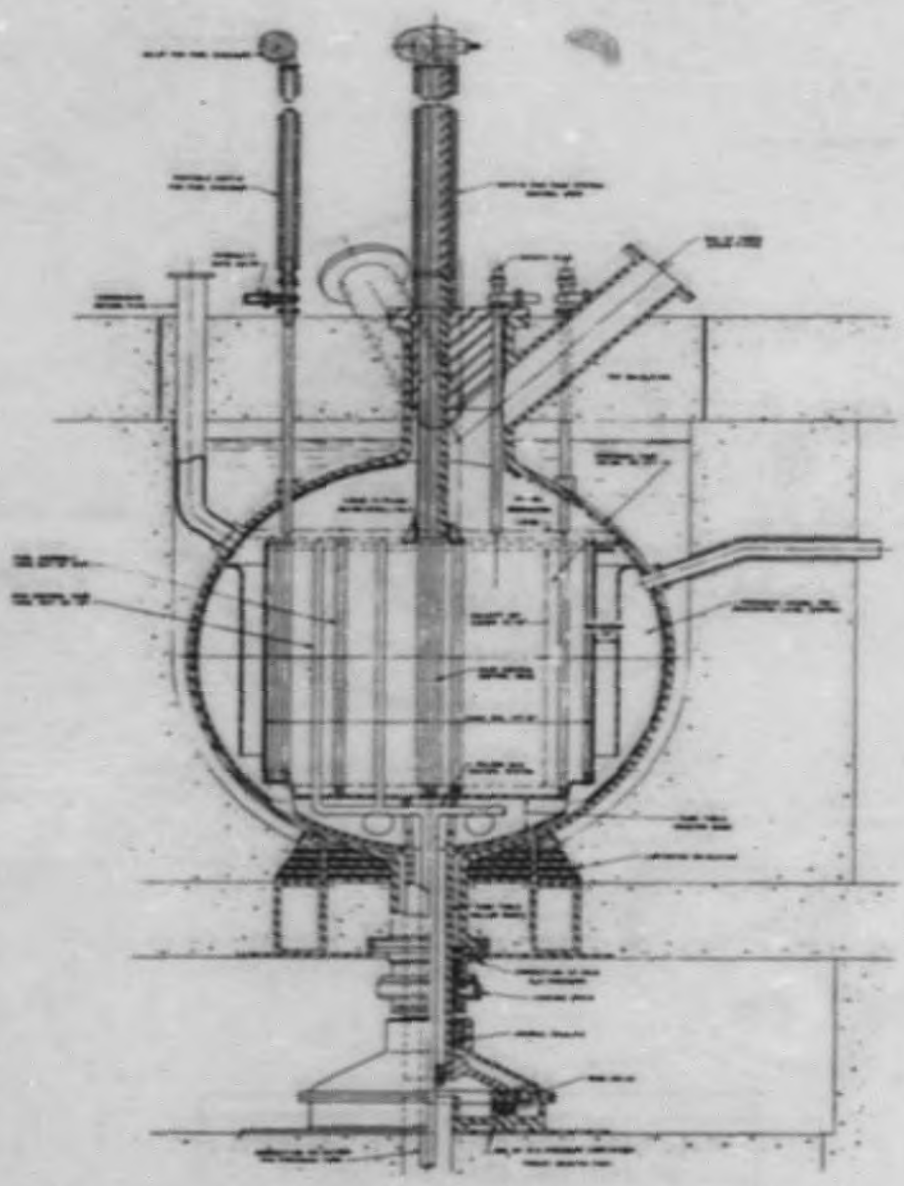

FIG. 42
VERTICAL SECTION OF
BOILING REACTOR TYPE I

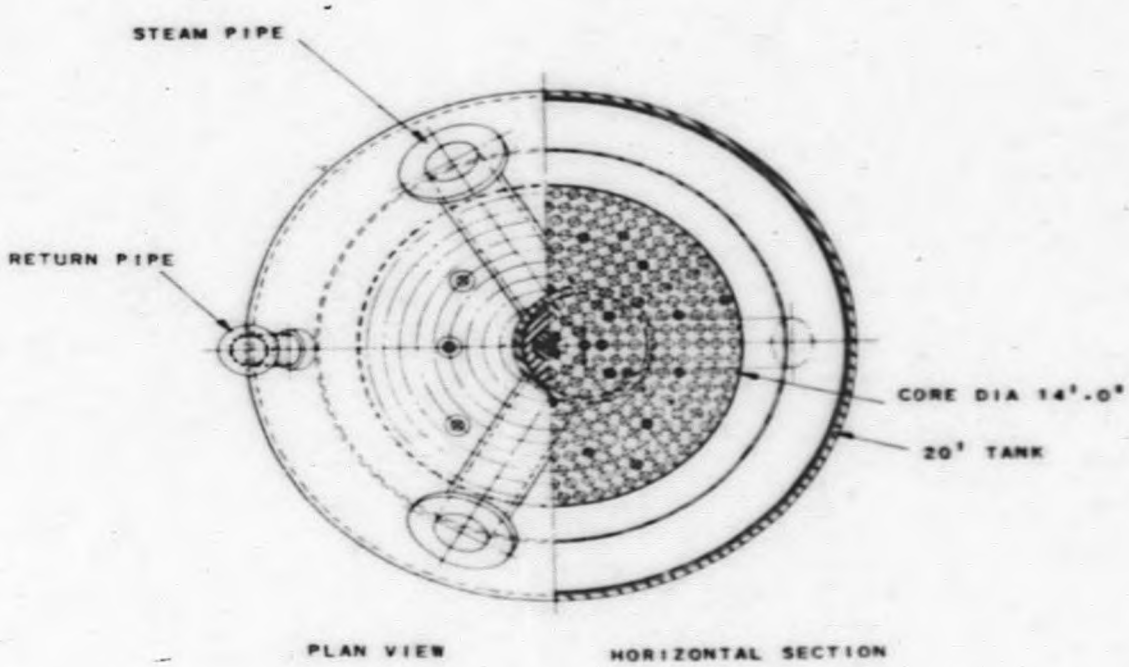

FIG. 43
PLAN VIEW AND HORIZONTAL SECTION
OF BOILING REACTOR TYPE I

(3) It was considered that the boiler tank could be built to operate safely at a pressure of 750 psi. The tank is spherical with a diameter of 20 ft. The spherical shape offers the best relative strength. The tensile stress in a 3 in. thick wall would be 15,000 psi under normal circumstances. This must, however, be considered in connection with a shell temperature close to 500F. The shell sections would have to be welded together in the field and stress relieving facilities would have to be provided.

(4) The design is considered to be the largest size feasible of this type and operating pressure. In fact, it is only made possible by avoiding the extensive perforation of the shell which is usually required for fuel exchange purposes; only ten such fuel holes have been allowed. The exchange of fuel assemblies is accomplished by having the reactor core installed on what amounts to a turntable inside the reactor tank. This feature can be engineered, but it could undeniably be the cause of complications with regard to safety devices and control rods.

(5) The total power rating of the reactor is estimated to be 1060 mw.

(6) Moisture separation would be accomplished by separators installed outside and above the reactor with the precipitated water drained back to the tank.

(7) Due to the movable reactor core, the control system must be essentially limited to central vertical rods, liquid poison tubes in the core and control by lowering the moderator and reflector level Furthermore, a change of steam pressure will change the fluid density and, thereby, the reactivity.

The subsequent reactor designs, Type II and III, are better suited for control rods throughout the core.

Design Data For Boiling Reactor Type I

Boiler tank diameter, ft	20
Core diameter, ft	14
Core height, ft	12
Number of fuel tubes in lattice	372
Number of control locations	22
Number of fuel exchange openings	10
Radial reflector thickness, in. D_2O	12

Vertical reflector at each end, in. D_2O	112
Lattice arrangement - fuel tubes spaced 7½ in. in concentric circles with 7½ in. radial increment	
Fuel in reactor, tons	50.6 (101,200 lbs)
Fuel assembles - Uranium plates 0.104 in. (buckled zone) and 0.124 in. (flat zone) with 0.010 in. zirconium cladding inside of stationary fuel tubes. Clearance between plates - 1/2 in.	
Fuel tubes - Zirconium tubes, 4½ in. ID with 0.030 in. walls	
Cooling surface, sq ft	19,000
Moderator and coolant	D_2O
Pressure, psi	720
Saturation Temperature, F	503
Total amount of D_2O in system, tons	160
Pile power generated, mw	1,060
Maximum flux for heat transfer, Btu/(hr)(sq ft)	300,000
Net electrical output if D_2O steam used directly, mw	282

2. Reactor Physics - H. P. Iskenderian

	Buckled Zone	Flat Zone
Thickness of fuel (no alloy)	.104	.124
Thickness with 0.010 in. zirconium clad added, in.	.124	.144
Enrichment, % of U^{235} in uranium	.82	.68
Weight of uranium in pile, lb	75,100	26,100
Net fuel thickness x % of U^{235}	.085	.085
Radius of flattened zone, ft		4.4
Height of flattened zone, ft		4.13
For hot, boiling condition:		
f (including xenon)	.94	.94
p	.814	.795

	Buckled Zone	Flat Zone
ϵ	1.035	1.035
η	1.397	1.307
k_∞	1.10	1.01
τ	232.	232.
L^2	108.	104.
M^2	340.	336.
B^2	283×10^{-4}	26.5×10^{-4}
% of power	69.5	30.5
Conversion ratio	.92	1.079
Average flux at 1,060 mw	7.2×10^{13}	9.1×10^{13}
Average conversion ratio for reactor	.955	
Average flux in reactor at 1,060 mw	8.4×10^{13}	
k_{eff} hot, boiling	1.00 (with xenon)	
k_{eff}, not boiling	1.035 (with xenon)	
k_{eff} room temperature (70F)	1.072 (with xenon)	
k_{eff} room temperature	1.129 (without xenon)	

C. Boiling Reactor Type II - Pressurized Tube System

1. Reactor Design

The Type II boiler was designed primarily to overcome the limitation in regard to size and power which is inherent in Type I, and, at the same time, to avoid the necessity of a movable core. When the size is not limited, the allowable heat flux can be chosen as low as desired for safety.

The reactor design is shown in Figures 44 and 45. The design is based on the following assumptions and requirements:

(1) Although natural convection contributes to the circulation of coolant the plans include motor-or turbine-driven circulating pumps which can handle any volume of liquid water that may be found necessary to secure the heat transfer from fuel plates to the boiling water in the tubes. The separation of water from the steam takes place in two steam drums placed above the reactor.

(2) The maximum heat flux permitted is taken to be 300,000 Btu/(hr)(sq ft). This should provide a margin of safety better than

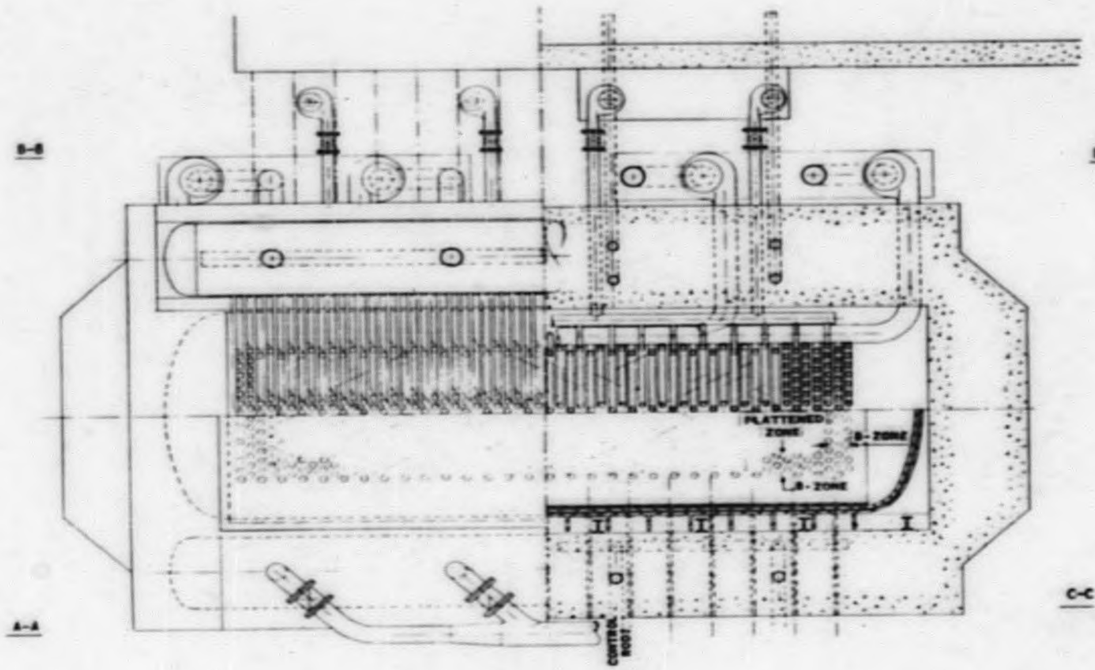

FIG. 44
PLAN VIEW OF BOILING REACTOR TYPE II

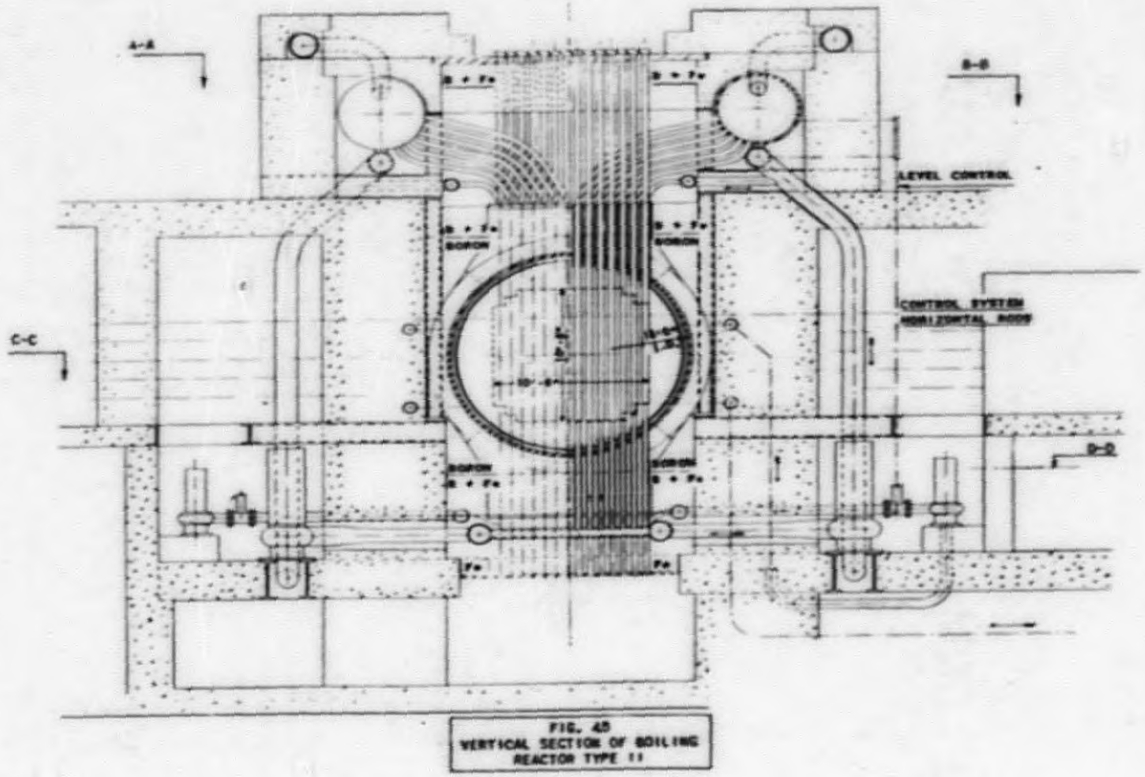

FIG. 45
VERTICAL SECTION OF BOILING
REACTOR TYPE II

100 %. However, realistic experiments will be needed before the exact factor will be known. This flexible design could take care of considerable variations in heat flux requirements.

(3) The structural strength of the boiler tank is no longer a great problem because the high pressure boiling water is confined to the tube system. The tank is primarily a moderator and preheater tank which arbitrarily carries a pressure approximately one-half that in the tube system. The water reaches a temperature of only 200F while in the tank. High temperatures are, therefore, avoided in the steel shell. The tank diameter is 16 ft. Its length, which determines the capacity of the boiler, is 44 ft. This is an important departure from the conventional reactor proportions.

(4) The tank is equipped with fuel exchange holes for each one of the fuel tubes. This is feasible due to the lower pressure in the tank and because the arrangement allows space for circumferential reinforcing rings between rows of fuel holes.

(5) The Type II design can be made for reactors of any large power rating which may be desired. The present plan is based on 2400 mw at a throttle pressure of 600 psi. Greater capacities would merely require a longer reactor and boiler tank. Furthermore, the system could be extended to steam pressures as high as 1000 psi if desired. The latter should only be considered if secondary cycles are used or if the boiler were to operate in connection with a super-heater, nuclear or conventionally heated.

(6) Increased clad thickness has been used in this reactor. The zirconium cladding is specified to be 0.020 in. minimum and not less than 0.040 in. at the edges of the fuel strips.

(7) The stationary pressure tubes which contain the fuel and the boiling water are 5 in. ID. They are spiral welded zirconium tubes (wall thickness 5/32 in.) designed to hold the pressure with a safety factor of 5. In case of an accident, it will be possible to replace any one of these tubes with most of the shielding intact.

(8) The control system consists of horizontal rods distributed between the fuel rods. There would be space enough for any number of rods which may be considered desirable.

The fuel is natural uranium in the buckled zone and slightly depleted uranium in the flattened zone (U^{235} = 0.635%). All the uranium is to be alloyed with 4% of zirconium for improved dimensional stability under irradiation.

Each fuel assembly consists of 37 fuel strips, which are flattened rods of zirconium clad fuel, 0.7 in. wide and 0.278 in. thick at the middle (flat zone) and 0.250 in. thick in the buckled zone.

Samples of fuel rods of this nature have been produced by the Argonne Metallurgy Division. When the originally round rods are rolled flat, the cladding material gains an increased thickness along the edges, which is an advantage for the present application with the fuel strips being supported only at points of the edges. The minimum thickness of cladding is 0.020 in. at the flat sides and 0.040 in. or more at the edges.

The water channels between strips are between 5/16 in. and 3/8 in. wide. The circulating water will be pumped into these channels with a minimum velocity of 5 fps increasing to about 30 fps at the top where one-seventh of the mass flow will have changed to steam. A cross section of a fuel assembly made of 37 such strips is shown in Figure 46 together with an alternate assembly which uses round rods furnished with helical ribs. The strips or rods are twisted in such a manner that they only touch on the edges or ribs while together. They form a hexagon bundle which is contained in a hexagon wrapper sheet of 0.030 zirconium. This whole cartridge forms the removable fuel assembly which is placed inside the 5-inch fuel or boiler tube in the reactor.

Pressure drop tests in two-phase flow have been conducted on a mock-up of an assembly of twisted strips; the results are reported on page 141.

Figure 47 shows the installation of the tube and fuel assembly. The segmental spaces between the fuel wrapper sheet and the 5 in. tube will fill up with slow moving liquid water, which functions as an insulating layer; it is estimated that not more than about 4% of the generated heat is transferred to the moderator by conduction through the tube walls. This heat serves to preheat the feedwater which passes through the moderator tank before entering the boiler tube system.

Design Data for Boiling Reactor Type II

Boiler tank diameter, ft	16
Core height, ft	10
Core width, ft	10½
Core length, ft	41
Reflector at each end and side, ft	1½
Reflector at top and bottom, ft	2
Width of flattened zone, ft	7

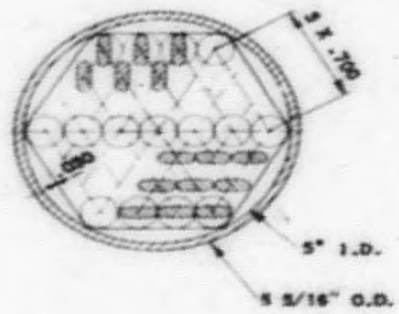

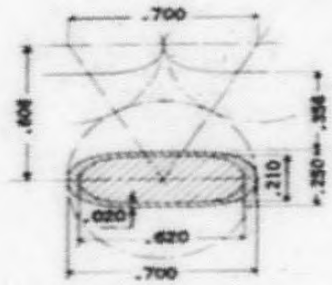

RIBBON TYPE.
TWISTED

NOTE:
DESIGN APPLIES TO SYSTEMS 4, 5, 6 AND 7
RIBBON DIMENSIONS SHOWN FOR BUCKLED ZONE.
FOR FLATTENED ZONE AND .028" TO THICKNESS.

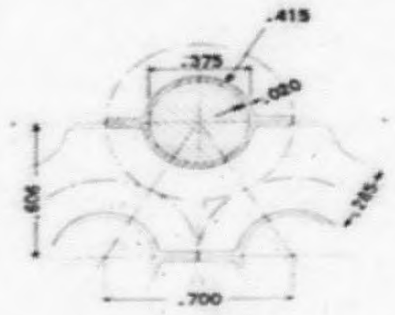

ROUND TYPE.
TWISTED

FIG. 48
CROSS SECTION OF FUEL ASSEMBLY.
BOILING REACTOR TYPE II

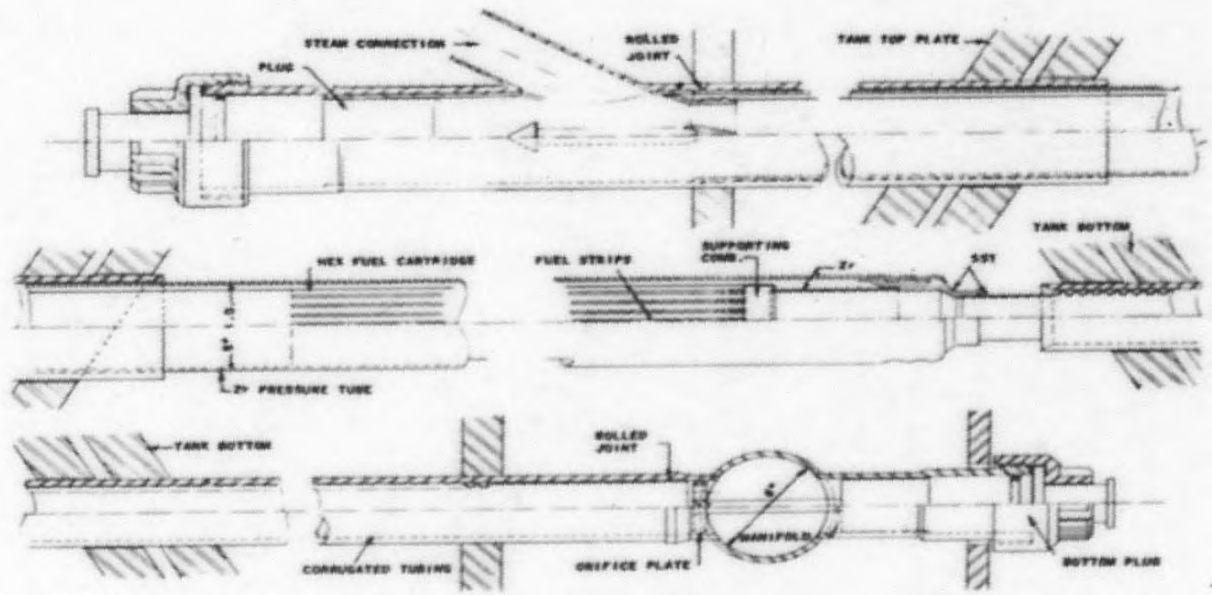

FIG. 47
TUBE AND FUEL ASSEMBLY.
BOILING REACTOR TYPE II

Length of flattened zone		36 ft 5 in.
Number of fuel tubes in reactor		840 (486 in flat zone + 354 in buckled zone)
Lattice arrangement	- 60 rows in length, spaced 8.2 in. times 14 rows in width, spaced 9 in.; every other of the 60 rows staggered to form a triangular lattice with approximately 60 deg angles.	
Fuel used in reactor	- 105,000 lb natural uranium in buckled zone plus 177,000 lb depleted uranium with U^{235} = 0.635% in flat zone.	
Total weight of uranium, tons		141
Fuel assemblies	- Uranium plus 4% zirconium alloy with 0.02 in. zirconium clad, 37 strips per tube; 0.70 in. wide.	
Cooling channel clearance, in.		5/16 to 3/8
Stationary fuel tubes	- Zirconium with 2½% tin spiral welded, 5 in. ID and 5/32 in. walls.	
Moderator D_2O		
Pressure, psia		250
Temperature, F		100-200
Boiling D_2O		
Pressure, psia		600
Temperature, F		486
Total amount of D_2O in system, tons		375
Total number of fuel tubes		840
Power transferred from cooling surface, mw		2280
Total reactor power, mw		2400
Cooling surface, sq ft		42,000
Maximum flux for heat transfer, Btu/(hr)(sq ft)		300,000
Net electrical output when D_2O steam used directly, mw		616
Steam production, lb/hr		7.7×10^6

Condenser back pressure, in. Hg	1½
Throttle pressure, psi	600
Condensate removed by intermediate separator	11% of flow at 25 psia
Total D_2O mass flow through reactor channels	7 times steam production

2. Reactor Physics - H. P. Iskenderian

	Buckled Zone	Flat Zone
Thickness of fuel including 4 wt % Zr alloy, in.	.210	.238
Thickness with 0.020 in. Zr clad added, in.	.250	.278
Enrichment, % of U^{235} in uranium	.72	.635
Net fuel thickness x % of U^{235}	.1348	.1348
For hot boiling condition:		
f (per lattice cell, including xenon)	.934	.936
p	.842	.829
ϵ	1.030	1.030
η	1.330	1.265
k_∞	1.078	1.010
τ	165.	165.
L^2	96.	92.
M^2	261.	257.
B^2	300×10^{-6}	38×10^{-6}
Number of fuel tubes	354.	486.
Conversion ratio	.922	1.047
Per cent of total power	37.8	62.2
Average flux at 2,400 mw	7.4×10^{13}	8.6×10^{13}
Exposure	754 mwd/ton = 44.3 days	
Average conversion ratio for reactor	1.00	
Average flux in reactor (2400 mw)	8.1×10^{13}	
Maximum/average flux, in width	1.04	
in height	1.24	
in length	1.02	

Maximum/average flux, within fuel tube cross section	1.17
Over-all maximum/average flux	1.54
k_{eff} hot, boiling, with xenon	1.00
k_{eff} hot, not boiling, with xenon	1.003
k_{eff} at room temperature, with xenon	1.016
k_{eff} at room temperature, without xenon	1.069

D. Boiling Reactor Type III - Horizontal Pressure Tank

The study of the specially designed semi-pressurized horizontal tank used in Type II revealed the possibility of building this type of tank for pressures as high as 600 psi. With this pressure limitation and with the same fluid for moderator and coolant, it would be possible to operate without extra strength of the fuel tubes within the reactor. This would, of course, result in considerable saving of zirconium and would lower the parasitic neutron absorption.

The proposed design of the Type III boiler is shown in Figures 48 and 49. The conditions applied to this type are as follows:

(1) As in the case of Type II, circulating pumps are depended on for sufficient coolant flow.

(2) The maximum heat flux allowed is 300,00 Btu/(hr)(sq ft).

(3) The structural strength of the tank depends on laminated reinforcing rings placed between the rows of fuel exchange openings. Furthermore, the shell temperature is kept low by means of the return condensate water. The pressure is limited to 600 psi.

(4) Inasmuch as the length of the tank and the reactor core are not limited, the total power capacity can be determined solely by economic considerations.

(5) The control system will consist of horizontal rods as in Type II.

(6) The steam outlets are all placed at the outer ends of the boiler tank to avoid conflict with the fuel openings.

(7) The upper segment of the tank forms the steam duct. The height of the reactor core will, therefore, be somewhat smaller than Type II if installed in the same size tank. This will decrease slightly the power output per unit length of tank.

(8) The preliminary moisture separation takes place at both ends of the boiler tank near the steam outlets.

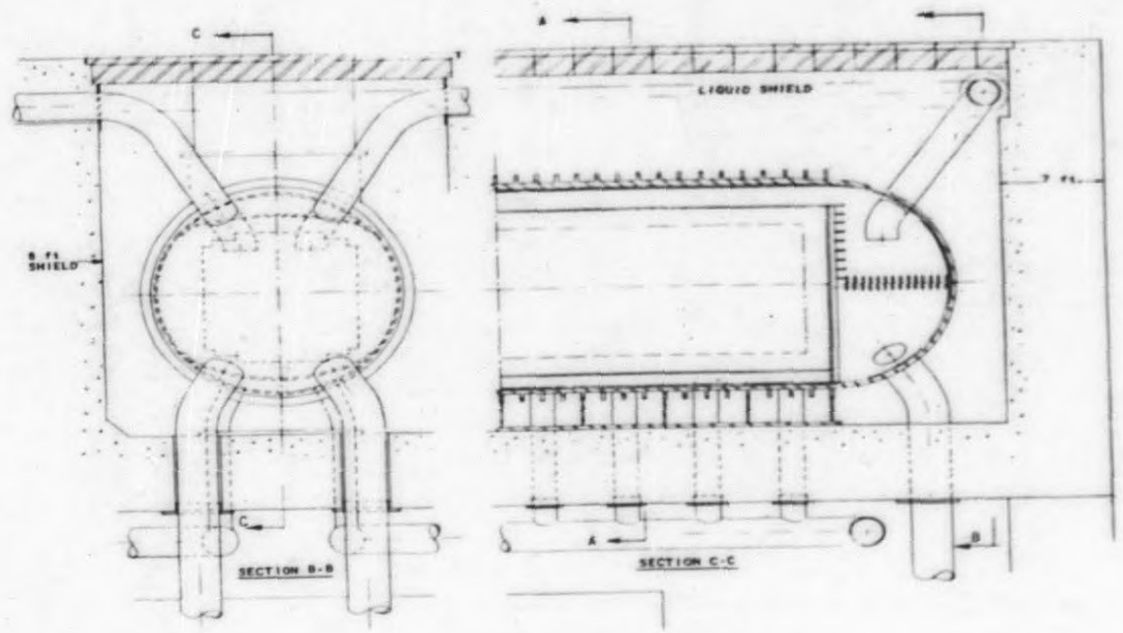

FIG. 48
VERTICAL SECTION OF BOILING REACTOR TYPE III

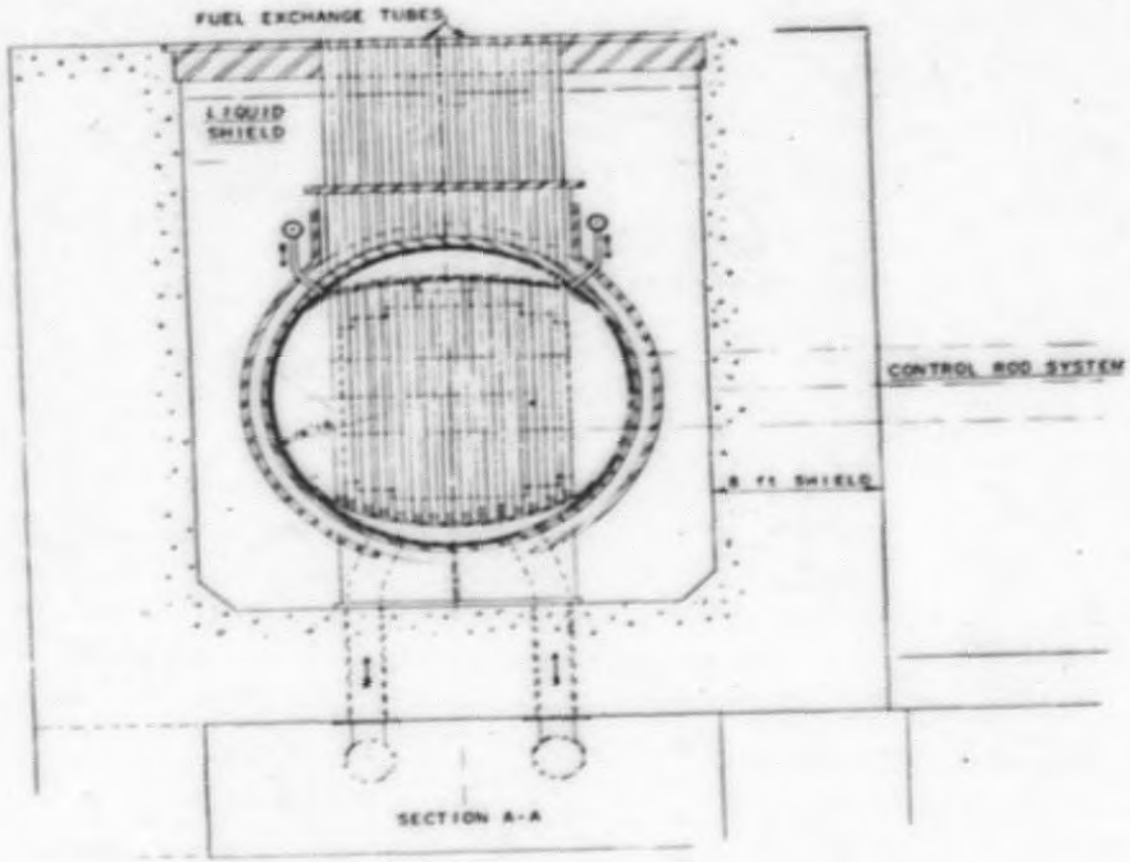

FIG. 49
VERTICAL CROSS SECTION OF BOILING REACTOR TYPE III

(9) The reactor is submerged in a concrete basin filled with water (suitably insulated) or oil for shielding.

(10) Only a temporary study has been made, as yet, of this design and its calculations. It is mentioned here as it would seem to be a type which would be practical for some intermediate size of a plant.

E. Heat Flux Limit in Boiling Reactors

As mentioned earlier, large scale experiments will be necessary in order to ascertain the heat flux limitations in the types of reactors discussed. However, the heat flux, defined as Btu/(hr)(sq ft), may not always serve as a criterion in determining the margin of safety; a large cooling surface and too small a flow of water passing through the cooling channels would result in a too high steam quality with too low cooling capacity.

At present, natural circulation in a reacter is uncertain. Not a great deal can be done to regulate this circulation. Forced circulation has been introduced in many modern boiler plants and would seem to be particularly useful in case of boiling power reactors with their higher rate of heat transfer per unit area.

Types II and III boiling reactors employ forced circulation to a rate of 7 lb of total flow passing through the reactor for each pound of steam generated. This is comparable to ratios used for existing operating boilers. The arrangement allows for a certain amount of orificing to be applied at the lower ends of such fuel tubes which might use too large a portion of the flow. The orifices can be changed as desired.

A preliminary estimate on the permissible heat flux in boiler Types II and III was calculated using the equation [11]

$$(q/a)\ \max = 4 \times 10^5 \times v^{1/3} + 4800\ (t_s - t) \times v^{1/3} \qquad (1)$$

Applying Eq. (1) to the point of the channels where the subcooling is zero and the water velocity is still at a minimum (equal to the inlet velocity (5.5 fps)) we get

$$(q/a)\ \max = 685{,}000\ \text{Btu/(hr) (sq ft)}$$

At this point of the channel, the actual heat flux is estimated to be 260,000, corresponding to 300,000 at the center. The factor of safety against burnout

---

[11] W. H. McAdams, et al, "Heat Transfer at High Rates to Water With Surface Boiling," ANL-4268, December, 1948.

should, therefore, be 2.6 as far as this transition point is concerned. Eq. (1) is considered applicable for velocities between 1 and 12 fps and for pressures from 30 to 90 psia. It is expected that the proposed higher pressures will increase the safety margin. The equation also refers to equivalent diameters of approximately 0.52 in., which are of the order of magnitude under consideration.

A report by Jens and Lottes[12] concludes that under the circumstances that applied to their experiments, burnouts occur when steam qualities are allowed to exceed 80% by weight. As mentioned previously, the vapor content in the Type II boiler tubes is only allowed to reach one-seventh of the total flow (steam quality = 14.2%). The report also refers to data from experiments carried out by Purdue and by UCLA. Some of these data dealing with net steam generation appear applicable; a few typical examples are tabulated.

Reported by	Mass Flow lb/(hr)(sq ft)	Per cent steam by weight	Per cent steam by volume	Burnout flux, Btu/(hr)(sq ft)	Pressure psia
UCLA	925,000	33.5	90.5	680,000	1,000
UCLA	890,000	37.0	90.	550,000	1,300
UCLA	3,890,000	7.1	58.3	1,080,000	1,100
Purdue	1,100,000	25.	94.	2,650,000	500
Purdue	910,000	31.	97.5	3,130,000	280
Purdue	970,000	18.	91.	2,850,000	500
Proposed Type II Boiling Reactor	940,000	14.2	86.	Suggested max. 300,000	650

To determine the amount of conservatism in this design, realistic boiling experiments of the type planned by the Heat Engineering Section will be necessary. In any case, it is felt that the controlled forced circulation will eliminate a great deal of the uncertainty.

The Type II reactor is considered to utilize, but is not limited to the use of moderator and coolant. The boiling liquid is confined to the high pressure tube system and it could be entirely separated from the moderator. It is conceivable that the coolant could be light water and that the moderator could be either heavy water or graphite. The present plan

[12] W. H. Jens, P. A. Lottes, "Analysis of Heat Transfer Burnout, Pressure Drop and Density Data for High-Pressure Water," ANL-4627, May, 1951.

is, therefore, merely one application of a system which employs an individual fuel tube system for pressurized boiling fluid. Heavy water is chosen in the present case due to the special emphasis on neutron economy.

If Type II is operated with same pressure in the tube system and in the moderator tank so that the tube wall thickness can be limited to 1/32 in., the conversion ratios can be improved by approximately 4%.

F. Effect of Some Design Conditions on Neutron Economy and Reactor Power

The boiling D_2O reactors which have been described above can be operated: (1) with natural circulation or forced circulation, (2) with equal pressures in reactor tank and fuel tubes, or (3) with excess pressure in the boiling fuel tube system. The power will depend on the system chosen.

Systems 1, 2, and 3 in Figure 50 employ natural circulation. The reactors are Types I, II, and III.

Systems 4, 5, 6, and 7 in Figure 51 employ forced circulation. The reactors are Type III for System 4 and Type II for Systems 5, 6, and 7.

System 1 is the reactor with a spherical tank, whereas System 6 is a Type II reactor with cylindrical tank and high pressure tubes. System 4 is a Type III reactor operated without excess tube pressure.

System 7 is different from the first six in that it contains both a primary D_2O cycle and a secondary H_2O cycle. The problem of keeping D_2O and H_2O separated would be transferred from the turbine condenser to the high pressure heat exchanger.

Typical characteristics for each of these systems are tabulated.

	System						
	1	2	3	4	5	6	7
Steam Cycles	direct	direct	direct	direct	direct	direct	Heat exch. to H_2O
Circulation	natural	natural	natural	forced	forced	forced	forced
Moderator temp, F (avg)	450	400	150	160	150	150	150
Moderator pressure, psi	780	520	520	520	620	250	450
Steam temp, F	503	468	468	468	496	496	518 D_2O, 500 H_2O
Tube wall thickness, in	1/32	1/32	1/32	1/32	1/32	5/32	5/32
Steam pressure, psi	700	500	500	500	600	600	800 D_2O, 500 H_2O
Estimated Conversion Ratio	.955	.97*	1.04	1.02*	1.04	1.00	.98*
Maximum reactor power, mw	1,960	2,000	2,000	2,000	2,400	2,400	2,400

*Rough evaluations obtained by comparison with the other more accurate figures

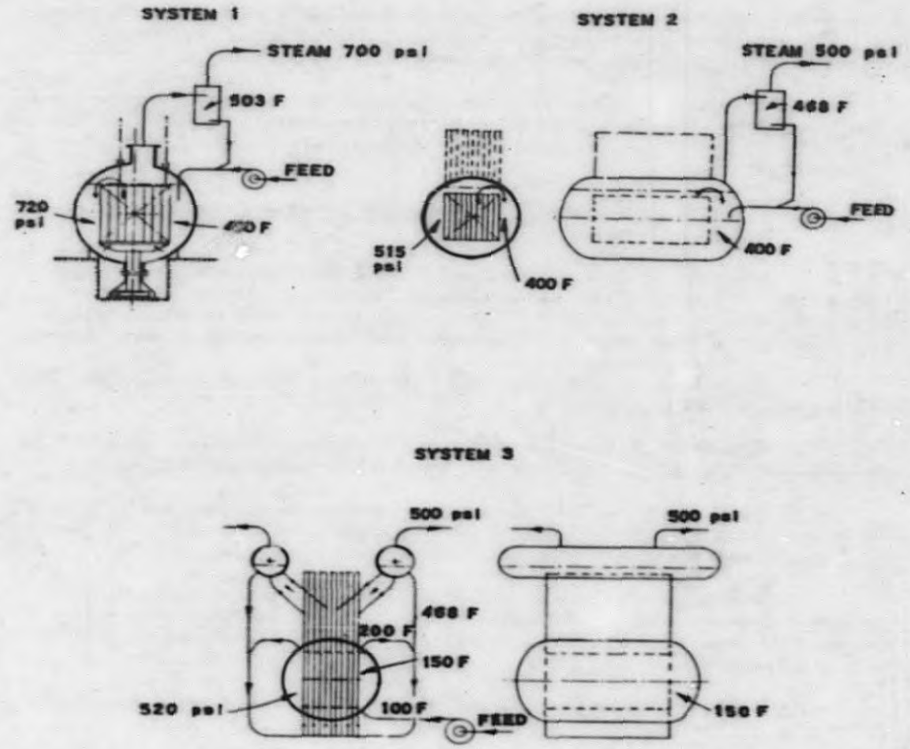

FIG. 50
BOILING REACTORS - NATURAL CIRCULATION

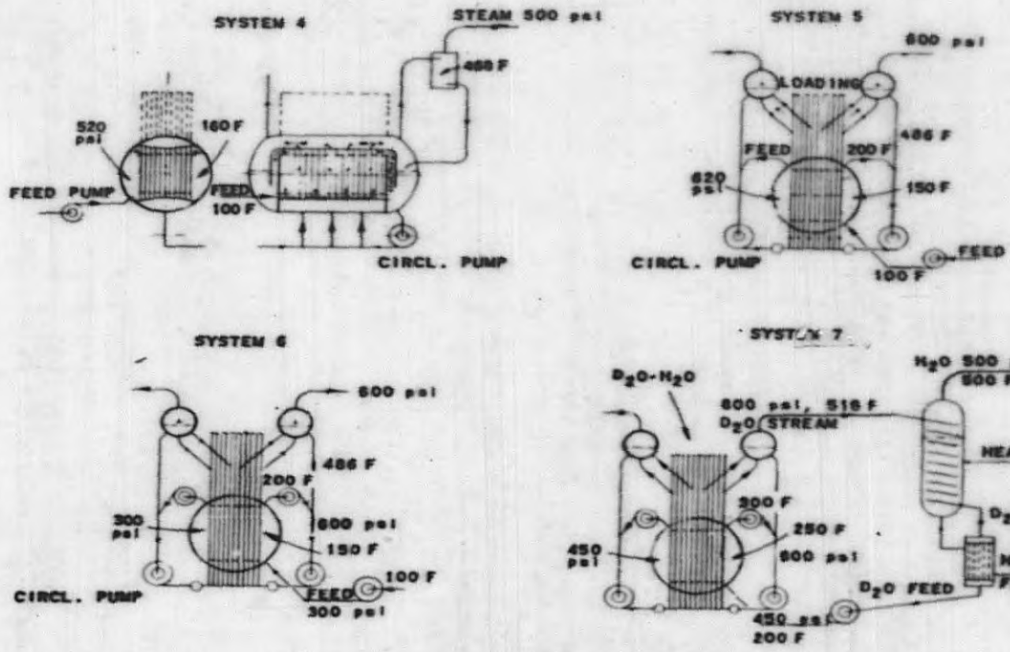

FIG. 51
BOILING REACTORS - FORCED CIRCULATION

REACTOR RESEARCH

REACTOR PHYSICS

A. Method for Calculation of Long-Term Changes in Reactors - R. Avery

During the lifetime of a power or production reactor some materials will build up or be burned out, control devices must be introduced in varying degree to maintain reactivity, and the flux and power distribution will change. The problem of calculating these and other related effects may be characterized by saying that we wish to determine: $n^j(r,x)$, the number of atoms per unit volume of material j at the point r at the "time" x; and $\phi^k(r,x)$, the neutron flux in the kth energy group at the point r at the "time" x, suitably normalized.

The variable x need not be the actual time. In some cases it may be more convenient to use some other variable to measure the age of the reactor (e.g., fractional burnup of the fuel, time integral of the flux, total number of fissions, etc.).

Although the flux is described in terms of a multi-group model, this is not essential to the method of solution. This is done for definiteness and also because multi-group diffusion theory techniques will probably be computationally the most feasible.

Before the quantities $n^j(r,x)$ and $\phi^k(r,x)$ are uniquely determinable, the initial distribution of atoms $n^j(r,o)$, which must correspond to a critical assembly, and the type of control must be specified.

We define x to be the cumulative neutron path length per unit volume in the first (highest) energy group at r = 0 (i.e., x is the integral of the product of the time and the flux in the first energy group at r = 0).

We also define:

$$\phi^k(r,x) = \frac{\text{path length in kth energy group at r at "time" x}}{\text{unit path length in first energy group at r = 0}}$$

Therefore, $\phi^k(r,x)$ is proportional to the neutron flux with the normalization $\phi^{k=1}(o,x) = 1$.

The essence of the following method for obtaining the functions $n^j(r,x)$ and $\phi^k(r,x)$ is to expand both of the functions in a power series in x.

$$n^j(r,x) = n_0^j(r)+xn_1^j(r)+x^2n_2^j(r)+x^3n_3^j(r)+ \ldots\ldots \quad (1)$$

$$\phi^k(r,x) = \phi_0^k(r)+x\phi_1^k(r)+x^2\phi_2^k(r)+x^3\phi_3^k(r)+\ldots\ldots \quad (2)$$

From $n_0^j(r)$, the initial distribution of atoms one can obtain $\phi_0^k(r)$, the initial flux distribution. Having obtained $\phi_0^k(r)$ one can then obtain $n_1^j(r)$. Knowing $n_1^j(r)$ one then obtains $\phi_1^k(r)$ from which one obtains $n_2^j(r)$ and so forth, alternating between the $n_\alpha^j(r)$ and the $\phi_\beta^k(r)$. The series approaches the true solution so that one cuts off the series when the desired degree of accuracy has been reached. Where this point will be depends primarily on how large a value of x is being considered (i.e., the degree of burnout). A detailed description of the method now follows:

We begin by requiring that the steady-state diffusion equation be satisfied identically in x (i.e., at all times).

$$\nabla\cdot\frac{1}{3\sum_j n^j(r,x)\sigma^j_{tr\ k}}\nabla\phi^k(r,x) - \sum_j n^j(r,x)\left[\sigma^j_{a\ k}+\sigma^j_{r\ k}\right]\phi^k(r,x) \quad (3)$$

$$+\sum_{\ell=1}^{k-1}\left(\sum_j n^j(r,x)\sigma^j_{\ell-k}\right)\phi^\ell(r,x)+\beta_k\sum_{\ell=1}^{G}\left(\sum_j \nu^j n^j(r,x)\sigma^j_{f\,\ell}\right)\phi^\ell(r,x) = 0$$

$k = 1,\cdots, G$

where G = number of groups,

σ^j_{ik} = the microscopic cross section for i-th event in material j for energy group k

i = a, absorption (fission + capture)

c, capture

f, fission

r, removal by scattering (elastic + inelastic)

tr, transport

$\sigma_{r\ell-k}$ is the cross section for transfer by scattering from 1 th to kth group

β_k, fraction of fission neutrons born in group k

ν^j, number of neutrons emitted per fission by material j.

Symbolically Eq. (3) may be written:

$$H(r,x)\,\Phi(r,x) = 0$$

If we now substitute Eq. (1) and (2) into Eq. (3), and then collect terms containing the same power of x, we obtain an equation:

$$H_0(r)\Phi_0(r)+xH_1(r)\Phi_1(r)+x^2H_2(r)\Phi_2(r)+\cdots\cdots = 0 \qquad (4)$$

where:

$$H_0(r)\Phi_0(r) = \nabla\cdot D_0^k(r)\,\nabla\phi_0^k(r) - \left(\sum_j n_0^j(r)\left[\sigma_a^{j\,k}+\sigma_r^{j\,k}\right]\right)\phi_0^k(r)+\sum_{\ell=1}^{k-1}\left(\sum_j n_0^j(r)\sigma_r^{j\,\ell-k}\right)\phi_0^\ell(r)$$

$$+\beta_k\sum_{\ell=1}^{G}\left(\sum_j \nu^j n_0^j(r)\sigma_f^{j\,\ell}\right)\phi_0^\ell(r)$$

$$H_1(r)\Phi_1(r) = \nabla\cdot D_0^k(r)\,\nabla\phi_1^k(r) - \left(\sum_j n_0^j(r)\left[\sigma_a^{j\,k}+\sigma_r^{j\,k}\right]\right)\phi_1^k(r)+\sum_{\ell=1}^{k-1}\left(\sum_j n_0^j(r)\sigma_r^{j\,\ell-k}\right)\phi_1^\ell(r)$$

$$+\beta_k\sum_{\ell=1}^{G}\left(\sum_j \nu^j n_0^j(r)\sigma_f^{j\,\ell}\right)\phi_1^\ell(r)+\nabla D_1^k(r)\,\nabla\phi_0^k(r) - \left(\sum_j n_1^j(r)\left[\sigma_a^{j\,k}+\sigma_r^{j\,k}\right]\right)\phi_0^k(r)$$

$$+\sum_{\ell=1}^{k-1}\left(\sum_j n_1^j(r)\sigma_r^{j\,\ell-k}\right)\phi_0^\ell(r)+\beta_k\sum_{\ell=1}^{G}\left(\sum_j \nu^j n_1^j(r)\sigma_f^{j\,\ell}\right)\phi_0^\ell(r)$$

$$H_2(r)\Phi_2(r) = \nabla\cdot D_0^k(r)\,\nabla\phi_2^k(r) - \left(\sum_j n_0^j(r)\left[\sigma_a^{j\,k}+\sigma_r^{j\,k}\right]\right)\phi_2^k(r)+\sum_{\ell=1}^{k-1}\left(\sum_j n_0^j(r)\sigma_r^{j\,\ell-k}\right)\phi_2^\ell(r)$$

$$+\beta_k\sum_{\ell=1}^{G}\left(\sum_j \nu^j n_0^j(r)\sigma_f^{j\,\ell}\right)\phi_2^\ell(r)\;\nabla\cdot D_2^k(r)\nabla\phi_0^k(r) - \left(\sum_j n_2^j(r)\left[\sigma_a^{j\,k}+\sigma_r^{j\,k}\right]\right)\phi_2^k(r)$$

$$+\sum_{\ell=1}^{k-1}\left(\sum_j n_1^j(r)\sigma_r^{j\,\ell-k}\right)\phi_1^\ell(r)+\beta_k\sum_{\ell=1}^{G}\left(\sum_j \nu^j n_1^j(r)\sigma_f^{j\,\ell}\right)\phi_1^\ell(r)+\nabla\cdot D_2^k(r)\nabla\phi_0^k(r)$$

$$-\left(\sum_j n_2^j(r)\left[\sigma_a^{j\,k}+\sigma_r^{j\,k}\right]\right)\phi_0^k(r)+\sum_{\ell=1}^{k-1}\left(\sum_j n_2^j(r)\sigma_r^{j\,\ell-k}\right)\phi_0^\ell(r)+\beta_k\sum_{\ell=1}^{G}\left(\sum_j \nu^j n_2^j(r)\sigma_f^{j\,\ell}\right)\phi_0^\ell(r)$$

etc.

$$k = 1, \cdots\cdots, G$$

and

$D_{\ell}^{k}(r)$ is defined by:

$$\frac{1}{3\sum_{j}\left[n_0^j(r)+xn_1^j(r)+x^2n_2^j(r)+\cdots\cdots\right]\sigma_{tr\,k}^{j}} = D_0^k(r)+xD_1^k(r)+x^2D_2^k(r)+\cdots\cdots$$

The requirement that Eq. (4) holds for all x implies that

$$H_0(r)\phi_0(r) = 0 \tag{5a}$$

$$H_1(r)\phi_1(r) = 0 \tag{5b}$$

$$H_2(r)\phi_2(r) = 0 \tag{5c}$$

etc.

In addition to the requirement that the steady-state diffusion equation be satisfied for all x (in each region) we also require that for all x the usual boundary conditions be satisfied, i.e., continuity of flux and current across boundaries, vanishing of flux at outer (extrapolated) boundary, finiteness everywhere, etc. The boundary conditions on the flux imply that each of the ϕ_{ℓ} have to satisfy the boundary conditions, since they are to be satisfied for all x.

$$\left.\begin{aligned} &\phi_0^k(\text{interface}) \\ &\phi_1^k(\text{interface}) \\ &\phi_2^k(\text{interface}) \end{aligned}\right\} \quad \text{Each continuous across boundaries} \tag{6a, 6b, 6c}$$

etc.

and

$$\phi_0^k(\text{outer boundary}) = 0 \tag{7a}$$

$$\phi_1^k(\text{outer boundary}) = 0 \tag{7b}$$

$$\phi_2^k(\text{outer boundary}) = 0 \tag{7c}$$

etc.

To satisfy the condition of continuity of current, $\vec{J}$, we have that

$$-\vec{J}^k(r,x) = D^k(r,x)\nabla\phi^k(r,x)$$

$$= \left[D_0^k(r)+xD_1^k(r)+x^2D_2^k(r)+\cdots\right]\nabla\left[\phi_0^k(r)+x\phi_1^k(r)+x^2\phi_2^k(r)+\cdots\right]$$

$$= D_0^k(r)\nabla\phi_0^k(r)+x\left[D_0^k\nabla\phi_1^k(r)+D_1^k(r)\nabla\phi_0^k(r)\right]$$

$$+x^2\left[D_0^k(r)\,\phi_2^k(r)+D_1^k(r)\nabla\phi_1^k(r)+D_2^k(r)\nabla\phi_0^k(r)\right]+\cdots$$

has to be continuous across boundaries for all x, or

$$D_0^k(r)\nabla\phi_0^k(r) \qquad (8a)$$

$$D_0^k(r)\nabla\phi_1^k(r)+D_1^k(r)\nabla\phi_0^k(r) \qquad (8b)$$

$$D_0^k(r)\nabla\phi_2^k(r)+D_1^k(r)\nabla\phi_1^k(r)+D_2^k(r)\nabla\phi_0^k(r) \qquad (8c)$$

} Each must be continuous across boundaries

etc.

In addition, from the normalization of $\phi_1^{k-1}(0,x) = 1$, we have as a normalization on the $\phi^k(r)$

$$\phi_0^1(o) = 1 \qquad (9a)$$

$$\phi_1^1(o) = 0 \qquad (9b)$$

$$\phi_2^1(o) = 0 \qquad (9c)$$

etc.

The equations in (5) are to be solved under the boundary conditions in (6), (7), (8) and (9).

Eq. (5a), which represents the reactor in its initial condition may be solved immediately. We now show how having obtained $\phi_\alpha^k(r)$ we can obtain $n_1^j(r)$ and in general, obtain $n_\alpha^j(r)$ once we know all the $\phi_{\beta<\alpha}^k(r)$, so that we can alternate between the ϕ and the n to obtain as many terms as desired.

From Eq. (1) we have:

$$\frac{dn^j(r,x)}{dx} = -n_1^j(r)+2xn_2^j(r)+3x^2n_3^j(r)+\cdots\cdots \qquad (10)$$

But we may also obtain:

$$\frac{dn^j(r,x)}{dx} = -n^j(r,x)\sum_{k=1}^{G}\sigma_{a\,k}^{j}\phi^k(r,x)+n^p(r,x)\sum_{k=1}^{G}\sigma_{(p\to j)\,k}^{p}\phi^k(r,x) \qquad (11)$$

where p labels the type of atom (if any) which produced atom j through some reaction of cross section $\sigma_{p\to j}$. We now substitute Eq. (1) and (2) into the right hand side of Eq. (11), equate it to the right hand side of Eq. (10), and finally equating terms which equal powers of x in the resulting equation, we obtain:

$$n_1^j(r) = -n_0^j(r)\sum_{k=1}^{G}\sigma_{a\ k}^{j}\phi_0^k(r)+n_0^p(r)\sum_{k=1}^{G}\sigma_{(p-j)\ k}^{p}\phi_0^k(r) \tag{12a}$$

$$n_2^j(r) = 1/2\left\{-n_1^j(r)\sum_{k=1}^{G}\sigma_{a\ k}^{j}\phi_0^k(r)-n_0^j(r)\sum_{k=1}^{G}\sigma_{a\ k}^{j}\phi_1^k(r)\right. \tag{12b}$$

$$\left.+n_1^p(r)\sum_{k=1}^{G}\sigma_{(p-j)\ k}^{p}\phi_0^k(r)+n_0^p(r)\sum_{k=1}^{G}\sigma_{(p-j)\ k}^{p}\phi_1^k(r)\right\}$$

$$n_3^j(r) = 1/3\left\{-n_2^j(r)\sum_{k=1}^{G}\sigma_{a\ k}^{j}\phi_0^k(r)-n_1^j(r)\sum_{k=1}^{G}\sigma_{a\ k}^{j}\phi_1^k(r)-n_0^j(r)\sum_{k=1}^{G}\sigma_{a\ k}^{j}\phi_2^k(r)\right. \tag{12c}$$

$$\left.+n_2^p(r)\sum_{k=1}^{G}\sigma_{(p-j)\ k}^{p}\phi_0^k(r)+n_1^p(r)\sum_{k=1}^{G}\sigma_{(p-j)\ k}^{p}\phi_1^k(r)+n_0^p(r)\sum_{k=1}^{G}\sigma_{(p-j)\ k}^{p}\phi_2^k(r)\right\}$$

Having applied Eq. (12a), using the ϕ_0^k obtained in the solution of (5a), and thus having obtained the n_1^j we are in a position to solve Eq. (5b). At this stage a decision as to the type of control desired has to be made. If in Eq. (5b) we use only the n_1^j obtained from the original n_0^j, in general there will be no solution to Eq. (5b) satisfying the boundary conditions given by Eqs. (6b), (7b), (8b) and (9b). This, of course, is due to the fact that, in general, the reactor either loses or gains reactivity with time and is therefore, no longer critical unless control devices are introduced. We, therefore, introduce one or more $n_1^{control}(r)$ into Eq. (5b) such that it yields a solution satisfying the boundary conditions. The control associated with the $n_1^{control}(r)$ is, therefore, control that has to be introduced linearly in x.

Having obtained a solution to Eq. (5b) one then applies Eq. (12b) in order to evaluate the $n_2^j(r)$. These $n_2^j(r)$ are then used in Eq. (5c) along with some new $n_2^{control}(r)$ necessary to achieve criticality. The control associated with this $n_2^{control}(r)$ has to be introduced quadratically in x.

So far nothing has been said about the actual solution of the various equations (5). Equation (5a) is, of course, the usual criticality equation and can be solved by the usual multi-group diffusion theory techniques. The subsequent equations given by (5) are of the same nature except that instead of being a set of linear homogeneous differential equations they also include inhomogeneous terms (containing the previously determined ϕ's). However the multi-group equations are solved by iteration assuming an inhomogeneous fission source, so that the presence of additional fixed inhomogeneous terms should cause no basic difficulty. The same limitations on geometry will exist as in an ordinary criticality problem. Thus, if the problem is being worked in spherical symmetry we can only introduce control devices having this symmetry.

In an actual problem, there usually will be only a few type atoms in whose long term changes of concentration we are interested. The others, say the structure and coolant atoms, even if they suffer transmutations the resultant atoms have nuclear properties which are sufficiently unchanged to make it unnecessary to find the change in concentrations. Also, even for the atoms in whose long term changes we are interested, there may be certain nuclear properties, such as the scattering cross section, which are unchanged by the transmutations. If this is the case, then one would certainly simplify the problem by not considering any changes in these macroscopic cross sections (i.e., set the $n^j_{\alpha>0}(r) = 0$ whenever they multiply the microscopic cross sections of these unchanged properties.

Once we have obtained the functions $n^j(r,x)$ and $\phi^k(r,x)$ to the desired number of terms, we might wish to express the results in terms of some variable other than x and therefore want the relationship between this variable and x. This will usually be fairly easy to do. For example, suppose that we wish to operate the reactor at a total constant power corresponding to P fissions per second, and want the relationship between the time, t, and x. Let:

$$N^F(x) = xN_1 + x^2N_2 + x^3N_3 + \cdots \tag{13}$$

be the number of fissions that have occurred in the reactor at time x.

$$\frac{dN^F(x)}{dx} = N_1^F + 2xN_2^F + 3x^2N_3^F + \cdots \tag{14}$$

Let us also assume that atoms of type A and B are the fissionable ones. Therefore:

$$\frac{dN^F(x)}{dx} = \int \left(\sum_{k=1}^{G} \left[n^A(r,x)\sigma_{f\,k}^A + n^B(r,x)\sigma_{f\,k}^B \right] \phi^k(r,x) \right) dV \tag{15}$$

Expanding $n(r,x)$ and $\phi(r,x)$ in the right hand side of (15) and equating terms corresponding to equal powers of x with those in the right hand side of (14) we obtain:

$$N_1^F = \int \left(\sum_{k=1}^{G} \left[n_0^A(r)\sigma_{1_k}^A + n_0^B(r)\sigma_{1_k}^B \right] \phi_0^k(r) \right) dV \tag{16a}$$

$$N_2^F = 1/2 \int \sum_{k=1}^{G} \left(\left[n_1^A(r)\sigma_{1_k}^A + n_1^B(r)\sigma_{1_k}^B \right] \phi_0^k(r) + \left[n_0^A(r)\sigma_{1_k}^A + n_0^B(r)\sigma_{1_k}^B \right] \phi_1^k(r) \right) dV \tag{16b}$$

etc.

By definition $N^F(x) = Pt$. Therefore, from Eq. (13) we obtain:

$$t = \frac{1}{P} \left[xN_1^F + x^2 N_2^F + x^3 N_3^F + \cdots \right] \tag{17}$$

which gives us the relation between t and x.

There are, however, cases, where it will not be possible to defer to the end of the problem the relationship of x and some other variables which can be used to measure the age of the reactor, particularly the time.

In Eq. (11), it has tacitly been assumed that the transmutation of one atom to another occurred directly with some microscopic cross section and that no radioactive decay period was involved. Usually, in the chains of interest this is not always true, but often it is a good enough approximation. However, if the approximation is not sufficiently good we may proceed as follows. It is, of course, now necessary to specify the conditions under which the reactor will operate (i.e., at what power of flux level). Let us take the same example as before, operation at constant power of P fissions per second. Furthermore, let us now assume that as in Eq. (11) atoms of the type j may be produced from atoms of type p with the cross section $\sigma_{(p\to j)}$ but in addition are also produced by radioactive decay from atoms of type d with a time constant λ^d. Also instead of being destroyed only by absorption of a neutron we assume that type j atoms may also be destroyed by decay with a time constant λ^j. If we include all these processes the analogous equation to Eq. (11) becomes:

$$\frac{dn^j(r,x)}{dx} = -n^j(r,x) \sum_{k=1}^{G} \sigma_{a_k}^j \phi^k(r,x) + n^p(r,x) \sum_{k=1}^{G} \sigma_{(p\to j)k}^p \phi^k(r,x) - n^j(r,x)\lambda^j \frac{dt}{dx} + n^d(r,x)\lambda^d \frac{dt}{dx} \tag{18}$$

From Eq. (17) we have:

$$\frac{dt}{dx} = \frac{N_1^F}{P} + \frac{2N_2^F x}{P} + \frac{3N_3^F x^2}{P} + \ldots \qquad (19)$$

Comparing Eqs. (10) and (18) and, as usual, equating terms with equal powers of x we have:

$$n_1^j(r) = -n_0^j(r)\left(\sum_{k=1}^{G} \sigma_a^j{}_k \phi_0^k(r) + \frac{\lambda^j N_1^F}{P}\right) + n_0^P(r) \sum_{k=1}^{G} \sigma^P_{(P-j)k} \phi_0^k(r) + n_0^d(r) \frac{\lambda^d N_1^F}{P} \qquad (20a)$$

$$n_2^j(r) = 1/2 \left\{ -n_1^j(r)\left(\sum_{k=1}^{G} \sigma_a^j{}_k \phi_0^k(r) + \frac{\lambda^j N_1^F}{P}\right) - n_0^j(r) \sum_{k=1}^{G} \sigma^P_{(P-j)k} \phi_1^k(r) + \frac{2\lambda^j N_2^F}{P} \right. \qquad (20b)$$

$$\left. + n_1^P(r) \sum_{k=1}^{G} \sigma^P_{(P-j)k} \phi_0^k(r) + n_0^P(r) \sum_{k=1}^{G} \sigma^P_{(P-j)k} \phi_1^k(r) + n_1^d(r) \frac{\lambda^d N_1^F}{P} + 2n_0^d(r) \frac{\lambda^d N_2^F}{P} \right\}$$

etc.

From Eq. (16) we see that N_1^F depends only on n_0 and ϕ_0 and therefore $n_1^j(r)$ may be directly evaluated; N_2^F depends on n_0, n_1, ϕ_0 and ϕ_1, all of which are already known by the time $n_2^j(r)$ is to be calculated. Therefore, the calculation is carried on in the same sequence, except that now, of course, it depends on the power, since the various $n_a^j(r)$ depend on the power.

B. One-Group Calculation of Long-Term Changes in a Spherically Symmetric Fast Converter.

The method described above has been applied to calculate some of the long term changes in a fast converter. The model used is that of a spherical core 50 cm in radius surrounded by a spherical blanket 60 cm thick. The core and blanket compositions are initially uniform. For simplicity, the problem is treated in a one-group picture and the solution carried only to the first order correction in the flux distribution and to the second order in the atomic concentrations.

With the above simplifications the problem can be solved analytically. The chief difficulty of the one group pictures is the lack of an appropriate fission cross section for U^{238}, particularly near the core blanket interface where the energy distribution and hence the average U^{238} fission cross section

is a very rapidly varying function of position. In an attempt to reduce this difficulty the fission cross section of U^{238}, as such, was set equal to zero, and its effect was taken into account as a "fast fission effect." Specifically, the fission cross sections of the other fissionable isotopes were increased by an amount designed to take into account the U^{238} fissions. The main error introduced by this method is that it neglects the diffusion of the neutrons from the place of birth to where they cause a fast fission. Thus the fast fissions in the inner region of the blanket which are caused by neutrons leaking from the core will not be accounted for, but will be assumed to occur in the outer regions of the core. However, this effect should not vary particularly with time and, therefore, the results of this calculation, which are primarily concerned with effects which do vary with time, can be adjusted, with results obtained from a two-group calculation, so as to largely correct this error.

The atoms whose concentrations as a function of time and position will be investigated, are:

U^{235} (25)

U^{238} (28)

Pu^{239} (49)

Pu^{240} (40)

Fission Products (F); by one "atom" of F we mean the fission products resulting from one fission.

The structure and coolant atoms (S and C), are assumed to not change from their initial concentrations. We take into account the effect on reactivity due to absorption of neutrons by the fission products, but they are, of course, not thereby assumed to be destroyed. Therefore, the number of fission product "atoms" is also a record of the number of fissions that have occurred and their rate of growth corresponds to the fission rate. In this calculation all radioactive decay periods will be neglected.

Defining x as the cumulative neutron path length at r = 0, and $\phi(r,x)$ as the ratio of the path length at r to that at r = 0 at "time" x, we have:

$$\frac{dn^{25}(r,x)}{dx} = -\sigma_a^{25}\, n^{25}(r,x)\phi(r,x) \qquad (1a)$$

$$\frac{dn^{28}(r,x)}{dx} = -\sigma_a^{28}\, n^{28}(r,x)\phi(r,x) \qquad (1b)$$

$$\frac{dn^{49}(r,x)}{dx} = \left[\sigma_c^{28}\, n^{28}(r,x) - \sigma_a^{49}\, n^{49}(r,x)\right] \phi(r,x) \qquad (1c)$$

$$\frac{dn^{40}(r,x)}{dx} = \left[\sigma_c^{49}\, n^{49}(r,x) - \sigma_a^{40}\, n^{40}(r,x)\right] \phi(r,x) \tag{1d}$$

$$\frac{dn^{F}(r,x)}{dx} = \left[\sigma_f^{25}\, n^{25}(r,x) + \sigma_f^{28}\, n^{28}(r,x) + \sigma_f^{49}\, n^{49}(r,x) + \sigma_f^{40}\, n^{40}(r,x)\right] \phi(r,x) \tag{1e}$$

$$\frac{dn^{S\ \&\ C}(r,x)}{dx} = 0 \tag{1f}$$

also, expanding n and ϕ in a power series in x, we have

$$n^{j}(r,x) = n_0^{j}(r) + x n_1^{j}(r) + x^2 n_2^{j}(r) + \cdots \tag{2}$$

$$\phi(r,x) = \phi_0(r) + x\phi_1(r) + x^2\phi_2(r) + \cdots \tag{3}$$

$$\frac{dn^{j}(r,x)}{dx} = n_1^{j}(r) + 2x n_2^{j}(r) + \cdots \tag{4}$$

Substituting Eqs. (2) and (3) into (1) and then equating terms of equal powers of x in the right hand sides of Eqs. (1) and (4), we obtain:

$$n_1^{25}(r) = -\sigma_a^{25} n_0^{25}(r)\phi_0(r) \tag{5a}$$

$$n_2^{25}(r) = -1/2\left\{\sigma_a^{25} n_1^{25}(r)\phi_0(r) + \sigma_a^{25} n_0^{25}(r)\phi_1(r)\right\} \tag{5b}$$

$$= 1/2\left\{(\sigma_a^{25})^2 n_0^{25}(r)\phi_0^2(r) - \sigma_a^{25} n_0^{25}(r)\phi_1(r)\right\}$$

$$n_1^{28}(r) = -\sigma_a^{28} n_0^{28}(r)\phi_0(r) \tag{6a}$$

$$n_2^{28}(r) = 1/2\left\{(\sigma_a^{28})^2\, n_0^{28}(r)\phi_0^2(r) - \sigma_a^{28}(-)\phi_1(r)\right\} \tag{6b}$$

$$n_1^{49}(r) = \left[\sigma_c^{28} n_0^{28}(r) - \sigma_a^{49} n_0^{49}(r)\right]\ \phi_0(r) \tag{7a}$$

$$n_2^{49}(r) = 1/2\left\{\left[-\sigma_c^{28}\sigma_a^{28} n_0^{28}(r) - \sigma_a^{49}\sigma_c^{28} n_0^{28}(r) + (\sigma_a^{49})^2 n_0^{49}(r)\right]\ \phi_0^2(r)\right. \tag{7b}$$

$$\left. + \left[\sigma_c^{28} n_0^{28}(r) - \sigma_a^{49} n_0^{49}(r)\right]\ \phi_1(r)\right\}$$

$$n_1^{40}(r) = \left[\sigma_c^{49} n_0^{49}(r) - \sigma_a^{40} n_0^{40}(r)\right]\ \phi_0(r) \tag{8a}$$

$$n_2^{40}(r) = 1/2\left\{\left[\sigma_c^{49}\sigma_c^{28} n_0^{28}(r) - \sigma_c^{49}\sigma_a^{49} n_0^{49}(r) - \sigma_a^{40}\sigma_c^{49} n_0^{49}(r) + (\sigma_a^{40})^2 n_0^{40}(r)\right]\ \phi_0^2(r)\right. \tag{8b}$$

$$\left. + \left[\sigma_c^{49} n_0^{49}(r) - \sigma_a^{40} n_0^{40}(r)\right]\ \phi_1(r)\right\}$$

$$n_1^{F}(r) = \left[\sigma_f^{25} n_0^{25}(r) + \sigma_f^{28} n_0^{28}(r) + \sigma_f^{49} n_0^{49}(r) + \sigma_f^{40} n_0^{40}(r)\right]\ \phi_0(r) \tag{9a}$$

$$n_1^F(r) = 1/2 \left\{ \left[-\sigma_f^{25}\sigma_a^{25}n_0^{25}(r) - \sigma_f^{28}\sigma_a^{28}n_0^{28}(r) + \sigma_f^{49}\sigma_c^{28}n_0^{28}(r) - \sigma_f^{49}\sigma_a^{49}n_0^{49}(r) + \sigma_f^{40}\sigma_c^{49}n_0^{49}(r) \right.\right.$$
$$\left.\left. - \sigma_f^{40}\sigma_a^{40}n_0^{40}(r) \right] \phi_0^2(r) + \left[\sigma_f^{25}n_0^{25}(r) + \sigma_f^{28}n_0^{28}(r) + \sigma_f^{49}n_0^{49}(r) + \sigma_f^{40}n_0^{40}(r) \right] \phi_1(r) \right\} \quad (9b)$$

$$n_1^S \text{ \& } C(r) = n_2^S \text{ \& } C(r) = 0 \quad (10)$$

We assume that none of the changes in atomic concentrations will have any effect on the scattering properties and, therefore, each region will retain its uniform diffusion constant.

The one-group diffusion equations for each region are, with the assumptions that have been made,

$$D_0\nabla^2\phi_0(r) + C_0\phi_0(r) = 0 \quad (11a)$$

$$D_0\nabla^2\phi_1(r) + C_0\phi_1(r) + C_1\phi_0(r) + C_2\phi_0^2(r) = 0 \quad (11b)$$

where,

$$C_0 = \sum_j n_0^j \sigma^j$$

$$C_1 = \sum_j b_1^j \sigma^j$$

$$C_2 = \sum_j a_{10}^j \sigma^j$$

$$\sigma^j = \nu^j\sigma_f^j - \sigma_a^j$$

$$n_1^j(r) = a_{10}^j \phi_0(r).$$

The a_{10}^j being defined through Eqs. (5a) to (9a), and b_1^j represents the atoms that are inserted linearly in x for control purposes.

Equation (11) was obtained by substituting Eqs. (2) and (3) into the one-group diffusion equations and then requiring that each of the coefficients of the various powers of x shall separately equal zero. Equation (11a) corresponds to the constant term and (11b) to the term linear in x.

$$\text{Let } k_c^2 = \frac{C_{oc}}{D_{oc}}$$

and

$$k_B^2 = -\frac{C_{oB}}{D_{oB}}$$

The solution of Eq. (11a) is:

$$\phi_{oc}(r) = \frac{\sin k_c r}{k_c r}$$

and

$$\phi_{oB}(r) = A_{oB} \frac{\sinh k_B(R_B - r)}{k_B r}$$

ϕ_{oc} satisfies the required normalization condition, $\phi_o(o) = 1$. A_{oB} is an arbitrary constant which is to be determined by the boundary conditions. The solution of Eq. (11b) is:

$$\phi_{1c}(r) = A_{1c} \frac{\sin k_c r}{k_c r} + \frac{C_{1c}}{2C_{oc}} \cos k_c r + \frac{C_{2c}}{4k_c r C_{oc}} \left\{ \cos k_c r \left[3Si(k_c r) - Si(3k_c r) \right] - \sin k_c r \left[Ci(k_c r) - Ci(3k_c r) \right] \right\} \tag{14}$$

and

$$\phi_{1B}(r) = A_{1B} \frac{e^{k_B r}}{k_B r} + B_{1B} \frac{e^{-k_B r}}{k_B r} - \frac{C_{1B}}{2C_{oB}} A_{oB} \cosh k_B(R_B - r) - \frac{C_{2B} A_{oB}^2}{8k_B r C_{oB}} \left\{ 2 \left[e^{k_B r} Ei(-k_B r) - e^{-k_B r} Ei(k_B r) \right] + e^{-2k_B R_B} \left[e^{-k_B r} Ei(3k_B r) - e^{k_B r} Ei(k_B r) \right] + e^{2k_B R_B} \left[e^{-k_B r} Ei(-k_B r) - e^{k_B r} Ei(-3k_B r) \right] \right\} \tag{15}$$

where

$$Si(x) = \int_0^x \frac{\sin t}{t} dt \qquad Ei(x) = \int_{-\infty}^x \frac{e^t}{t} dt$$

$$Ci(x) = \int_\infty^x \frac{\cos t}{t} dt \qquad -Ei(-x) = \int_x^\infty \frac{e^{-t}}{t} dt$$

and are all well tabulated functions.

A_{1c}, A_{1B}, and B_{1B} are arbitrary constants to be determined by the boundary conditions. C_{1c} and C_{1B} are not arbitrary but one or both of them will be adjusted (thereby determining the amount and type of control) so that the boundary conditions will be satisfied.

The boundary conditions on ϕ_1 are:

$$\phi_{1c}(o) = 0 \tag{16a}$$

$$\phi_{1B}(R_B) = 0 \tag{16b}$$

$$\phi_{1c}(R_c) = \phi_{1B}(R_c) \tag{16c}$$

$$D_{oc}\frac{d\,\phi_{1c}(R_c)}{dr} = D_{oB}\frac{d\,\phi_{1B}(R_c)}{dr} \tag{16d}$$

The last boundary condition is of this simple form only because we have assumed that the diffusion constants remain unchanged. Had this assumption not been made, the boundary condition on the current at the interface would have been:

$$D_{oc}\frac{d\,\phi_{1c}(R_c)}{dr} + D_{1c}(R_c)\frac{d\,\phi_{oc}(R_c)}{dr} = D_{oB}\frac{d\,\phi_{1B}(R_c)}{dr} + D_{1B}(R_c)\frac{d\,\phi_{oB}(R_c)}{dr} \tag{16d'}$$

In some problems we might be willing to assume that the scattering properties are unchanged by the various nuclear reactions, but want to consider the possibility of introducing uniform scattering into a region for control. In that case all of the above equations would hold, with (16d') replacing (16d) and the definition of C_1 in Eq. (11b) containing the additional term, $-\frac{D_1}{D_o} C_o$.

$$C_1 = -\frac{D_1}{D_o} Co + \sum_j b_1^j \sigma^j$$

However, this type of control will not be used in this problem.

The following constants and cross sections are used. The composition of core and blanket is initially:

Core	Blanket	
R_c = 50 cm	R_B = 110 cm	t = 60 cm
$^{25}_{28}$ } 0.30		
Na 0.55	0.20	
Fe 0.15	0.10	

The relative amounts of 25 and 28 were determined by the condition that the reactor be initially critical.

The following microscopic cross sections (barns) were used.

	25	28	49	40	fission (product) "atoms" F	Na	Fe
σ_a	1.9	0.25	2.1	--	0.4	0.0008	0.03
σ_c	0.3	0.19	0.2	--	0.4	0.0008	0.03
σ_{core}	2.825	-0.25	4.396	--	-0.4	-0.0008	-0.03
$\sigma_{blanket}$	3.25	-0.25	5.005	--	-0.4	-0.0008	-0.03
σ_{tr}	7.0	7.0	7.0	--	---	3.5	3.5
σ_f	1.6	---	1.9	--	0	0	0
$Nx10^{-24}$	0.0482	0.0482	---	--	---	0.022	0.0847

We assume that:

$$\left(\frac{\text{fissions 28}}{\text{fissions 25}}\right)_{core} = .18 \qquad \left(\frac{\text{fissions 28}}{\text{fissions 25}}\right)_{blanket} = .29$$

$$\left(\frac{\text{fissions 28}}{\text{fissions 49}}\right)_{core} = .21 \qquad \left(\frac{\text{fissions 28}}{\text{fissions 49}}\right)_{blanket} = .336$$

in obtaining σ_{core} and $\sigma_{blanket}$ for 25 and 49 where $\sigma = \nu\bar{\sigma}_f - \sigma_a$.

and

$$\bar{\sigma}_f^{25} = \left[1 + \frac{\text{fissions 28}}{\text{fissions 25}}\right]$$

or

$$\bar{\sigma}_f^{49} = \sigma_f^{49}\left[1 + \frac{\text{fissions 28}}{\text{fissions 49}}\right]$$

From the blanket composition and the cross section we obtain:

$D_{oB} = 1.18529$

$C_{oB} = -.00845644$, $k_n = .0844659$

$y = k_B t = 5.06795$

$z = k_B R_c = 4.2233$

The core diffusion constant is independent of the 25 to 28 ratio and is:

$$D_{oc} = 1.7403$$

If we define $x = k_c R_c$, the initial criticality equation is:

$$x \cot x = 1 - \frac{D_{oB}}{D_{oc}} (1 + z \coth y)$$

which yields

$$x = 2.39007,$$

from which we obtain:

$$C_{oc} = .0039765,\ k_c = .0478013$$

$$n_{oc} = .0025959 \times 10^{24} \text{ and } \frac{\text{Vol 25}}{\text{total volume}} = .053857$$

From the boundary conditions at the interface we obtain:

$$A_{oB} = .0151904$$

The initial flux distribution is, therefore:

$$\phi_{oc}(r) = \frac{\sin .0478013\ r}{.0478013\ r} \tag{17a}$$

$$\phi_{oB}(r) = .17984 \frac{\sinh .0844659\ (110 - r)}{r} \tag{17b}$$

C_{2c}, and C_{2B} may now be calculated and are:

$$C_{2c} = -.00524506 \times 10^{-24}$$

$$C_{2B} = .033653 \times 10^{-24}$$

We choose to obtain criticality by adjusting C_{1c} for criticality and setting C_{1B} equal to zero (i.e., we will introduce enough uniform cross section in the core to maintain criticality but will introduce no control in the blanket).

The set of four equations (16) may now be solved for the four unknowns A_{1c}, C_{1c}, A_{1B} and B_{1B} and we obtain:

$$\begin{aligned} 10^{24} A_{1c} &= -.00035456 \\ 10^{24} C_{1c} &= .00288396 \\ 10^{24} A_{1B} &= -.53762 \times 10^{-4} \\ 10^{24} B_{1B} &= 63.954 \end{aligned} \tag{18}$$

The resulting flux distribution $\phi_1(r)$ becomes:

$$10^{24}\phi_{1c}(r) = -.00035456\,\frac{\sin k_c r}{k_c r} + .362622\cos k_c r - .329750\, f_c(k_c r) \qquad (19a)$$

where

$$f_c(\alpha) = \frac{1}{\alpha}\left\{\cos\alpha\left[3Si(\alpha)-Si(3\alpha)\right] - \sin\alpha\left[Ci(\alpha)-Ci(3\alpha)\right]\right\}$$

and

$$10^{24}\phi_{1B}(r) = -.53762\times10^{-4}\,\frac{e^{k_B r}}{k_B r} + 63.954\,\frac{e^{-k_B r}}{k_B r} - .00022957\, f_B(k_B r) \qquad (19b)$$

where:

$$f_B(\alpha) = \frac{1}{\alpha}\left\{2\left[e^{\alpha}Ei(-\alpha) - e^{-\alpha}Ei(\alpha)\right] + e^{-2k_B R_B}\left[e^{-\alpha}Ei(3\alpha) - e^{3\alpha}Ei(\alpha)\right] + e^{2k_B R_B}\left[e^{-\alpha}Ei(-\alpha) - e^{3\alpha}Ei(-3\alpha)\right]\right\}$$

The fluxes $\phi_0(r)$ and $\phi_1(r)$ are plotted in Figure 52. The flux distribution at any x is given in this first order approximation by:

$$\phi(r,x) = \phi_1(r) + x\phi_1(r)$$

where x is defined as the integral of the product of the time and the flux at r = 0.

The fluxes $\phi_0(r)$ and $\phi_1(r)$ defined in Eqs. (17) and (18), together with the value of C_{1c} which stipulates the amount of control necessary, and the various $n_1^j(r)$ and $n_2^j(r)$ defined by Eqs. (5) through (9) and which may now be evaluated complete the solution of the problem in this approximation.

The total number of the various type atoms in the core or blanket can be obtained from the integrals of the functions $\phi_0(r)$, $\phi_0^2(r)$, $\phi_1(r)$ over the core or blanket. These functions can be evaluated analytically by straight forward methods. Their numerical values in this problem are:

$$\frac{1}{V_c}\int_{core}\phi_{0c}(r)\,dV = .533738 \qquad \frac{1}{V_B}\int_{blanket}\phi_{0B}(r)\,dV = .0254315$$

$$\frac{1}{V_c}\int_{core}\phi_{0c}^2(r)\,dV = .317393 \qquad \frac{1}{V_B}\int_{blanket}\phi_{0B}(r)\,dV = .00300191$$

$$\frac{1}{V_c}\int_{core}\phi_{1c}(r)\,dV = .135433\times10^{-24} \qquad \frac{1}{V_B}\int_{blanket}\phi_{1B}(r)\,dV = .0165598\times10^{-24}$$

R.AVERY:T.W.L.,7-14-53

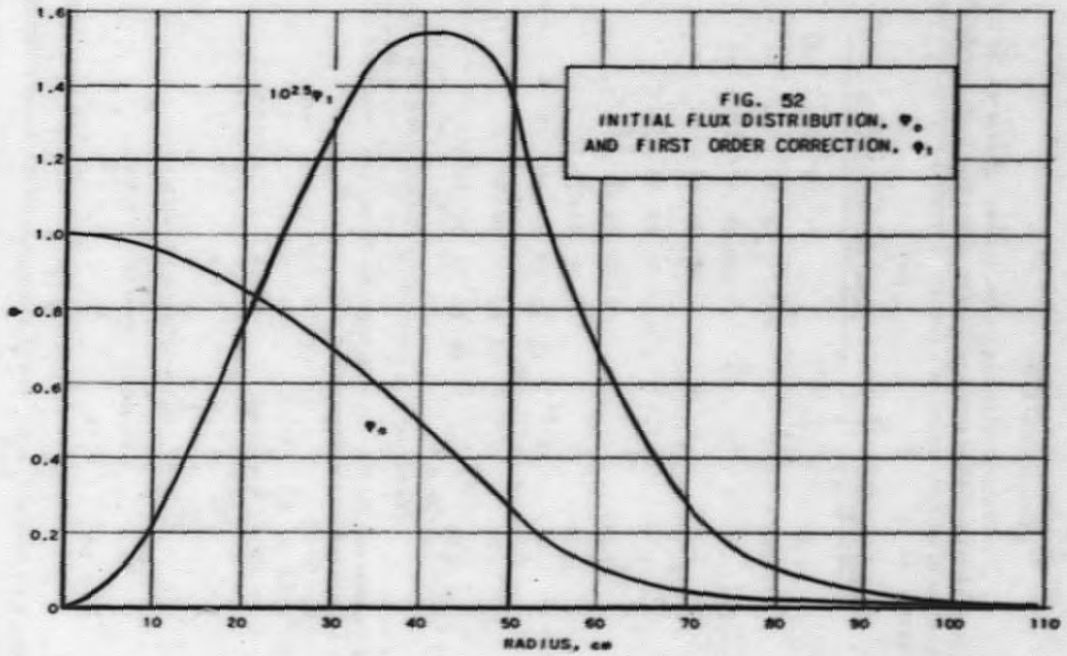

FIG. 52
INITIAL FLUX DISTRIBUTION, ϕ_0
AND FIRST ORDER CORRECTION, ϕ_1

RE-7-11457-A
ANL-AEJ-11457

C. Variation of Reactivity with Irradiation Time in $U^{234} - U^{235}$ and $Th^{232} - U^{235}$ Systems* - J. C. Carter

1. $U^{234} - U^{235}$ System

Work is continuing on this system. At present, the following range of enrichments and initial conversion ratios have been investigated and curves of isotopic content as a function of irradiation time have been prepared.

% Enrichment	Initial Conversion Ratio
.50	.90 1.0 1.1 1.2
.60	.80 .90 1.0 1.1 1.2
.72	.70 .80 .90 1.0 1.1 1.2
.80	.70 .80 .90 1.0 1.1
.90	.70 .80 .90 1.0 1.1
1.00	.60 .70 .80 .90 1.0 1.1
1.25	.60 .70 .80 .90 1.0 1.1
1.50	.50 .60 .70 .80 .90 1.0
1.75	.50 .60 .70 .80 .90 1.0
2.00	.50 .60 .70 .80 .90 1.0

The variation of reactivity is represented by $\frac{(f\eta)}{(f\eta)_0}$ where f and η represents the thermal utilization and the number of neutrons released per capture in fuel, respectively.

$$f\eta = \frac{\nu \Sigma_f^f}{\Sigma_a^f + \Sigma_a^m + \Sigma_a^p}$$

Σ_a^p — fission products

Σ_a^m — structure + moderator + xenon

Therefore, when the Σ_a^m and Σ_a^p are known for a specific reactor, the values of Σ_f^f and Σ_a^f can be determined for the isotopic abundance curves and the reactivity variation can be quickly determined for a given point in the reactor.

*To be reported in future under Central Station Water Reactors.

If the flux distribution throughout the reactor is known, it is possible to determine the change in isotopes and reactivity for the reactor as a whole.

The variation in reactivity for the specific conditions listed below has been calculated with initial conversion ratios (ICR) as parameter and is presented in Figure 53.

Initial Thermal Flux = 6.6×10^{13}

Enrichment = 72% U^{235}

Initial U^{238} = $2,320 \times 10^{24}$ atoms/ton

1,000 mwd/ton = 52 days = 4.49×10^{6} sec

Fission/mw = 3.1×10^{16}/sec

Cross section/fission products = 50 barns/fission

	U^{235}	U^{238}	Pu^{239}	Pu^{240}	Pu^{241}
σ_a	640	2.8	1,150	540	1,420
σ_f	540	0.0	765	0	1,060
σ_c	100	2.8	385	540	360
η	2.12		2.02		2.02
ν	2.5		2.95		2.95

2. <u>Th^{232} - U^{235} System</u>

The series of reactions which produce fissionable isotopes is shown in the following diagram.

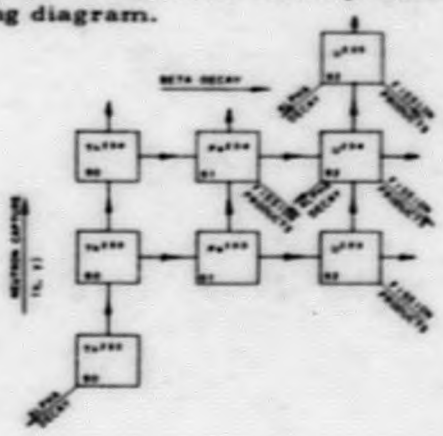

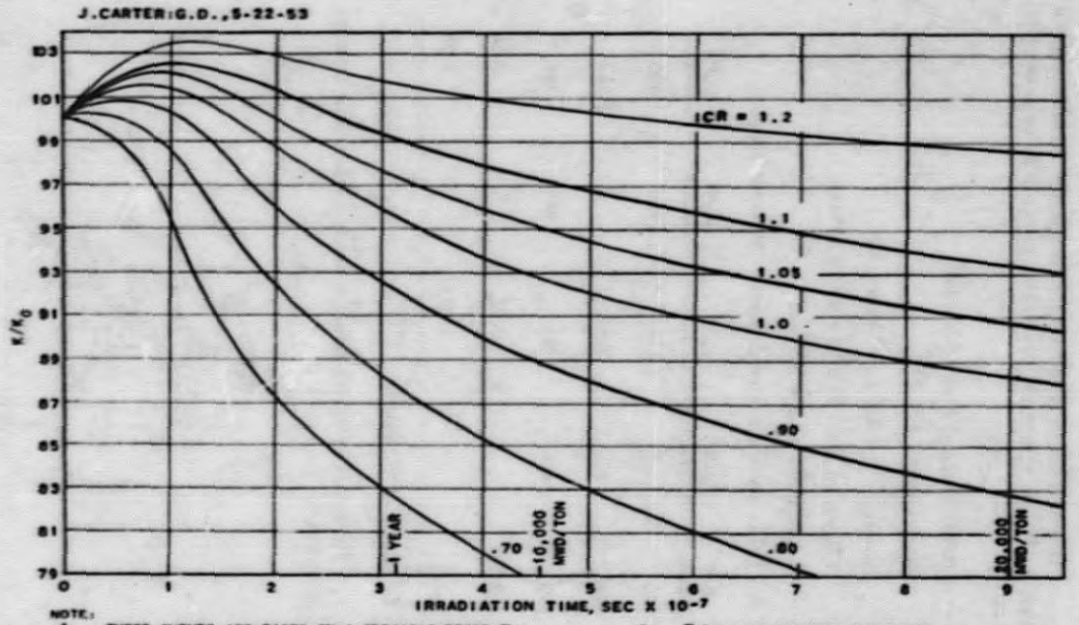

NOTE:
1. THESE CURVES ARE BASED ON A SPECIFIC POWER = 19.27 mw/ton. FOR ANY OTHER SPECIFIC POWER VARY TIME DIRECTLY AS THE SPECIFIC POWER.
2. Σ_a & ρ ARE ASSUMED CONSTANT
3. Σ_a MOD + STRUCTURE + XENON = 98 Σ_a
4. σ_a FISSION FRAGMENTS = 50 BARNS/FISSION

FIG. 53
VARIATION OF REACTIVITY VS IRRADIATION TIME

RE-7-11006-A

The fuel consists of a mixture of U^{235}, U^{238} and Th^{232}. The production of Pu by capture in U^{238} and the formation of Th^{234} are neglected. The system of equations which define the production of significant amounts of fissionable isotopes is considered to be

$$\frac{d N^{U^{235}}}{dt} = + N^{U234} \sigma_a^{U^{234}} \phi_{(t)} - U^{235} \sigma_a^{U^{235}} \phi_{(t)}$$

$$\frac{d N^{Th^{232}}}{dt} = -N^{Th^{232}} \sigma_a^{Th^{232}} \phi_{(t)} - (1-p) \left\{ N^{U^{235}} \sigma_a^{U^{235}} \eta_{U^{235}} + N^{U^{233}} \sigma_a^{U^{233}} \eta_{U^{233}} \right\} \phi_{(t)}$$

$$\frac{d N^{Th^{233}}}{dt} = N^{Th^{232}} \sigma_a^{Th^{232}} \phi_{(t)} + (1-p) \left\{ N^{U^{235}} \sigma_a^{U^{235}} \eta_{U^{235}} + N^{U^{233}} \sigma_a^{U^{233}} \eta_{U^{233}} \right\}$$

$$\phi_{(t)} - N^{Th^{233}} \lambda^{Th^{233}}$$

$$\frac{d N^{Pa^{233}}}{dt} = N^{Th^{233}} \lambda^{Th^{233}} - N^{Pa^{233}} \lambda^{Pa^{233}}$$

$$\frac{d N^{U^{233}}}{dt} = N^{Pa^{233}} \lambda^{Pa^{233}} - N^{U^{233}} \sigma_a^{U^{233}} \phi_{(t)}$$

$$\frac{d N^{U^{234}}}{dt} = N^{U^{233}} \sigma_c^{U^{233}} \phi_{(t)} - N^{U^{234}} \sigma_a^{U^{234}} \phi_{(t)}$$

The variation of reactivity as a function of irradiation time was determined for the following set of conditions and is shown on Figure 54.

Fissions/mw-sec = 3.1×10^{8}

Initial flux = 6.6×10^{13} neutrons/(cm^2)(sec)

Cross section for fission products = 50 barns/fission

$\lambda^{Th^{233}} = .495 \times 10^{-3}$ sec^{-1}

$\lambda^{Pa^{233}} = .294 \times 10^{-6}$ sec^{-1}

	U^{235}	U^{233}	U^{234}	Th^{232}
σ_a	650	564	89	7
σ_f	549	514	0	0
σ_c	101	50	0	0
η	2.12	2.37		
ν	2.50	2.60		

RE-7-11530-A

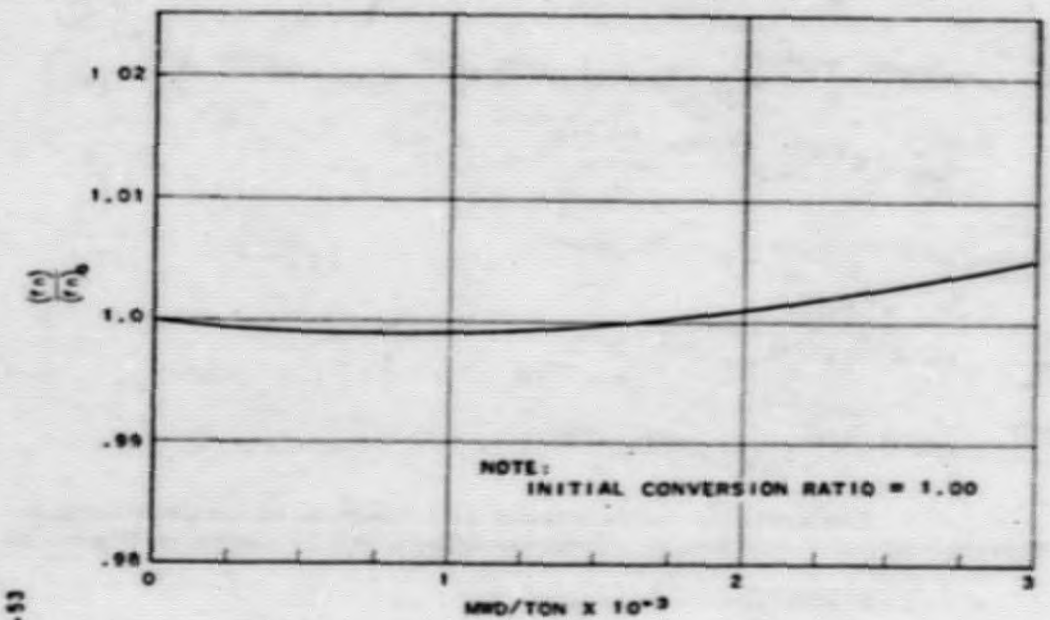

J.C. CARTER: E.K., 8-24-53

FIG. 54
VARIATION OF REACTIVITY WITH IRRADIATION TIME FOR Th^{232}–U^{235} SYSTEM

It is recognized that there is very little precedent for the design of thorium reactors and that the conditions chosen may be unrealistic, therefore, it is planned to make a parametric study over a wide range of initial conversion ratios.

D. Shielding Measurements in the EBR (CP-4) - C. D. Curtis, M. P. Tubinis

As an aid in understanding the efficiency of the upper shield of the Experimental Breeder Reactor, neutron flux traverses have been made along axes passing through the core center and through the inner blanket. Small fission pulse counters[13] with coatings of U^{235}, Pu^{239}, Np^{237}, U^{238} and Th^{232} were used. In addition, copper and manganese wires were threaded through iron shielding plugs and lowered into empty thimbles. The wires were exposed with and without cadmium covers which consisted of cadmium tubing with a 0.030 in. wall thickness. Traverses were made through the core center in rod position No. 1 and through the inner blanket in rod position No. 279 which is at a radius of 13.4 cm. The rod positions in the core and inner blanket are shown in Figure 55. All measurements were made at pile powers of 0.45 kw and above.

Data were collected with the U^{235} and wire detectors for points beginning below the core and extending out through the concrete shield above the reactor. With the threshold detectors, data were collected up to approximately 100 cm above the core center line.

The results from U^{235} counters and wires exposed in hole No. 1 are shown in Figure 56. The U^{235} fission rate and the copper data are normalized, independently, to unity at the core center. Because the relative cross sections of Cu^{65} and Mn vary with neutron energy spectrum, little significance should be attached to the joining of the copper and manganese curves. The approximate composition of the reactor through which the traverses were made is indicated at the bottom of the graph. The use of a cadmium cover over the U^{235} counter as well as over the wires showed, as expected, that no significant thermal flux existed below the large regions of void which are above the long fuel rod assembly.

The effects of the regions of different composition can be seen from the changing slopes of the curves. The thermal flux attenuation length over the last 20 cm in the top concrete shield two feet thick is approximately 8 cm.

---

[13] Reactor Engineering Division Quarterly Report, ANL-5012, March 15, 1953, p. 26.

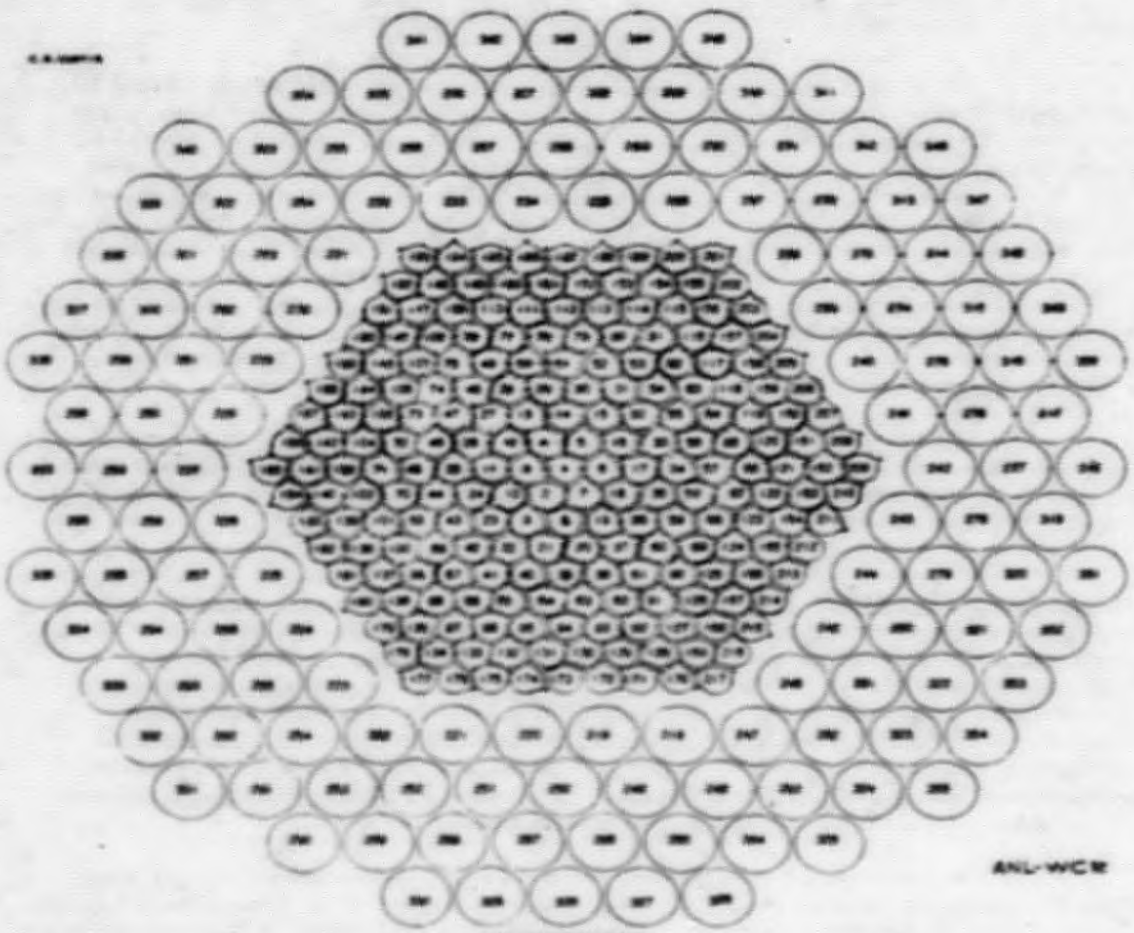

ANL-WCR

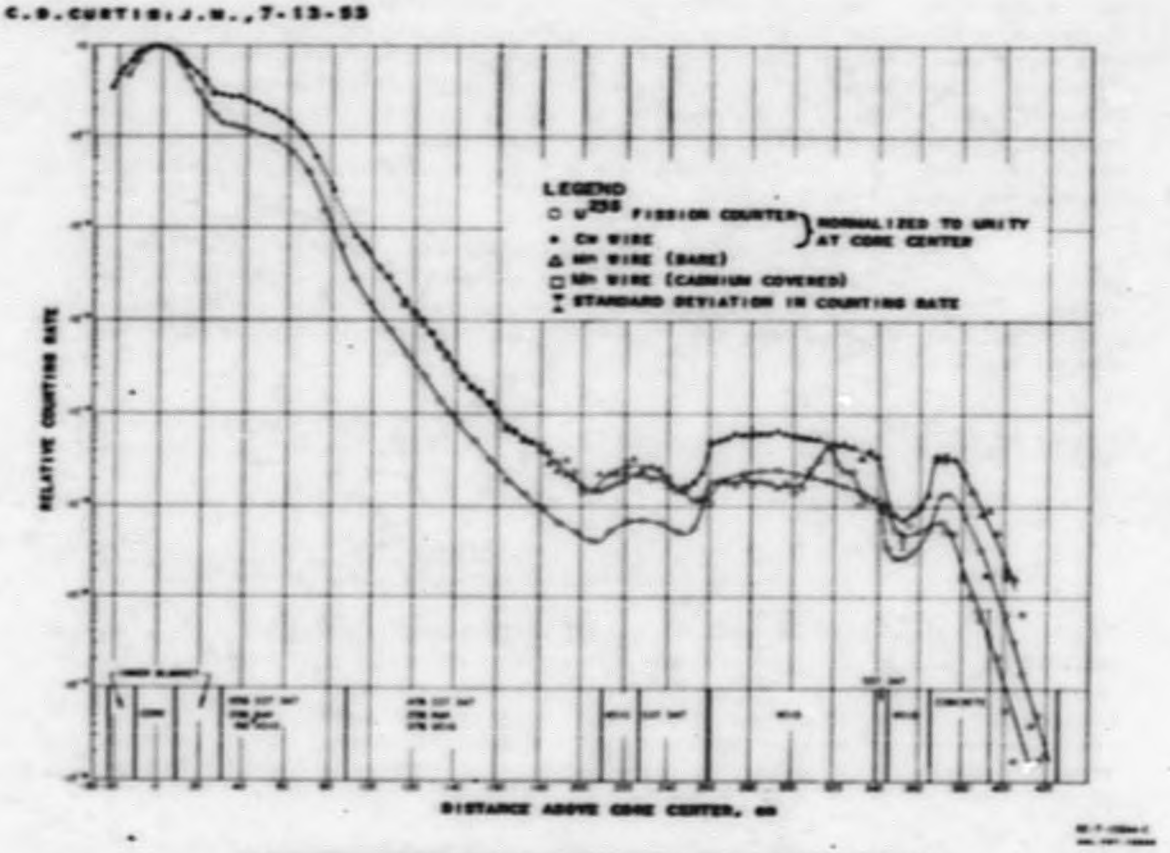

FIG. 56
AXIAL FLUX TRAVERSES. ROD POSITION NO. 1

Figure 57 compares the data obtained from the fission counters in rod position No. 1. The data are normalized to unit fission rate for U^{235} at the core center by using relative fission cross sections previously determined.[14] For some of the traverses, an iron rod one foot in length was hung below the counter to reduce neutron streaming in the hole. The difference in the resulting counting rate was barely detectable in the tank above the core. As expected, the fission rates fall off near the edge of the core more abruptly as the fission thresholds increase. At greater heights this variation among the threshold materials is less pronounced. At a distance of 80 cm above the core center, all the attenuation lengths lie between 11 and 13 cm. The characteristics of the thorium counter used invalidated the data obtained in the core. At distances beyond 15 cm above the core center, the thorium data should be reliable with the exception that the normalization is in doubt.

Traverses were made through the inner blanket rod position hole No. 279 with U^{235} and Np^{237} counters and with copper and manganese wires. The features of the plotted curves were quite similar to those obtained for rod position No. 1 with the exception of less intense flux, as shown in Figure 58.

FUEL ELEMENT DEVELOPMENT

A. Corrosion

1. High-Temperature, Water-cooled Reactor Fuel Elements - J. W. Frank, W. W. Galbreath, Jr., A. H. Roebuck

As part of an evaluation of fuel materials and fuel elements for possible use in high-temperature, water-cooled reactors (200-500F), a study is being made of methods to minimize serious corrosion effects usually accompanying exposure of unalloyed fuel material to water. The uranium-water reaction produces corrosion products of approximately twice the volume of the original metal; this reaction proceeds rather rapidly at temperatures above 300F.

The study is directed primarily toward evaluating fuel materials that would have considerably more resistance to water attack than pure uranium in the event of failure of the protective clad. It is known that some uranium alloys and uranium oxide have improved corrosion resistance over that for the unalloyed metal. Corrosion tests are currently being made on these materials, and data are included for uranium oxide. In addition to the

---

[14] S. Untermyer, "Fission Rate Measurements in the Experimental Breeder Reactor (CP-4)," ANL-4811, April 18, 1952.

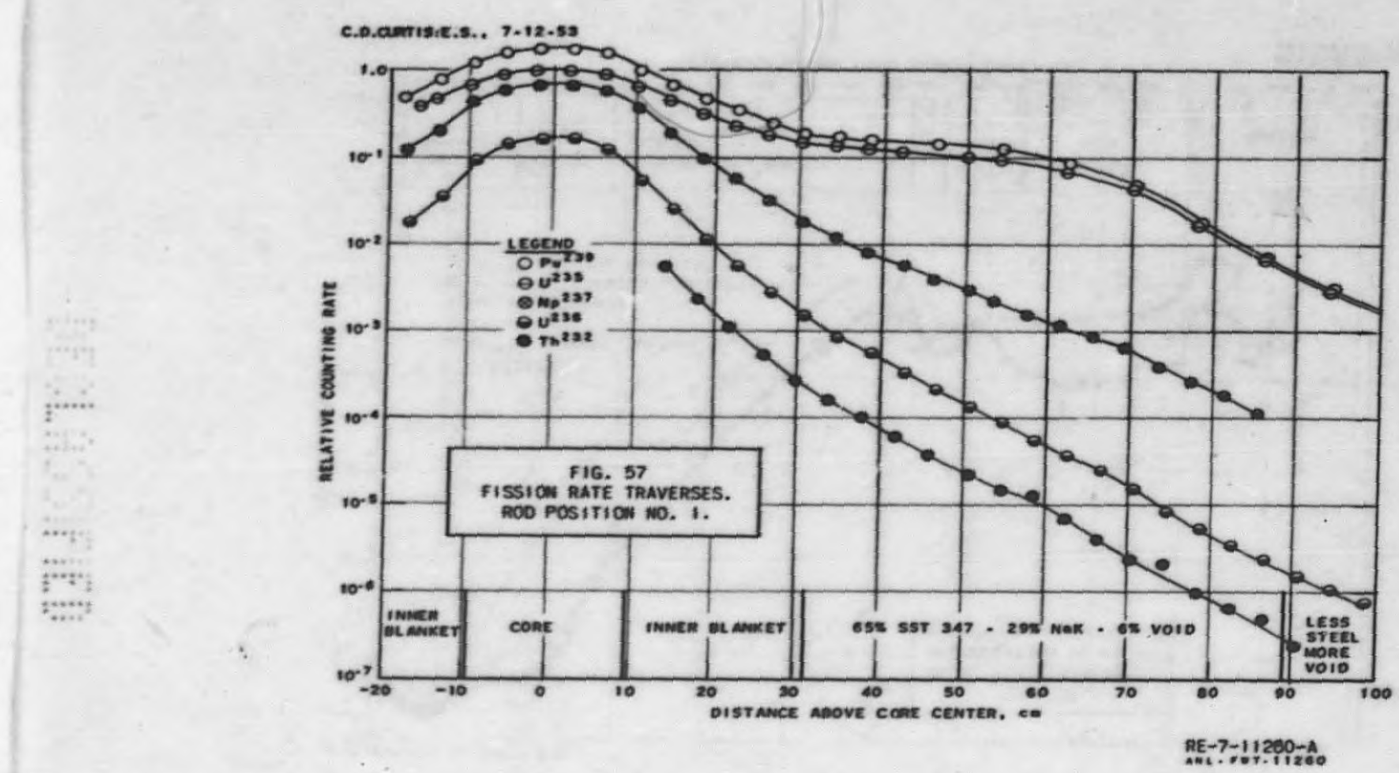
C.D.CURTIS:E.S., 7-12-53
1.0
10^{-1}
10^{-2}
10^{-3}
10^{-4}
10^{-5}
10^{-6}
10^{-7}
RELATIVE COUNTING RATE
LEGEND
Pu^{239}
U^{235}
Np^{237}
U^{236}
Th^{232}
FIG. 57
FISSION RATE TRAVERSES.
ROD POSITION NO. 1.
INNER BLANKET
CORE
INNER BLANKET
65% SST 347 - 29% NaK - 6% VOID
LESS STEEL MORE VOID
-20
-10
0
10
20
30
40
50
60
70
80
90
100
DISTANCE ABOVE CORE CENTER, cm
RE-7-11260-A
ANL - FBT - 11260

C.D.CURTIS:E.S.. 7-12-53

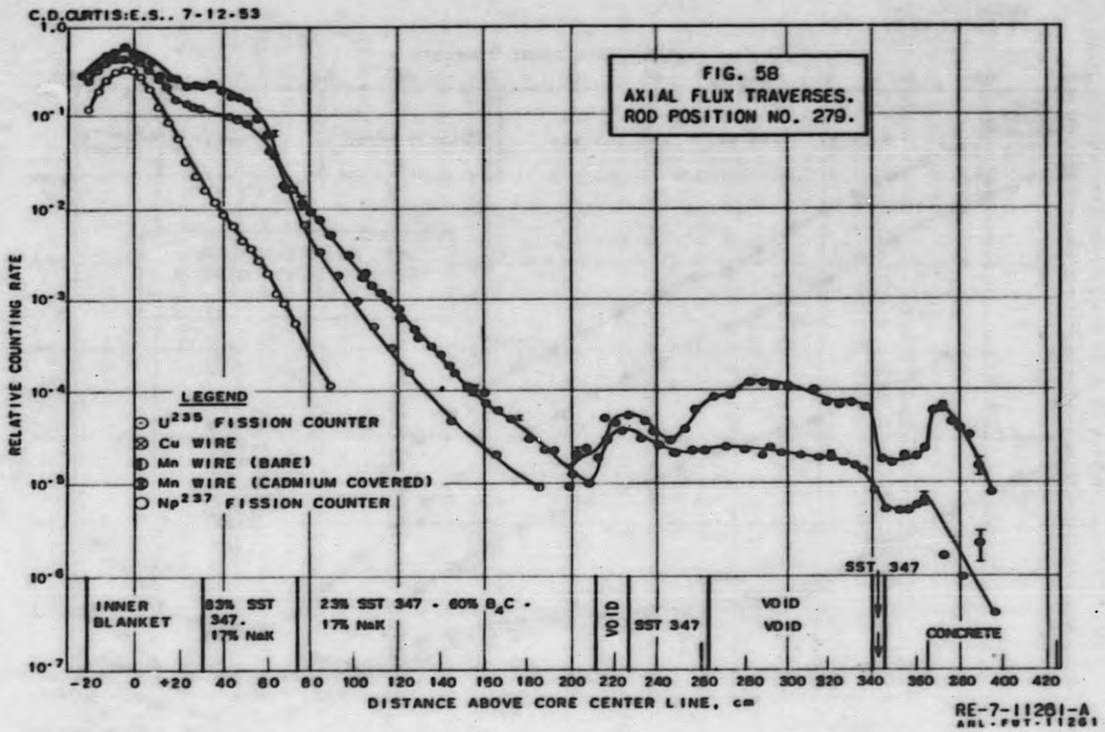

RE-7-11261-A
ANL-FUT-11261

corrosion behavior, it is necessary to evaluate the results of rapid development of corrosion products on the stability of a fuel element following failure of a clad. Thus, additional tests are being made to observe the effect of corrosion of fuel material on a simulated can structure.

Corrosion tests have been made on samples of uranium dioxide having specific gravities of 5.0, 9.3, 10.3, and 10.6. The samples were fabricated by the Metallurgy Division using extrusion, slip casting and hydraulic pressing techniques. The samples were exposed to either 500 or 600F water, either degassed or containing dissolved oxygen; one sample was tested at 600F in both liquid and vapor phase. A description of the samples, test conditions, and test results are given in Table II. The data indicate that the UO_2 tested to date is slightly more resistant in degassed water than in oxygenated water. A small amount of yellow oxide formed on the samples tested in degassed water, indicating that the samples underwent more oxidation in the presence of oxygen. The effect of temperature was not apparent in the data. It was noted that the water resistivity decreases about the same amount as that experienced in corrosion tests of highly resistant materials such as stainless steel. However, the pH decreased from a value of about 7 to about 5.5 in the 500F test and from about 7 to about 6 during the 600F test, indicating that there was some solution of the UO_2 in the test water.

2. Zirconium Clad, Natural Uranium Plates - R. M. Robinson and Metallurgy Division

Samples, prepared by the Argonne Metallurgy Division for the evaluation of zirconium clad natural uranium plates, were corrosion tested in a large-scale thermal syphon autoclave. Slow recirculation of water past the samples was accomplished by the use of internal heaters, internal baffling, and an external cooler. The samples were examined for bond failures after exposure for 24 hr at 338F, 410F, and 482F, respectively. The plates were then exposed for 120 hr at 482F to complete the test.

All plates were fabricated by a modified picture frame process. Graphite-melted uranium was clad with Grade III crystal bar zirconium by a combination of gamma and alpha rolling. Two groups of plates were tested. The samples in Group 1 consisted of two plates, 42 in. long (Nos. 51 and 52). Both plates were reduced 11% in the gamma phase, 88% in the alpha phase, and cold-reduced 12% after removal from the steel can. A 1/2 in. wide strip of nickel was flash-welded to the exposed zirconium at each end, and a 1/2 in. wide strip of copper was flash-welded to the nickel. The descriptions of the second set of samples, tested as Group 2, are given in Table III. Further details on the fabrication will be included in an Argonne Metallurgy Division topical report.[15]

---

[15] J. J. Lawless, et al, "Development of Zirconium Clad Uranium Plates for Reactor Fuel," ANL-5076, May 6, 1953.

Table II

CORROSION OF URANIUM DIOXIDE

Material Identification	Sample No.	Test Conditions: Temp. F and Gas*	Time, hr	pH: Before	pH: After	Resistivity: Before	Resistivity: After	Wt. Change, mg/(cm²)(sec)	Appearance After Test
Sp. gr. 10.6. Hydrostatically pressed. Fired at 1750C. Mat. Div. No. 1645	4003-1	500 degassed	330	7.1	5.8	195,000	45,000	- 4.4	Very small pieces chipped off of sample edges. Sample completely covered with dull black coating. No appreciable amount of H_2 was found in autoclave after test.
Repeat test on above sample		500 degassed	333	7.0	5.7	180,000	28,000	- 2.4	During second 2-week test period, sample turned a dull brownish black in color.
Sp. gr. 10.6. Hydrostatically pressed. Fired at 1750C. Mat. Div. No. 1645	4003-2	500 oxygenated	330	7.0	5.3	250,000	60,000	+ 0.76	Sample covered with a fairly heavy loose yellow-green oxide coating.
Repeat test on above sample		500 oxygenated	333	7.0	5.4	250,000	48,000	-15.4	During second 2-week test period, sample turned more yellowish and small pieces chipped off ends.
Sp. gr. 10.6. Hydrostatically pressed. Fired at 1750C. Mat. Div. No. 1645	4003-3	600 oxygenated steam phase	334	6.9	---	165,000	---	0.00	Two specimens were exposed in a single autoclave: one sample in the steam phase. The autoclave lost its water during the test. Both samples turned a lustrous black during test.
		600 oxygenated water phase						- 0.25	
Repeat on above sample		600 oxygenated steam phase	400	6.7	6.8	350,000	30,000	-36.9	Steam phase sample covered with a loose black scale. Water phase sample covered with a loose powdery dull coating.
		600 oxygenated water phase						+ 3.38	
Sp. gr. 10.3. Hydrostatically pressed. Fired at 1750C. Mat. Div. No. 1649	4012	600 degassed	258	6.7	6.0	470,000	47,000	+ 0.22	Small metallic specks in water after test. Loose gray-white coating with metallic luster on sample. Analysis showed this coating to contain traces Al, Si, and Cu.
Sp. gr. 9.8. Slip cast. Fired at 1750C. Mat. Div. No. 1653	4013	600 degassed	258	7.9	5.4	320,000	33,000	- 7.05	Loose powdery dull gray coating.
Sp. gr. 5. Extruded. Fired at 1700C. Mat. Div. No. 1654	4011	600 degassed	258	6.4	6.0	340,000	31,000	- 0.47	Sample covered with a loose porous brown-black coating.

*Oxygenated tests were made by initially saturating test water, in open autoclave at room temperature, with oxygen, resulting in a calculated gas concentration of 30 cc of oxygen per liter of water.

Table III

DESCRIPTION OF GROUP 2 ZIRCONIUM CLAD, NATURAL URANIUM SAMPLES

Plate No. Met. Div.	Sample No. E.E. Div.	Gamma Reduction, per cent	Alpha Reduction, per cent	Cold Roll Reduction, per cent	Nominal Length, in.	Fabrication
25A	4055	22	94	5	24	Sheared from end of rolled plate.
26A	4063	22	94	---	24	Exposed core sealed by welding
26A	4056	22	88	---	18	with Zr-3% Sn filler wire.
27A	4058	22	88	---	18	Natural end of plate sheared and seal welded.
26B	4057	22	88	---	18	Same as 25A except natural end
27B	4059	22	88	---	18	left as rolled.
42A	4060	45	80	5	22	Sheared from middle of rolled plate. Exposed core at each end sealed by welding with Zr-3% Sn filler wire.
43A	4061	45	80	---	22	Sheared from end of rolled plate. Exposed core sealed by welding with Zr-3% Sn filler wire. Natural end sheared only.
43B	4063	45	80	---	22	Same as 43A except natural end of plate left as rolled.
53	4053	11	90	20	42	Fabricated with strips of Ni and Cu as for plates 51 and 52.
54	4054	11	90	20	42	Same as plate 53.

During the test of Group 1 plates, the pH varied from 5.2 to 6.87, while the resistivity ranged from 460,000 to 83,000 ohm-cm. The pH of the water samples taken during the test of Group 2 plates varied from 6.28 to 7.05, while the resistivity was fairly constant at 160,000 to 180,000 ohm-cm. The plates exposed as Group 1 were coated with a loose gray-black powder, with white powder along the edges. A yellow powdery coating was observed near the bond between the copper strip and the zirconium.

During the first 24-hour exposure at 338F of Group 2 plates, a slit 2 in. long appeared on plate 28A causing exposure and oxidation of the natural uranium. The plate was removed and the test was resumed. A defect in the cladding apparently caused this failure. The zirconium cladding on plate 28A was 0.005 in. thick; that on all other plates was in the range 0.010 - 0.025 in. thick. During exposure at 410F and 482F, the top and bottom welded sections of one of the 42 in. long plates fell off. No further bond failures were detected.

Plates 53 and 54 had a large amount of yellow precipitate along the weld bonds between the nickel-copper and nickel-zirconium strips. Analysis of the deposition showed 30% zirconium, 20% uranium, and 18% nickel, plus lesser amounts of other elements. Most of the plates had a coating of loose gray-black powder and red-brown corrosion products; white powder was prevalent along the edges. Spectro-chemical analysis of the red-brown powder showed greater than 20% iron, 0.2% copper, 0.8% zirconium and 1% uranium (only metallic ions are identifiable by this type of analysis). A possible explanation for the large amount of uranium depositing on plates 53 and 54 is that some uranium may have been exposed during welding of the nickel and copper strips to the zirconium; the exposed uranium may have adhered to the weld during clean-up of the welded area.

3. Corrosion of Natural Uranium and Magnesium in Diphenyl - R. M. Robinson

Results of static corrosion tests of two samples of natural uranium and one sample of high purity magnesium in diphenyl at 500F in stainless steel autoclaves are summarized in Table IV. The volume of diphenyl used was computed to be sufficient to submerge the samples. The first test was made with air present in the autoclave; the second test was made with air evacuated from the autoclave. The exact composition of the uranium sample tested first is unknown; the major impurities in the second uranium sample are:

Al	15 ppm	Si	30 ppm
Fe	80 ppm	C	475 ppm
Ni	10 ppm	N	14 to 19 ppm

Table IV

CORROSION OF NATURAL URANIUM AND MAGNESIUM IN DIPHENYL

Medium: Diphenyl, Practical Grade (95-98 per cent, melting point 65-69C (149-156F))
Temperature: 500F

Sample	Argonne Sample No.	Dissolved Gas Content	Duration, hr	Rate of Weight Change, mg/(cm²)(mo)	Appearance After Test
Natural uranium, Beta annealed and degreased.	4003	Air*	15	---	Area, cm²: 5.8 Initial weight, gm: 20.4090 Weight change, gm: -0.2687 Loose black oxide coating.
Same sample, loose black oxide coating removed.	4003	Air*	257	-19.0	Very loose black oxide coating.
Natural uranium, Beta heat treated, grain size, 0.06 to 0.07 mm average diameter. Pickled 15 min at room temperature in nitric acid (25 per cent by weight), then degreased.	4014	Deaerated**	99	+ 0.3	Before test, metallic luster. After test dull gray-black coating, iridescent tarnish on bottom of sample.
Same sample, repickled.	4014	Deaerated**	692***	+ 8.4	Slightly loose, dull green-black coating.
Magnesium	1867	Air*	257	- 0.11	Retained original appearance.
Natural uranium coupled to magnesium	4014 1867	Deaerated**	339	- 0.38 + 0.21	Uranium: slightly loose, dull black coating, except green tarnish on contact area. Magnesium: light brown coating, except original appearance on contact area.

*No attempt to evacuate air was made.

**Air was evacuated by a vacuum pump from the autoclave containing the sample and diphenyl while heating from room temperature to 140F.

***Probable leak of autoclave seal indicated by large loss of diphenyl during test period.

The results show that natural uranium and coupled samples of natural uranium and magnesium may have satisfactory corrosion resistance to 500F diphenyl if oxygen and water are excluded. The corrosion resistance of magnesium to 500F diphenyl with a slight amount of oxygen present is satisfactory; the resistance of uranium does not appear satisfactory in the presence of oxygen.

4. Chemical Thermodynamics of Reactor Materials - W. K. Anderson and J. W. Frank

Standard free energies (ΔF) as functions of temperature calculated at 400K and 600K (about 261 and 621F) for several reactions of interest in current reactor studies at Argonne are given in Table V.

Table V

CALCULATED FREE ENERGIES AT 400K AND 600K FOR CHEMICAL REACTIONS IN REACTOR STUDIES

Reaction	ΔF Cal/gm-mole 400K	600K
$Cr_2O_3 + 6\ Na \rightleftharpoons 3\ Na_2O + 2\ Cr$	-14,950	-14,350
$Fe_3O_4 + 8\ Na \rightleftharpoons 4\ Na_2O + 3\ Fe$	-120,470	-105,340
$Fe_2O_3 + 6\ Na \rightleftharpoons 3\ Na_2O + 2\ Fe$	-89,257	-77,739
$FeO + 2\ Na \rightleftharpoons Na_2O + Fe$	-32,600	-28,210
$NiO + 2\ Na \rightleftharpoons Na_2O + Ni$	-37,901	-34,405
$UO_2 + 4\ Na \rightleftharpoons 2\ Na_2O + U$	-78,460	-86,270
$UO_2 + Zr \rightleftharpoons ZrO_2 + U$	+13,830	+14,360
$Ti + 2\ H_2O^* \rightleftharpoons TiO_2 + 2\ H_2$	-101,940	-107,200
$Zr + 2\ H_2O^* \rightleftharpoons ZrO_2 + 2\ H_2$	-133,830	-139,010
$UO_2 + H_2O^* \rightleftharpoons UO_3 + H_2$	+24,510	+25,430
$3\ UO_2 + 2\ H_2O^* \rightleftharpoons U_3O_8 + 2\ H_2$	+32,790	+26,300
$UO_2 + H_2O^{**} \rightleftharpoons UO_3 + H_2$	+29,130	+30,620
$Zr + 2\ H_2O^{**} \rightleftharpoons ZrO_2 + 2\ H_2$	-132,520	-128,630
$Ti + 2\ H_2O^{**} \rightleftharpoons TiO_2 + 2\ H_2$	-101,340	-97,820
$U + 2\ H_2O^* \rightleftharpoons UO_2 + 2\ H_2$	-147,660	-153,370
$U + 3\ H_2O^* \rightleftharpoons UO_3 + 3\ H_2$	-119,150	-127,940
$U + 2\ H_2O^{**} \rightleftharpoons UO_2 + 2\ H_2$	-146,380	-142,970
$U + 3\ H_2O^{**} \rightleftharpoons UO_3 + 3\ H_2$	-117,230	-112,370

*Liquid

**Vapor

References

Oedon Barta, Z. Electrochem. 43, 733-43.

G. N. Lewis, M. Randall, "Thermodynamics and the Free Energy of Chemical Substances," (New York: McGraw-Hill, 1953).

U.S. Dept. of Interior, Bureau of Mines Bulletin 476.

Reactions showing large negative free energies have a high probability of occurring, while those with large positive free energies never occur. Reactions with intermediate values of free energy up to a positive value near ten-thousand cal/gm-mole may sometimes occur, but are somewhat indeterminate. Therefore, the data of Table V indicate that sodium will reduce the oxides of such structural elements as iron, chromium, and nickel, and that uranium will reduce sodium oxide. In the water systems there is confirmation of the empirical fact that UO_2 is the stable form of uranium in the presence of either liquid or vapor phase water. Apparently water or steam should oxidize titanium and zirconium; the empirically known fact that these metals have fair stability in hot water can be explained on the basis of the formation of oxide films which are impervious to further attack.

B. Heat Transfer Experiments

Pressure Drop Studies on Twisted Ribbon Core Assemblies - A. B. Schultz

A coordinated mechanical test program has been set up to determine the pressure drop through core assemblies composed of twisted wires with variation of flow rate, metal to water ratio, pitch, and change of water density (by introducing air).

Twisted flat wire fuel elements appear to have several good features for reactor core construction. They can be built into a core assembly which is structurally self-supporting, except for thin tubes to separate the wires from the control rods. The water passages can be accurately controlled dimensionally, and warping or swelling of the wires cannot appreciably change the size of the passages. Good mixing of the bulk flow of the coolant minimizes local hot zones and uniform local mixing may break up laminar flow and permit some relaxation of hot channel factors. Point contact between adjacent wires is not considered critical from the standpoint of cooling. Almost any metal to water ratio can be obtained by proper selection of wire thickness and width. In particular, the larger ratios of metal to water can be obtained with a supporting structure that does not interfere with the water flow. By rolling to an elliptical shape, a tight mechanical bond of the cladding can be assured.

The range of wire sizes being considered at present are 0.039 in. x 0.148 in.; 1/16 in. x 3/8 in.; 0.109 in. x 5/8 in.; and 7/16 in. x 15/16 in. The configurations include closely-packed cores with tubular passages for control rods; bundles of wires encased in thin-walled tubes heterogeneously arranged; and bundles of wires encased in closely-packed tubes with central control rod spaces.

a. Test Apparatus and Procedure

The test assembly consists of a cluster of twisted ribbons 48 in. long retained in a 3-inch (across flats) hexagonal channel formed by a Lucite tube as shown in Figures 59 to 63. The specimens tested so far have been 3/8 in. x 1/16 in. ribbons twisted to 6-inch, 12-inch, and 24-inch pitch. Tests on the 6-inch pitch were made to determine the extreme tight twist limit, and the 24-inch pitch the flattest pitch of any possible interest. The ribbons have a metal to water ratio of 1:4.4 (Figures 64 and 65). The ribbons are twisted from 3/8 in. x 1/16 in. cold-rolled round edge flat steel wire commercially available. These are welded at one end to 5/8 in. x 1/16 in. steel plates which are positioned in slots in the end of the Lucite tube.

The assembly is inserted in a loop (Figures 66 and 67) through which water can be circulated up to 200 gpm or 10 fps at room temperature. Valves are provided to control the rate of flow and the pressure in the test section. To enable studies of two-phase flow, air can be injected to lower the density to 0.2 with velocities of the water and air mixture up to 20 fps. Mercury manometers are provided to show pressure drop and flow meters to show water and air flow. A pressure gauge at the center of the test section is used to determine average air density through the test section. A small air line into the side of the test section at the bottom is used for bubbling tests. The water is treated with sodium dichromate to prevent corrosion of the mild steel parts.

Calibration runs were first made comparing the pressure drop over the 48-inch section including entry and exit losses with the pressure drop between taps spaced 33 in. apart over the middle of the test section. Accumulated air was carefully vented from vital points, due allowance was made for the relative densities of the water in the manometer leads and in the test section, and also allowance was made for the weight of the water over the mercury column differential. The results are considered as accurate as the calibration and reliability of the instrumentation will permit.

Tests were run at water flows from 25 gpm up to 200 gpm at increments of 25 gpm. Air and water mixtures were run at densities of 1.6, 0.8, 0.6, 0.4, 0.2 and 0.1 to obtain data which might be applicable to two-phase flow studies for boiling-type reactors. Bubbling tests were made to determine the rate of mixing and to observe the degree of spread at the top. Slow motion movies (1000 frames/sec) were made to aid in studying the flow characteristics of the water and air mixtures.

b. Results

The test results for the pressure drop between 33-inch taps are shown graphically in Figures 68 to 71 inclusive. For convenience, all pressures are given in terms of direct manometer reading - water over

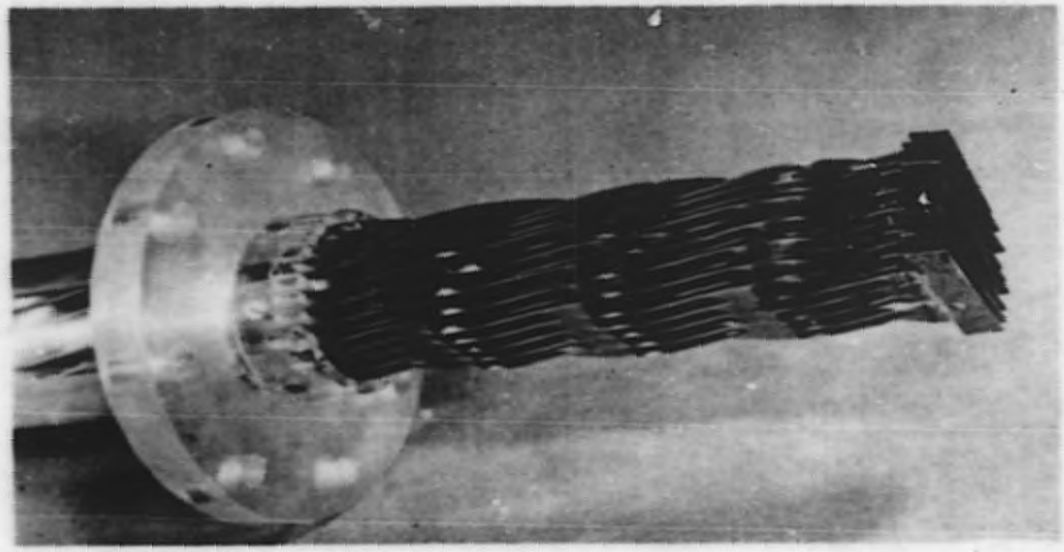

FIG. 59
TWISTED WIRE CORE ASSEMBLY

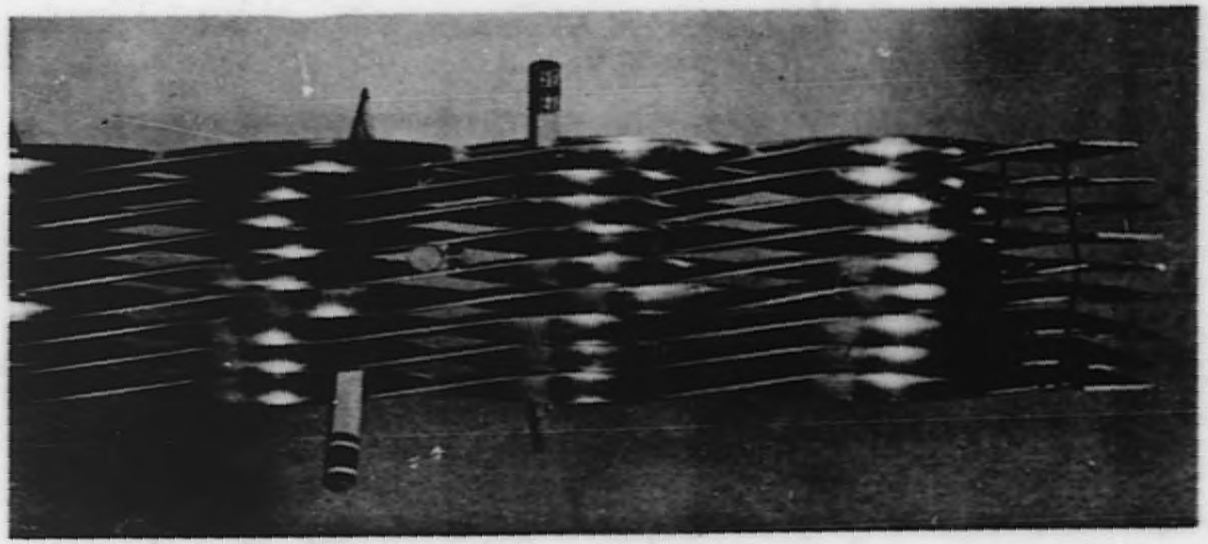

FIG. 60
ASSEMBLY OF 6-INCH PITCH TWIST WI S.
PENCILS INDICATE LINES OF SUPP

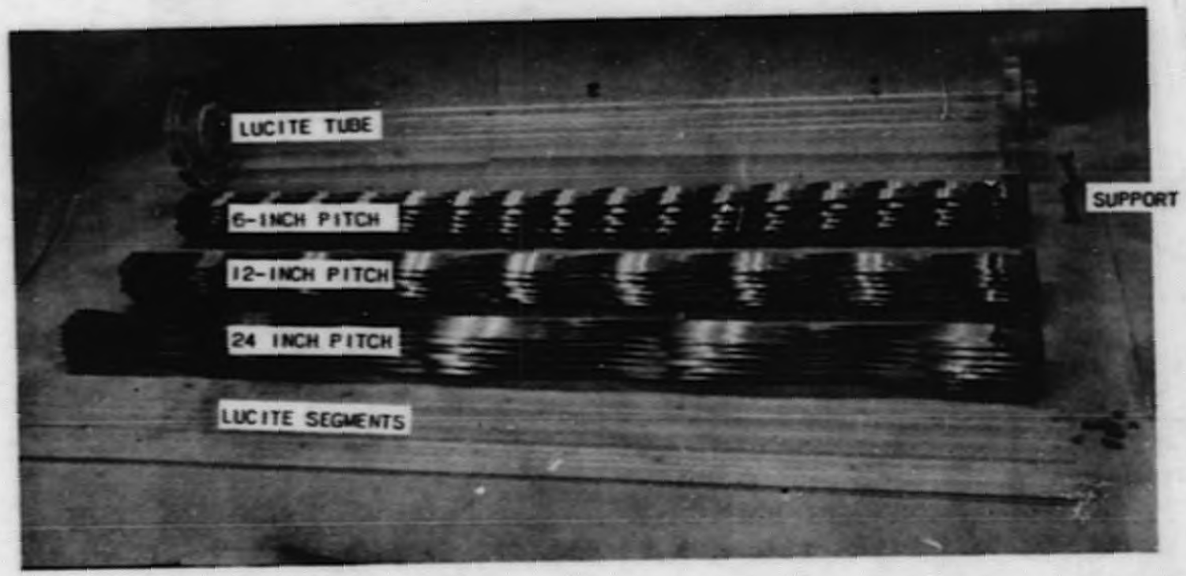

FIG. 61
DISASSEMBLED TEST SECTION AND THE THREE SPECIMENS TESTED

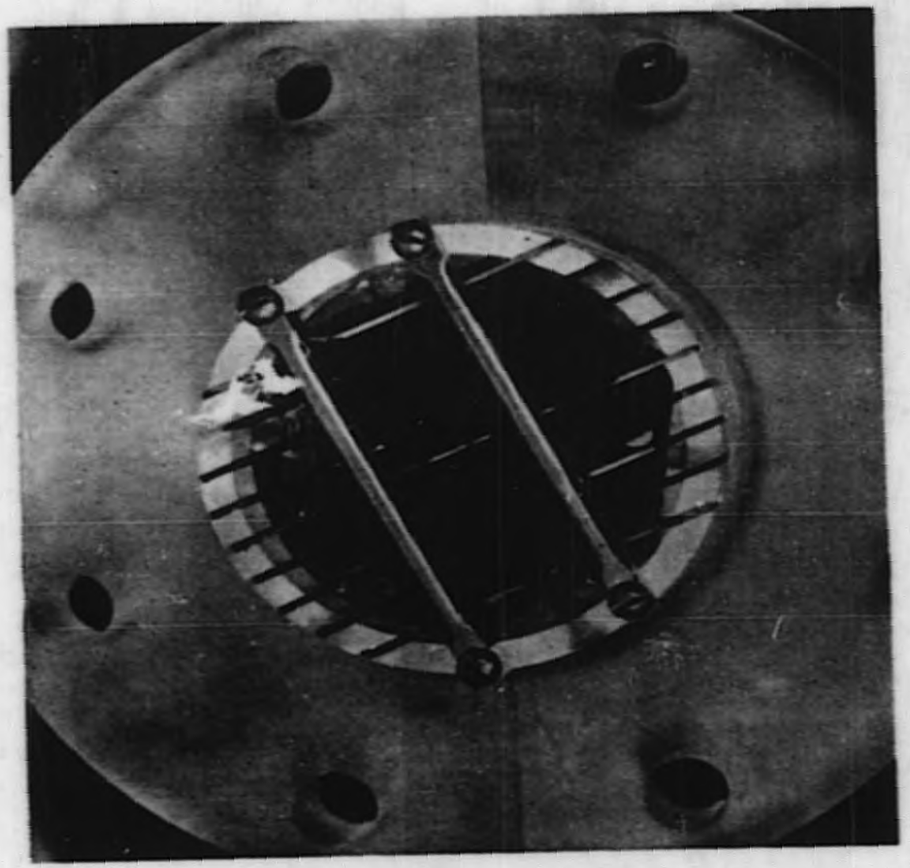

FIG. 62
END VIEW OF ASSEMBLED TEST SPECIMEN

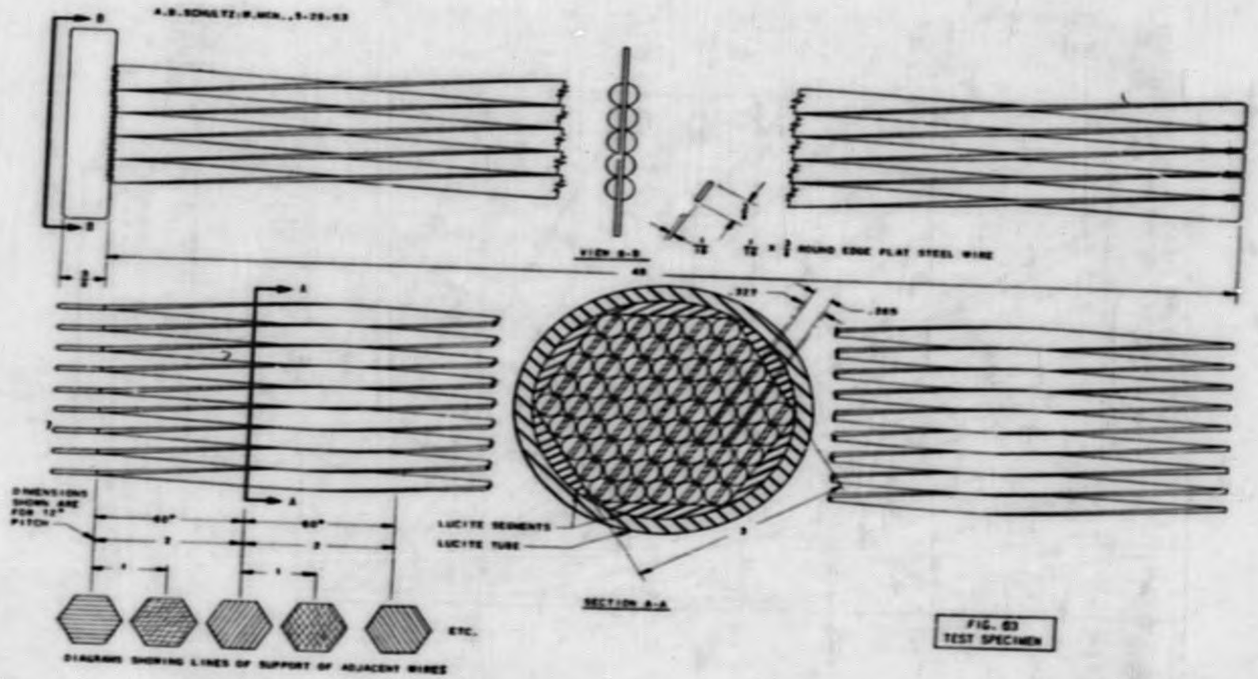

FIG. 63
TEST SPECIMEN

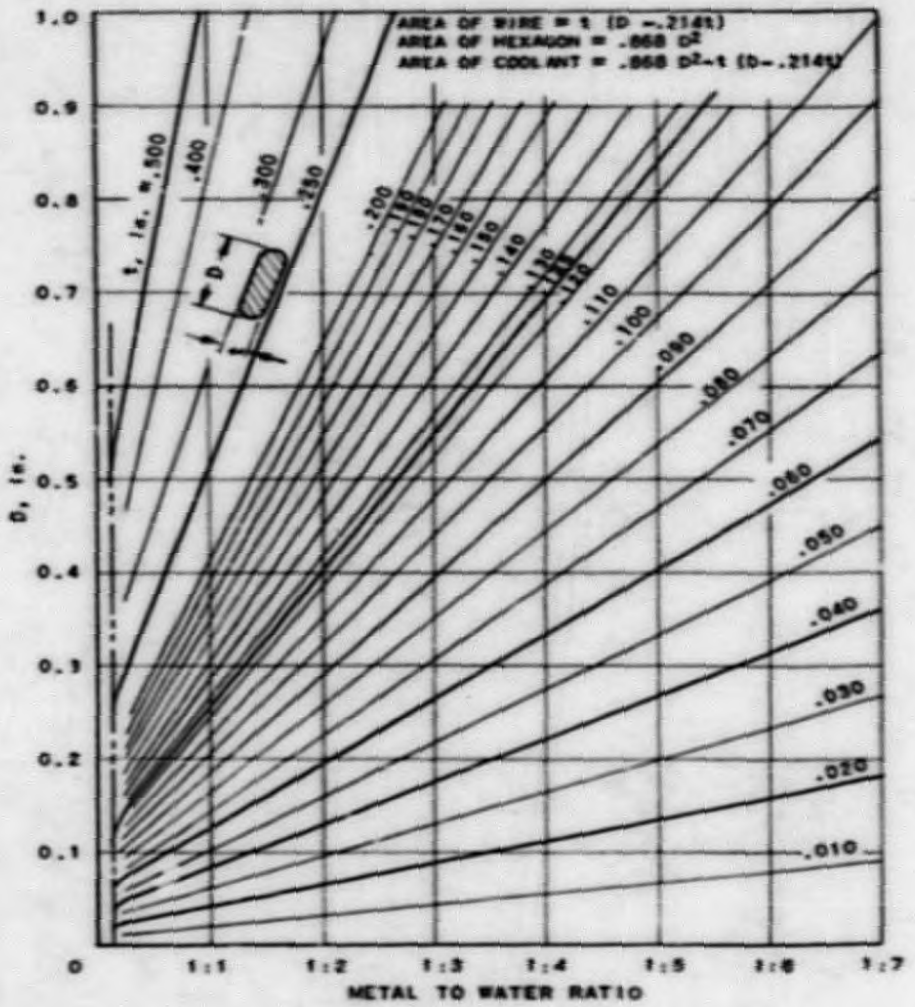

RE-7-11516-A

A. B. SCHULTZ: E. A. K., 8-21-53

FIG. 64
METAL TO WATER RATIOS FOR TWISTED ROUND EDGE FLAT WIRES

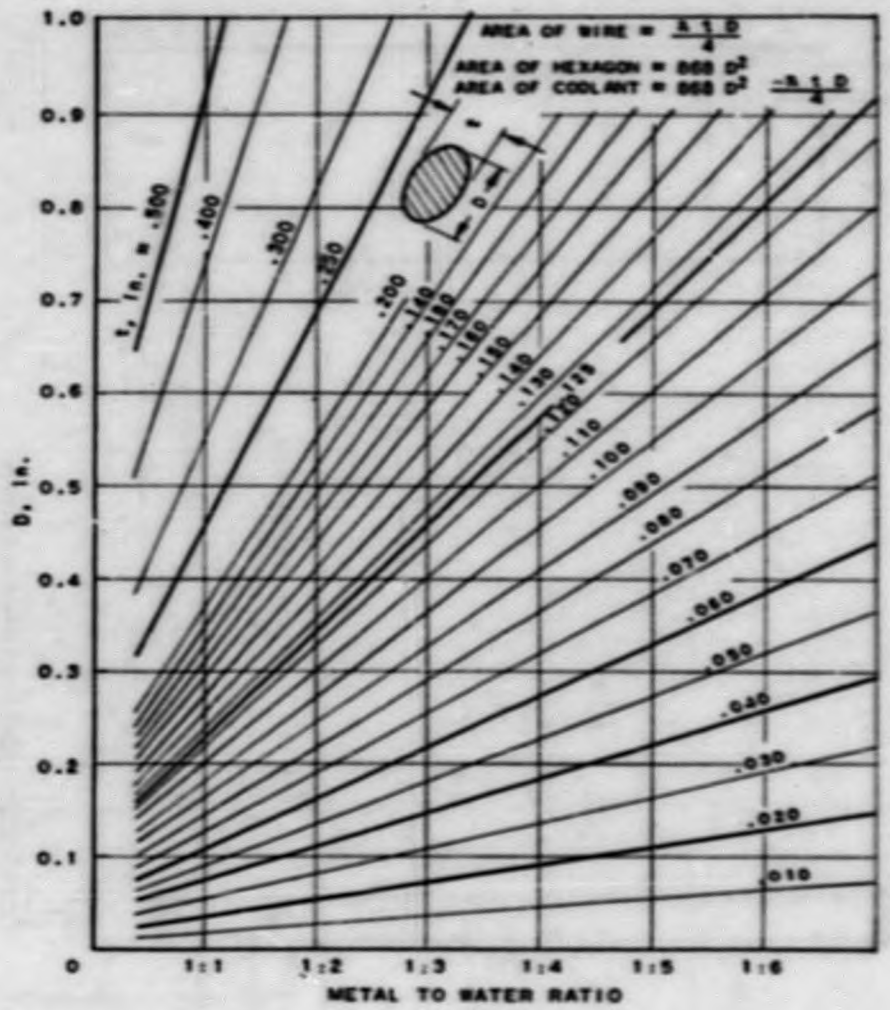

FIG. 65
METAL TO WATER RATIOS
FOR ELLIPTICAL WIRES

RE-7-11531-A

A.B.SCHULTZ:E.A.K.,8-21-53

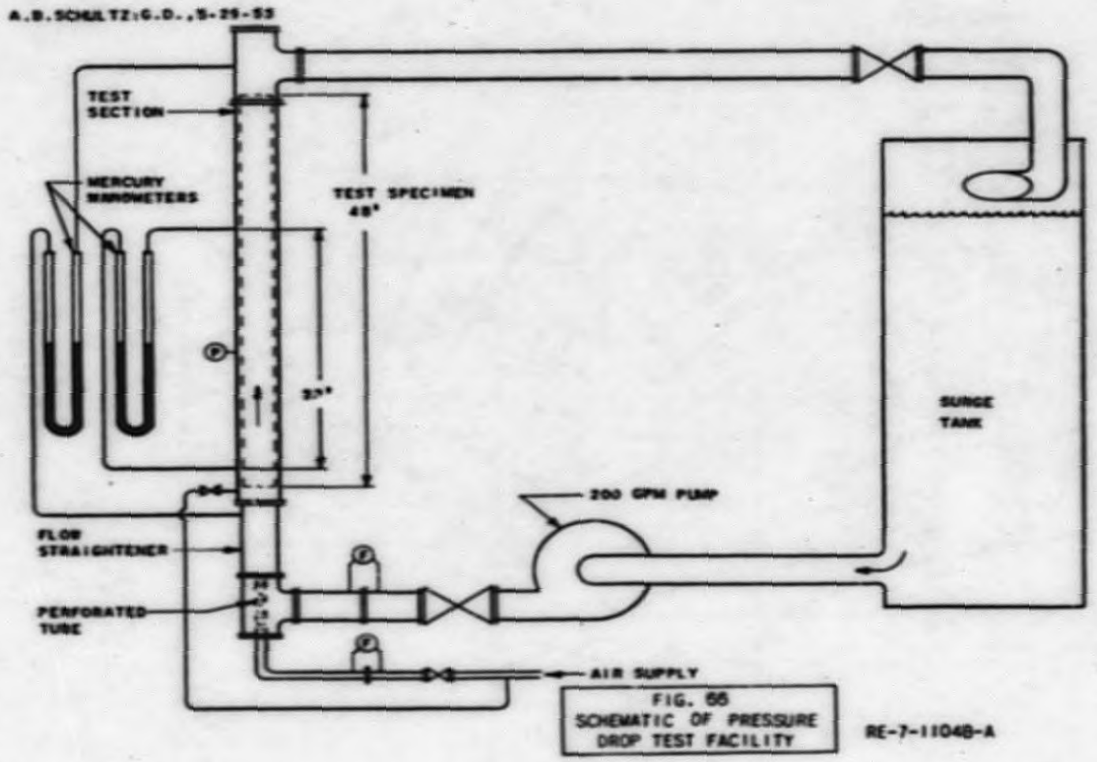

FIG. 66
SCHEMATIC OF PRESSURE DROP TEST FACILITY

RE-7-1104B-A

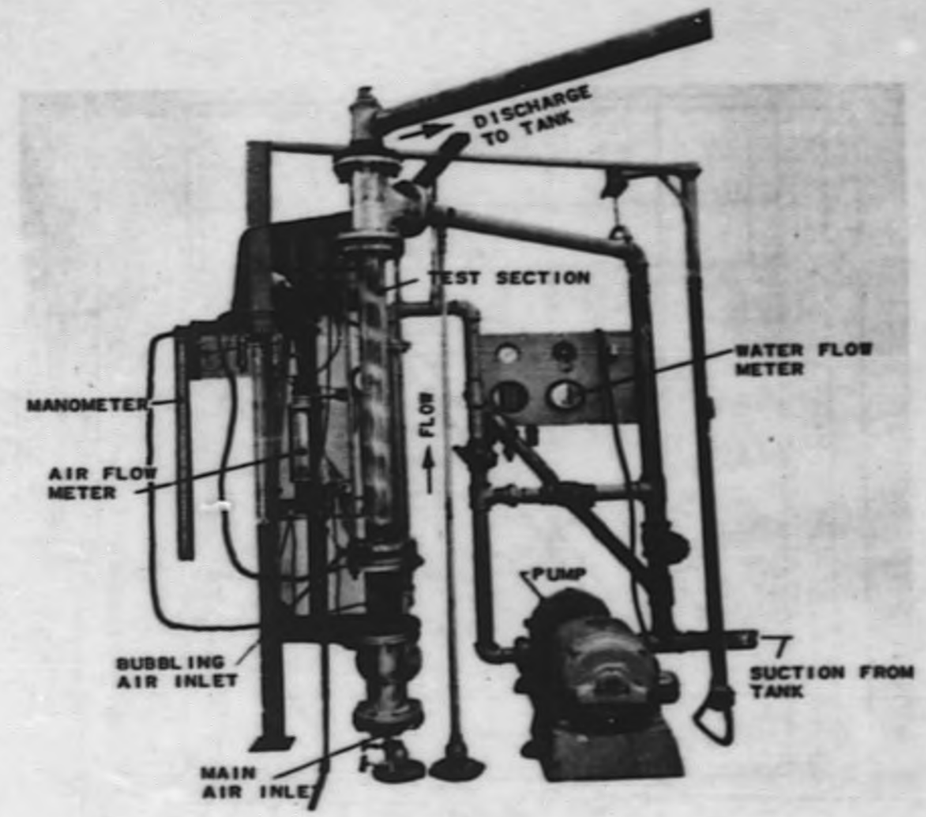

FIG. 67
PRESSURE DROP TEST FACILITY

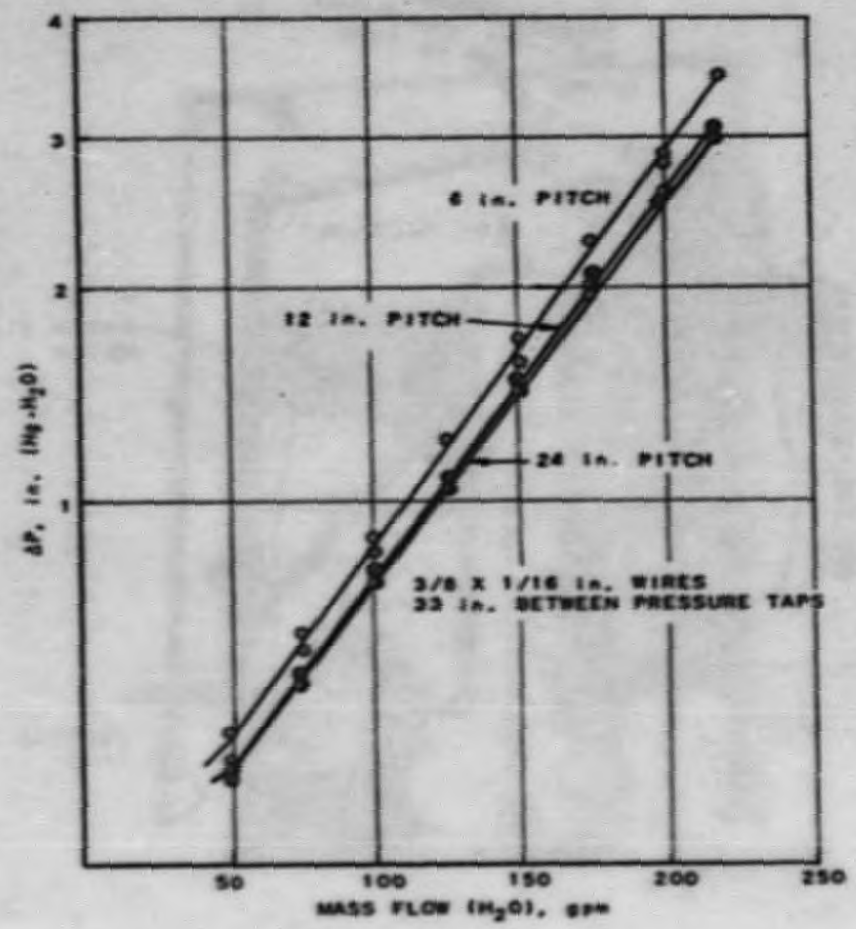

RE-7-11511-A

A.B.SCHULTZ & C.K.SOPPET:T.R.L.,8-15-53

FIG. 88
MASS FLOW VS PRESSURE DROP AND CHANGE OF PITCH OR TWIST, SOLID WATER

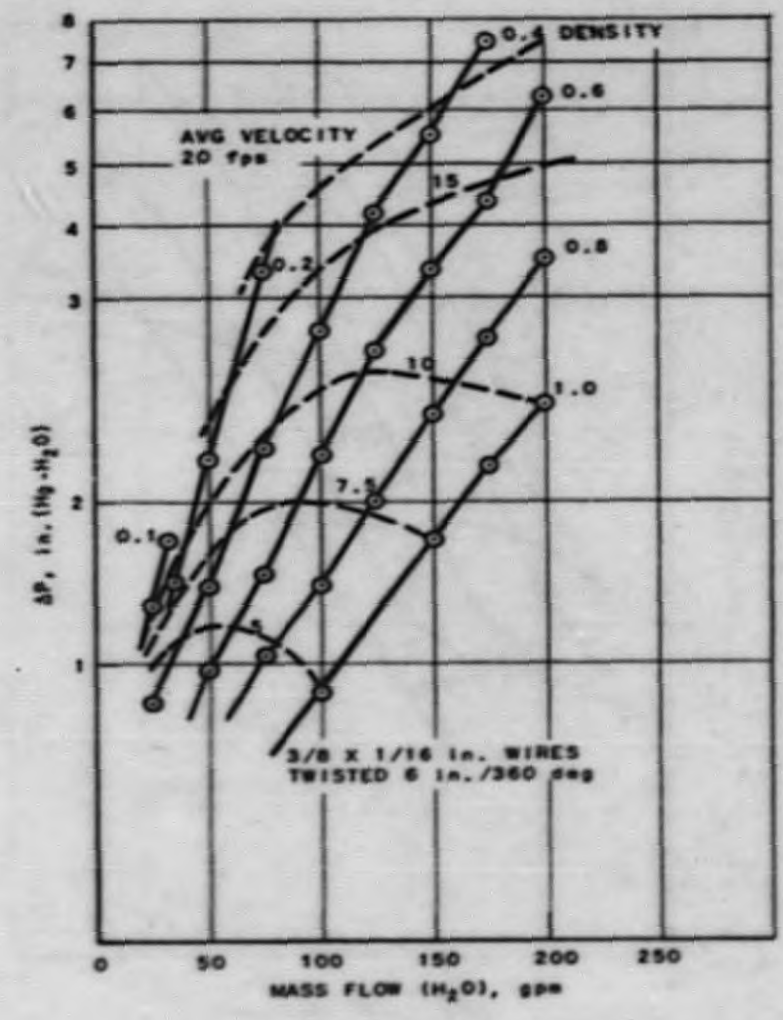

FIG. 69
MASS FLOW VS PRESSURE DROP.
WATER AND AIR MIXTURES

RE-7-11500-A

A.B.SCHULTZ & C.K.SOPPET:E.F.,8-19-53

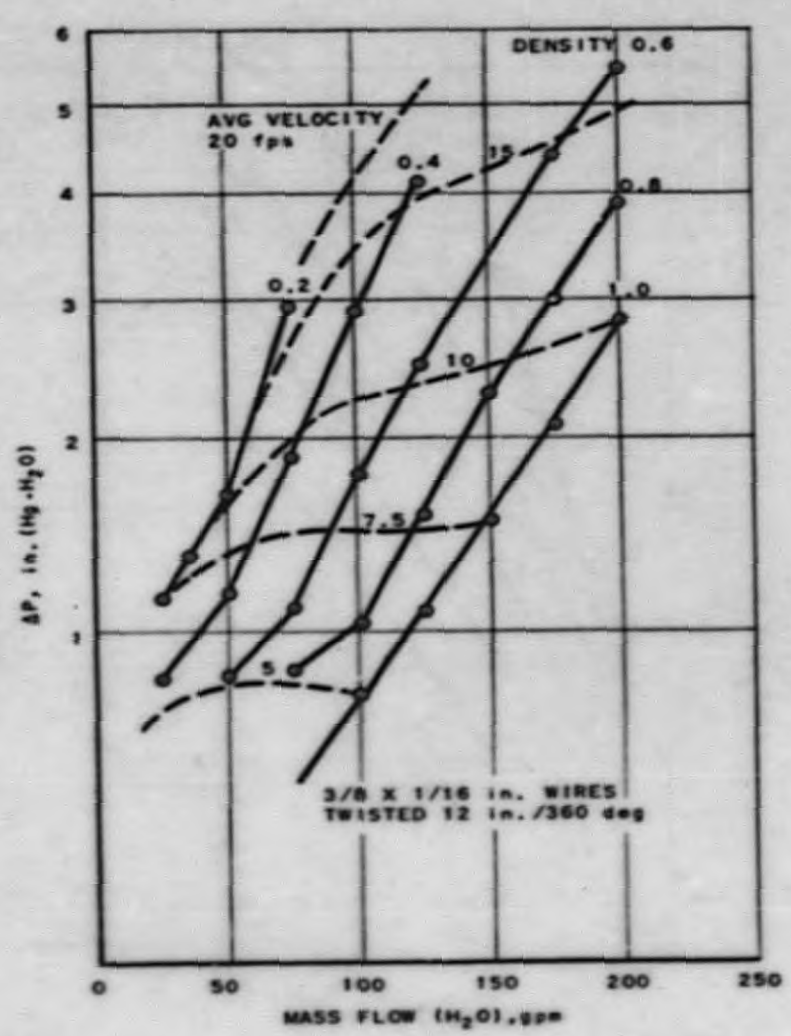

FIG. 70
MASS FLOW VS PRESSURE DROP.
WATER AND AIR MIXTURES

RE-7-11499-A

A.B.SCHULTZ:E.F.,8-18-53

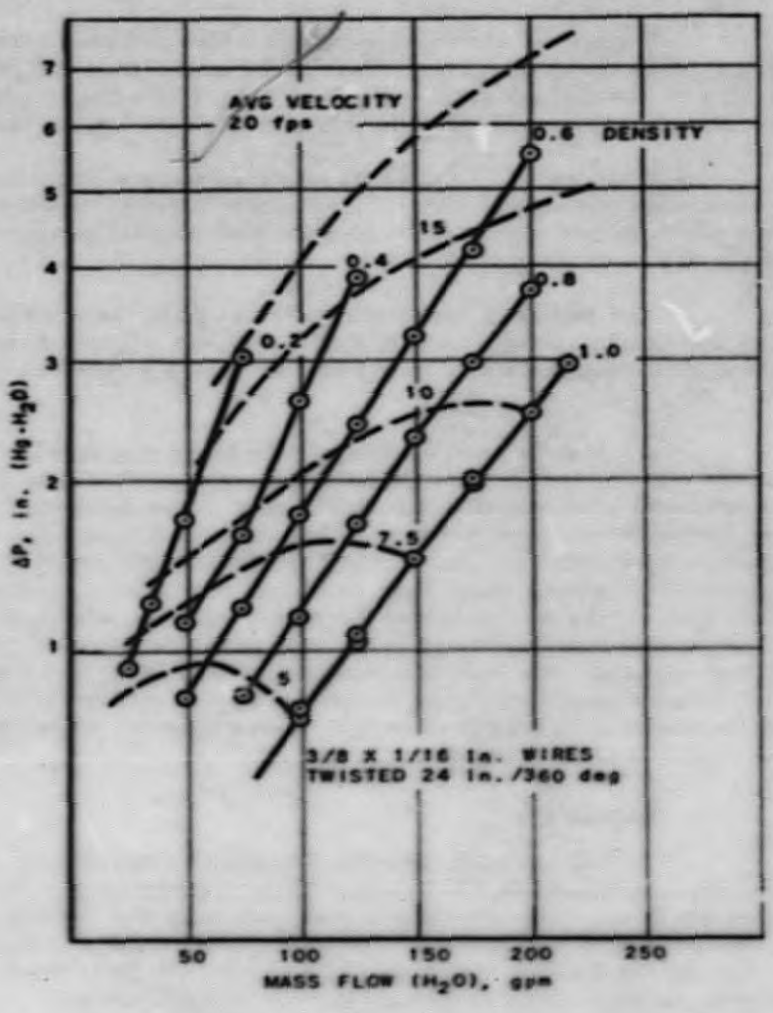

RE-7-11510-A

A.B.SCHULTZ & C.K.SOPPET:E.F.,8-19-53

FIG. 71
MASS FLOW VS PRESSURE DROP.
WATER AND AIR MIXTURES

mercury (in. Hg-H_2O). To convert to psi, the results must be multiplied by a factor of 0.455; to psi per foot of length by a factor of 0.165.

Figure 68 shows the comparative pressure drop for solid water for the three pitches tested. It is to be noted that the increase of pressure drop due to the tighter pitch is not great. The added resistance of the 12-inch versus the 24-inch pitch (nearly parallel) is negligible.

Figures 69, 70, and 71 show pressure drop through each test specimen with varying density. Again the difference between 12-inch and 24-inch pitch is not significant; and the 6-inch pitch over the others is of a small order of magnitude.

The bubbling tests showed that with the 6-inch pitch ribbons, the bubbles spread to approximately three-fourths of the channel. With the 24-inch pitch ribbons, the bubbles spread to only a scant one-fourth of the channel.

A condition not anticipated was an apparently uncontrollable surging of the air and water mixtures. Even though the flow of the mixture was fairly uniform at the bottom, it developed into a surging, slugging or burping action as it reached the top. This condition was apparent in all the mixed runs but was most violent in the lowest density conditions where the mixture alternated from a dead stop to a fast surge at a frequency of approximately 100 cycles per minute. Occasionally, at low flow and low density, the flow would even reverse for a fraction of a second. At high flow rates and high density, the surging was not so apparent but high-speed movies taken show that the condition still exists. Further study of the phenomenon is planned to see if it is inherent in two-phase flow or whether it is due to the nature of the test apparatus.

c. Conclusions

The calculated and the measured resistance of 1/16 in. x 3/8-in. parallel ribbons is 15% greater than calculated for flat plates of equal projected area. The measured resistance of the 6-inch pitch ribbons is 30% greater than calculated for flat plates, and 13% greater than measured for the 24-inch pitch ribbons. In general, the increased resistance of the ribbons is much less than was generally anticipated.

It appears possible to calculate, with reasonable accuracy, the pressure drop through twisted ribbons by using conventional calculation methods. The above comparisons indicate that for skin friction losses an average between the condition of infinite geometry and the condition including the confining walls will give results agreeing with experimental tests. The losses due to the twists may be calculated by assuming that one-sixth of the fluid, located at the periphery of the twists, will suffer complete loss of rotational kinetic energy at each point where the ribbons form parallel plates, i.e., six times per each 360 deg of twist.

Subsequent tests will be made to determine whether the above conclusions still hold for ribbon configurations and metal to water ratios tabulated below.

Wire Size, in.	Pitch of Twist, in.	Metal:Water Ratio
3/8 x 1/8	6	1:1.8
	24	
3/8 x 3/16	6	1:1
	24	
5/8 x 0.109	12	1:4.2
	24	
0.139 x 0.048	2-7/8	1:1.7

RADIATION STUDIES

Lubricants - W. K. Anderson, J. W. Frank

Several new greases have been received from the Standard Oil Company, Whiting, Indiana, in connection with the program to develop a grease with higher resistance to radiation damage than Dow-Corning High Vacuum Silicone Stopcock grease. The grease is to be used in the EBR.

One grease, LG-0147,[16] survived preliminary screening tests; the results of further testing are shown comparatively with the Dow-Corning grease in Table VI.

Grease LG-0147 has lower volatility than the silicone, shows equally good filming and wetting properties, does not corrode metals, and is superior to the Dow-Corning grease in lubricity. Its viscosity-temperature characteristic is about equivalent to that of the silicone material. It withstood without any particular harm radiation which rendered the silicone material useless as a lubricant.

It should be recognized that at temperatures near 100C (212F) the organic base oils used to compound the lubricants are almost at their practical volatility limit. If the temperatures and neutron fluxes which the greases must resist in service are appreciably higher than those used as criteria for these tests, it is unlikely that any organic material can long withstand such conditions.

---

[16] Composition data withheld - laboratory number assigned by Standard Oil Company for identification purposes only.

Table VI

COMPARISON OF STANDARD OIL COMPANY GREASE LG-0147
WITH DOW-CORNING HIGH VACUUM SILICONE STOPCOCK GREASE

	LG-0147	D-C High Vacuum Silicone Stopcock Grease
Volatility in oven at 100C (212F), per cent per hour	0.0008	0.0045
Film formation	Good	Good
Wetting ability	Good	Good
Corrosion	None	None
Lubricity data, (Precision Four Ball Wear Tester)		
Diameter of wear spot, mm	0.616	0.910
Mean specific pressure, psi	3898	1786
Micro-penetrometer data,		
Pentratiou at 25C (77F)	88	54
Pentration at 100C (212F)	128	90
Per cent change in penetration from 25C to 100C (77F to 212F)	45	67
Irradiation resistance:		
Total nvt*	3.7×10^{17}	5.5×10^{16}
Gas generation, cc/hr	0.25	6.8
Appearance after irradiation	Good, still a lubricant	Rubbery, no longer a lubricant

*At approximately 3×10^{12} fast neutrons/(cm^2)(sec).

END